SLAM/SAP signaling regulates discrete γδ T cell developmental checkpoints and shapes the innate-like γδ TCR repertoire

Somen K Mistri[1], Brianna M. Hilton[1], Katherine J. Horrigan[1], Emma S. Andretta[1], Remi Savard[1], Oliver Dienz[1], Kenneth J Hampel[2], Diana L. Gerrard[2], Joshua T. Rose[2], Nikoletta Sidiropoulos[2], Devdoot Majumdar[1], and Jonathan E. Boyson[*1]

[1]Department of Surgery, Larner College of Medicine, University of Vermont, Burlington, Vermont 05405, USA

[2]Department of Pathology and Laboratory Medicine, Larner College of Medicine, University of Vermont Medical Center, Burlington, Vermont 05405, USA

*Corresponding Author

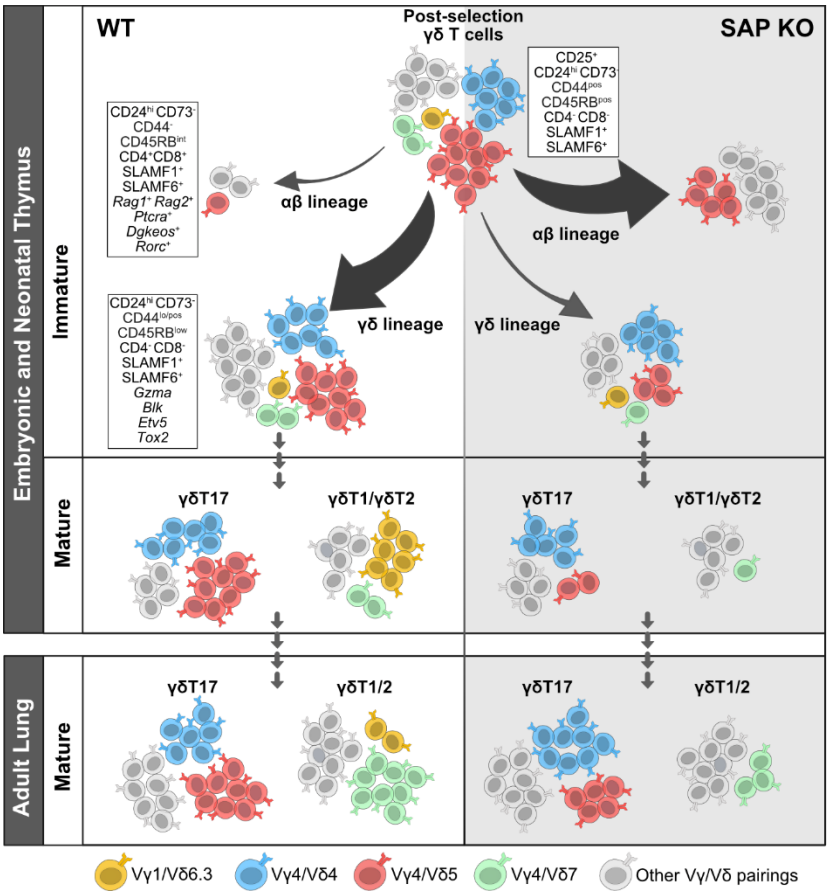

- SAP deficiency results in diversion of γδ T cells to the αβ T cell lineage
- SAP deficiency results in a loss of immature *Gzma*⁺*Blk*⁺*Etv5*⁺*Tox2*⁺ γδT17 precursors
- Identification of Vγ4/Vδ7 γδT1 cells as a novel SAP-dependent innate-like T cell subset

15

16 **Abstract**

17 During thymic development, most γδ T cells acquire innate-like characteristics that are critical for
18 their function in tumor surveillance, infectious disease, and tissue repair. The mechanisms,
19 however, that regulate γδ T cell developmental programming remain unclear. Recently, we
20 demonstrated that the SLAM-SAP signaling pathway regulates the development and function of
21 multiple innate-like γδ T cell subsets. Here, we used a single-cell proteogenomics approach to
22 identify SAP-dependent developmental checkpoints and to define the SAP-dependent γδ TCR
23 repertoire. SAP deficiency resulted in both a significant loss of an immature
24 *Gzma*$^{+}$*Blk*$^{+}$*Etv5*$^{+}$*Tox2*$^{+}$ γδT17 precursor population, and a significant increase in *Cd4*$^{+}$*Cd8*$^{+}$
25 *Rorc*$^{+}$*Ptcra*$^{+}$*Rag1*$^{+}$ thymic γδ T cells. SAP-dependent diversion of embryonic day 17 thymic γδ T
26 cell clonotypes into the αβ T cell developmental pathway was associated with a decreased
27 frequency of mature clonotypes in neonatal thymus, and an altered γδ TCR repertoire in the
28 periphery. Finally, we identify TRGV4/TRAV13-4(DV7)-expressing T cells as a novel, SAP-
29 dependent Vγ4 γδT1 subset. Together, the data suggest that SAP-dependent γδ/αβ T cell lineage
30 commitment regulates γδ T cell developmental programming and shapes the γδ TCR repertoire.

31 **Introduction**

32 Like αβ T cells, γδ T cells can be broadly grouped into innate-like IFN-γ-producing γδT1,
33 IL-4-producing γδT2, or IL-17-producing γδT17 subsets that are functionally programmed during
34 thymic development[1, 2, 3, 4], or inducible subsets that differentiate in the periphery[5]. These innate-
35 like γδ T cells are highly enriched in mucosal tissues such as the skin, gut, and lung and play
36 critical roles in the host response to pathogens, tumor surveillance, autoimmunity, and tissue
37 homeostasis. Accumulating data suggest that the relative balance of these functional γδ T cell
38 subsets can have important implications in disease susceptibility and progression. This is perhaps
39 best exemplified in the setting of cancer where IFN-γ-producing γδT1 have been shown to play a
40 critical role in tumor elimination[6, 7, 8], while γδT17 subsets promote tumor growth and metastasis[9,
41 10, 11, 12]. The thymic developmental programs, therefore, that regulate the balance of these
42 functional subsets in the periphery may have considerable impact on disease outcome. Unlike the
43 case for their αβ T cell counterparts, however, the mechanism that determine whether a developing
44 γδ T cell acquires an innate-like γδT1 or γδT17 phenotype during thymic development remain
45 unclear.

46 A significant body of data supports a model in which weak or strong TCR signal strength
47 might contribute to the development of innate-like γδT17 (weak signal) and γδT1 (strong signal)
48 subsets[4, 13, 14, 15, 16], and a strong TCR signal has been suggested to be necessary for the development
49 of the IFN-γ and IL-4 producing γδNKT cell subset[17]. However, there is also evidence of a TCR-
50 independent model in which pre-existing hard-wired transcriptional programs regulate the
51 development of some innate-like γδT17 subsets[18], and accumulating data suggest that γδT17
52 programming is associated with the use of distinct signaling pathways[19, 20, 21].

53 SLAM family receptors comprise a family of nine receptors, SLAMF1 (SLAM; CD150),
54 SLAMF2 (CD48), SLAMF3 (Ly9; CD229), SLAMF4 (2B4; CD244), SLAMF5 (CD84),
55 SLAMF6 (Ly108; CD352), SLAMF7 (CRACC; CD319), SLAMF8 (BLAME), and SLAMF9
56 (SF2001; CD84H), that are expressed primarily on hematopoietic cells and which play diverse
57 roles in immune development and function[22]. Most SLAM family receptors interact in a
58 homophilic manner, the exception to this rule being SLAMF4, which serves as the ligand for
59 SLAMF2. SLAM family receptor signals can be both activating or inhibitory, depending on the
60 recruitment of the cytosolic signaling adapter proteins SAP and EAT-2, and inhibitory SHP-1,
61 SHP-2, or SHIP phosphatases to immunoreceptor tyrosine switch motifs in the SLAM family
62 receptor cytoplasmic domain[22]. Although SLAM/SAP signaling has long been known to play a
63 role in innate-like NKT[23] and γδNKT[17] cell development, recent findings from multiple groups
64 demonstrating that this pathway is also involved in the development of innate-like γδT1, γδT17[24]
65 and innate-like MAIT cells[25, 26] indicates that SLAM/SAP signaling plays a fundamental role in
66 the development of a majority of the innate-like T cell lineages.

67 In this study, we set out to define the stage of thymic development during which SAP
68 mediates its effect on γδ T cell developmental programming and to define SAP-dependent changes
69 in the γδ T cells transcriptional program during their development. Finally, since SAP-dependent
70 innate-like T cell subsets are often characterized by highly restricted TCRs (e.g., $V\gamma1^{+}/V\delta6.3^{+}$
71 γδNKT[27]), we wished to identify whether specific TCR clonotypes were also associated with SAP-
72 dependent γδT1 and γδT17 T cells. Therefore, we utilized a single-cell proteogenomics approach
73 with V(D)J profiling that allowed us to simultaneously compare cell surface protein expression,
74 gene expression, and TCR clonotypes between B6 and B6.SAP$^{-/-}$ γδ T cells from embryonic,
75 neonatal, and adult thymus, as well as from peripheral lung γδ T cells. Collectively, these data

76 provide a comprehensive map of the SAP-dependent γδ T cell subsets and their developmental
77 checkpoints in perinatal and adult thymus.

78 **Results**

79 *SLAM family receptor expression marks transcriptionally distinct developmental stages among*
80 *E17 γδ T cells*

81 γδT17 developmental programming is thought to occur primarily during
82 embryonic/neonatal thymic development[2, 18, 28], and is tightly linked to the expression of discrete
83 TCR gamma and delta pairings[29]. To identify the specific developmental stages of thymic
84 development during which SLAM/SAP signaling pathway exerts its effects, we employed a single-
85 cell RNAseq approach coupled with feature barcoding (i.e., CITEseq[30]) and V(D)J profiling to
86 compare embryonic day 17 (E17) B6 and B6.SAP$^{-/-}$ thymic γδ T cells (**Fig. 1A**). FACS-sorted
87 thymic γδ T cells (**Suppl. Fig. 1**) from individual embryos (n = 4 B6 and 4 B6.SAP$^{-/-}$ mice) were
88 identified using hashtags, and Vγ1^{+} and Vγ4^{+} γδ T cells were identified using barcoded antibodies
89 (ADTs). To help define the developmental trajectories of the E17 γδ T cells, we also stained cells
90 with barcoded antibodies specific for CD24, CD73, CD44, and CD45RB, which define distinct
91 developmental pathways of γδT17 and γδT1 cells in the thymus[4, 31, 32], as well as for SLAMF1 and
92 SLAMF6. After data filtering and QC, we verified that clusters were evenly distributed among the
93 biological replicates (**Suppl. Fig. 1**). The resulting dataset represented a total of 5278 thymic γδ T
94 cells from B6 (n = 2597) and B6.SAP$^{-/-}$ (n = 2681) γδ T cells. Data were visualized using uniform
95 manifold approximation and projection (UMAP) for dimensionality reduction and a graph-based
96 clustering approach[33].

97 First, we annotated the B6 dataset using a combination of cell surface protein expression,
98 gene expression, and TCR clonotype sequence. This analysis revealed 11 B6 E17 γδ T cell clusters,
99 mostly distributed between two major branches (**Fig. 1B**). We observed the presence of
100 CD24^{low}73^{low}44^{high}45RB^{low}SLAMF1^{pos} (c8) and CD24^{low}73^{high}44^{high}45RB^{high}SLAMF6$^{low/pos}$ (c0,

101 c9) clusters, consistent with mature γδT17 phenotype and γδT1 phenotypes, respectively (**Fig. 1C,**
102 **Suppl. Fig. 1).** In support of this annotation, the c8 cluster was enriched in *Il17a*, *Il17f, Il23r,*
103 *Rorc*, and TRGV6/TRDV4 (IMGT nomenclature; encoding Vγ6/Vδ1) transcripts with limited
104 CDR3 diversity, while the c0/c9 cluster was enriched in *Ifng*, *Tbx21, Klrd1*, *Il2rb, Xcl1,* and
105 TRGV5/TRDV4 (encoding Vγ5/Vδ1) transcripts also with little to no diversity (**Figs. 1D – F,**
106 **Suppl. Fig. 2, Suppl. Tables 1 and 2**)[34, 35]. Consistent with previous observations[24], we noted that
107 the c0/c9 cluster was highly enriched in *Cd244a* (*Slamf4*), and was enriched in transcripts from
108 another SLAM family member, *Slamf7* (**Figs. 1D - E**). Flow cytometric analysis confirmed that
109 SLAMF7 was expressed primarily on mature γδ T cells and that its expression was mostly confined
110 to γδ T cells expressing the canonical $CD44^{+}CD45RB^{+}$ markers of γδT1 cells (**Suppl. Fig. 1**)[4, 36].
111 We identified a small $CD24^{low/int}73^{high}44^{high}45RB^{pos}$ c3 cluster characterized by enrichment
112 in *Cd200* (whose expression is upregulated upon TCR ligation[37]), *Il2rb, Nr4a1, Cd244a*, *Xcl1,* and
113 *Tnfrsf9* (encoding 4-1bb receptor). A high frequency of invariant TRGV5/TRDV4 clonotypes and
114 decreased TCR clonotype diversity (**Suppl. Fig. 2, Suppl. Table 2)** suggested that c3 represented
115 an immature γδT1 population. The $CD24^{low/pos}CD73^{low/pos}44^{low/pos}CD45RB^{low/pos}$ c4 cluster was
116 enriched in *Ms4a4b and Ms4a6b (*encoding CD20 homologues that modulate T cell activation[38,
117 39]), *S1pr1*, *Il6ra, Cd8a, Cd8b1,* and *Ccr9,* suggesting that the c4 cluster represents the previously
118 described emigrating thymic $Ccr9^{+}$ $S1pr1^{+}$ γδ T cells[40] (**Fig. 1C and 1E**). Consistent with the c4
119 cluster representing naïve emigrating thymic γδ T cells, the diversity of the c4 TCR clonotypes
120 was the highest among the $CD24^{low/int}$ (c0/c9, c8, c3) clusters (**Suppl. Fig. 2).**
121 We identified several immature $CD24^{high}CD73^{neg}$ ADT clusters (c1, c2, c7, c5, c6, and c10)
122 that also expressed SLAMF1 and/or SLAMF6 (**Fig. 1B and Suppl. Fig 1**). The c1 and c2 clusters
123 were enriched in γδT17-associated genes such as *Blk, Maf, Sox13, Ccr2, Tcf12, and Rorc*[32, 41, 42,

124 [43, 44], as well as *Sh2d1a* (encoding SAP) and *Ccr9*[16] **(Fig. 1E, Suppl. Table 1)**. Within these two
125 clusters, the CD44$^{low/pos}$CD45RB^{low} c2 cluster was especially enriched in genes previously
126 implicated in γδ T cell development such as *Etv5, Tox, Sox4, Tcf7*, *Zbtb16* [44, 45, 46, 47, 48], *Igfbp4* and
127 *Igf1r* which were recently implicated in Th17 differentiation[49], *Tnfsf11* (RANKL) which regulates
128 Aire^{+} mTEC development [50], as well as *Themis* and *Tox2* **(Fig. 1E, Suppl. Fig. 1)**. A high level of
129 *Gzma* expression identified c2 as the previously described *Gzma*$^{+}$ γδ T cell subset[40]. Interestingly,
130 in addition to expressing γδT17-associated genes, the c2 cluster was also enriched in γδT2-
131 associated *Gata3* and *Il4* transcripts (**Fig. 1D – E, Suppl. Table 1**). The CD44$^{low/pos}$CD45RB^{neg} c1
132 cluster, in contrast, exhibited significantly higher levels of *Il17a, Il17f, Rorc*, *Maf* [42], as well as
133 *Ifngr1,* consistent with the c1 cluster representing immature γδT17 cells (**Fig. 1D – E, 1G, and**
134 **Suppl. Fig. 1**).

135 Analysis of the c1 and c2 TCR transcripts revealed that the c2 cluster was notably enriched
136 in TRGV4-expressing cells and that 87% of Vγ4 T cells utilized just 3 TRDV chains (50%
137 TRDV5, 24% TRDV2-2, and 12% TRAV13-4/DV7) (**Fig. 1F, Suppl. Table 2**). Clonotype
138 analysis revealed a high frequency of semi-invariant TRGV4/TRDV5 and TRGV4/TRDV2-2
139 clonotypes previously associated with γδT17[51, 52, 53] (**Suppl. Fig. 2, Suppl. Table 2**). In contrast,
140 the c1 cluster possessed comparatively fewer of these TRGV4 clonotypes, and was enriched in
141 TRGV6, TRGV5, and TRGV1 paired with TRDV4 (**Suppl. Fig. 2, Suppl. Table 2)**. Indeed, we
142 noted that the Vγ1 repertoire, which is diverse in adult tissues, was dominated by TRGV1/TRDV4
143 clonotypes (35% of all TRGV1) in E17 thymus, and just two closely related semi-invariant
144 TRGV1/TRDV4 clonotypes comprised 17.4% of all TRGV1. The location of these clonotypes in
145 the immature γδT17-related clusters (**Suppl. Fig. 2)** suggested that they represent the dominant
146 IL-17-producing Vγ1 clonotypes at E17, which we verified using flow cytometry (**Suppl. Fig. 3**).

147 Since the IL-4-producing Vγ1/Vδ6.3 γδNKT cell subset develops in fetal thymus[1], we
148 asked whether the *Il4*-enriched γδ T cells in cluster 2 (**Fig. 1D**) were immature Vγ1 γδNKT cells
149 with previously identified canonical Vδ6.3 sequences[27]. Interestingly, while we did identify a
150 small number of Vγ1 T cells with these canonical sequences (encoded by TRAV15-1/DV6-1 or
151 TRAV15N-1) in our dataset, these were not present in the *Il4*-enriched c2 cluster.

152 The $CD44^{pos}CD45RB^{pos}$ c5 cluster was enriched in *Il2ra*, *Scin, Bex6, Cd5, Slamf6, Cd28,*
153 *Hivep3*, and cell-cycle/metabolism genes, consistent with γδ T cells that have recently developed
154 from DN2/DN3[40, 54, 55]. Within the c5 and c7 clusters, we noted that while there was expression of
155 γδT17-associated genes such as *Blk, Maf, Sox13,* and *Etv5*, there was relatively little *Rorc*
156 expression. *Rorc* expression became apparent in the c2 cluster (*Rorc*^{low}) and was significantly
157 increased in the c1 cluster (**Suppl. Fig. 1)**. Flow cytometric analysis confirmed BLK and PLZF
158 expression in $CD25^{high}$ E17 Vγ4 T cells, while RORγt expression was primarily observed in the
159 $CD25^{neg}$ population, suggesting that BLK is expressed soon after γδ T cell selection, followed by
160 RORγt (**Suppl. Fig. 3)**. These data were consistent with MAF-directed expression of *Rorc*[40, 42]
161 and suggested a c5 – c7 – c2 – c10 / c1 – c8 γδT17 developmental trajectory, which was supported
162 by trajectory inference analysis **(Fig. 1H).**

163 Finally, analysis of the $CD24^{high}73^{neg}44^{neg}45RB^{int}SLAMF1^{pos}SLAMF6^{pos}$ c6 population
164 revealed that it was highly enriched in *Cd8a, Cd8b1, Cd4, Rag1, Rag2, Ptcra, Arpp21, and*
165 *Dgkeos,* consistent with cells developing along the αβ T cell lineage **(Figs. 1E, 1G, Suppl. Fig. 1,**
166 **and Suppl. Table 1**)[56]. Analysis of the Vγ1 and Vγ4 ADTs confirmed that c6 cells were not simply
167 contaminating αβ T cells as both Vγ1- and Vγ4-expressing cells were present in the c6 cluster
168 **(Suppl. Fig. 3**) and analysis of the c6 TCR clonotypes revealed the presence of TRGV1, GV4,

169 GV5, GV6, and GV7 clonotypes, none of which appeared to be specific to the c6 cluster (**Suppl.**
170 **Table 2)**.

171 Since trajectory inference analysis suggested a strong relationship between the *Il2ra*$^{+}$ c5
172 and c6 clusters (**Fig. 1H**), we conducted differential gene expression analysis between the c5 and
173 c6 from B6 mice. Interestingly, we found that the c6 cluster was highly enriched in *Rorc,*
174 suggestive of a γδT17 phenotype, but was mostly lacking in the expression of *Maf, Blk, Ccr2*, and
175 other canonical γδT17-associated transcripts (**Fig. 1E, 1G, and Suppl. Fig. 1**). Indeed, flow
176 cytometric analysis of E17 TCRβ^{neg}TCRδ^{pos} γδ T cells confirmed that CD4CD8 DP γδ T cells
177 exhibited an immature CD44^{low}CD25^{low}MAF^{neg}BLK^{neg}RORγt^{pos} phenotype (**Suppl. Fig. 3**), and
178 that RORγt expression in the absence of BLK or MAF is a characteristic of Lin^{neg} DN thymocytes
179 as they progress from CD44^{low}25^{high} DN3 to CD44^{low}25^{low} DN4 (**Suppl. Fig. 3**). Together, these
180 data suggested that the c6 cluster γδ T cells represented previously described CD4CD8 DP γδ T
181 cells that were developing along an alternative αβ T cell pathway[57, 58, 59].

182

183 *SAP regulates γδ T cell clonotype diversion into both the γδT17 and the αβ T cell developmental*
184 *pathways.*

185 To identify SAP-dependent developmental checkpoints, we next compared the hashtag-
186 separated B6 and B6.SAP$^{-/-}$ E17 γδ T cell datasets. A comparison of the cluster frequencies
187 between B6 and B6.SAP$^{-/-}$ γδ T cells revealed significantly decreased frequencies of the
188 CD24^{high}73^{neg}44^{int}45RB^{int}SLAMF1^{pos}SLAMF6^{pos} c2 and c1 clusters in B6.SAP$^{-/-}$ mice, and a
189 striking increase in the frequency of the CD24^{high}73^{neg}44^{neg}45RB^{neg}SLAMF1^{high}SLAMF6^{high} c6
190 cluster (**Fig. 2A)**. A comparison of differentially expressed genes among the immature (c1, c2, c7,
191 c5, c6, and c10) clusters using pseudobulk analysis revealed 234 differentially expressed genes

192 with a p_{adj} threshold < 0.005 and log_2 fold change greater than 0.5, with 148 genes exhibiting
193 decreased expression in B6.SAP$^{-/-}$ γδ T cells, and 86 genes exhibiting increased expression (**Fig.**
194 **2B, Suppl. Table 3**). Consistent with the decreased frequencies of the c1/c2 clusters in B6.SAP$^{-/-}$
195 mice, a significant fraction of the differentially expressed genes that were down-regulated in
196 B6.SAP$^{-/-}$ mice reflected γδT17-associated genes (e.g., *Maf, Blk, Ccr2, Sox13, Etv5, etc.*) that were
197 present in the c2 and c1 clusters, as well as a number of c1/c2-enriched genes (e.g., *Cpa3, Tox2,*
198 *Pdcd1, Tmem121, Bex6*, and *Scin*) whose importance in γδ T cell development is unclear (**Fig. 2B-**
199 **C, Suppl. Table 2**). This was not solely due to the decreased frequency of the c2 and c1 clusters
200 in B6.SAP$^{-/-}$ mice, as a closer analysis revealed a decreased number of transcripts for many
201 signature genes (e.g., *Blk*, *Etv5*, *Ccr2*) prevalent in the c2 cluster and to a lesser extent the c7
202 cluster **(Suppl. Fig. 4**). Given the decreased expression of *Blk*, we also examined the expression
203 of Src tyrosine kinase family members *Lck* and *Fyn,* which have previously been implicated in T
204 cell development[60]. Unlike *Blk*, which was mostly restricted to γδT17 clusters, *Lck* and *Fyn*
205 expression was more broadly distributed (**Suppl. Fig. 1**). Using pseudobulk analysis to compare
206 their expression between B6 and B6.SAP$^{-/-}$ immature E.17 γδ T cells, we found that neither *Lck*
207 nor *Fyn* expression was appreciably altered (**Suppl. Fig. 4**), suggesting that *Blk* expression was
208 uniquely dependent on SAP. We did note, however, that the magnitude of *Lck* differential
209 expression was close to the 0.5 log_2 FC cut-off and that its expression was increased in B6.SAP$^{-/-}$
210 γδ T cells (**Suppl. Fig. 4**). Indeed, a large number of genes whose expression was increased in
211 B6.SAP$^{-/-}$ mice were those whose expression was mostly confined to the c6 cluster (e.g., *Cd4,*
212 *Cd8b1, Ptcra, Rag2*) or whose expression was highest in c6 (e.g., *Tcf7, Thy1, Lck*) (**Fig. 2B-C,**
213 **Suppl. Fig. 4)**. Together, these data identified the *Gzma*$^+$*Etv5*$^+$*Sox13*$^+$*Blk*$^+$*Tox2*$^+$ c2 and
214 *Cd4*$^+$*Cd8b1*$^+$*Ptcra*$^+$*Rag2*$^+$ c6 clusters as SAP-dependent developmental checkpoints.

215 Next, we asked whether these SAP-dependent alterations in γδ T cell development were
216 associated with any changes in the TCR repertoire. A comparison of all γδ TCR clonotypes
217 between E17 B6 and B6.SAP$^{-/-}$ γδ T cells revealed no significant changes in overall clonotype
218 frequency (**Fig. 2D**). However, a closer examination of TCR repertoire revealed significant
219 changes in the distribution of specific TCR clonotypes. For example, within the TRGV4 repertoire,
220 which represents the dominant TCR among immature clusters at E17, we observed a significant
221 decrease in TRGV4/TRDV5 clonotypes in the c2 cluster and a concomitant increase of these
222 clonotypes in the c6 cluster (**Fig. 2E**). Among the TRGV4 clonotypes, this appeared to be specific
223 to the TRDV5 clonotypes, as we observed no significant differences c2 and c6 frequencies among
224 TRGV4/TRDV2-2 and TRDV7 clonotypes (**Fig. 2E**). We did note, however, a significant increase
225 in the TRGV4/TRDV7 clonotypes in the *Il2ra*$^{+}$ c5 cluster (**Fig. 2E**). Within the TRGV1 repertoire,
226 we noted a significant increase in TRGV1/TRDV4 clonotypes within the c6 cluster (**Fig. 2E**).
227 Together, these data suggested that SAP operated at an early stage of γδ T cell development during
228 or soon after the down-regulation of *Il2ra,* and that it positively regulated entry into the γδT17
229 pathway at the c5/c7 to c2 transition, while at the same time inhibiting entry into the CD4^{+}CD8^{+}
230 αβ T cell-like c6 cluster. The net result of these changes appeared to be that specific TCR
231 clonotypes such as TRGV4/TRDV5 were diverted from the γδT17 pathway into the αβ T cell-like
232 pathway.
233
234 *SAP deficiency is associated with increased numbers of immature CD4^{+}CD8^{+}RORγt^{+} thymic γδ T*
235 *cells*
236 Next, we independently evaluated these observations using flow cytometry. This analysis
237 revealed that while SAP deficiency did not affect the overall number of E17 γδ T cells (**Suppl.**

238 **Fig. 5**), it did result in a significant decrease of immature CD24^{pos}BLK^{pos}MAF^{pos}RORγt^{pos} γδ T
239 cells in E17 B6.SAP$^{-/-}$ thymus (**Fig. 3A-B**). We found that this decrease was most pronounced in
240 the CD44^{pos} population after downregulation of CD25 (**Fig 3A, Suppl. Fig. 5**) and that this
241 population exhibited a high level of PLZF expression, suggesting it corresponded to the
242 CD44^{+}*Blk*$^{+}$*Maf*$^{+}$*Zbtb16*$^{+}$*Rorc*$^{+}$ c1 cluster (**Suppl. Fig. 5**). In addition, UMAP analysis of E17 Vγ4
243 T cells flow cytometric data revealed the presence of a SAP-dependent
244 CD24^{pos}BLK^{pos}PLZF^{pos}RORγt^{neg} population in B6.SAP$^{-/-}$ thymus **(Suppl. Fig. 5**) consistent with
245 the phenotype of the *Rorc*^{low} c2 cluster. In contrast, we found no evidence of a SAP-dependent
246 decrease in the CD25^{pos} population frequency, consistent with the notion that SAP exerts its effect
247 during or after this stage of development (**Fig. 3A**). We also noted that in addition to its effect on
248 the numbers of immature thymic γδT17, SAP deficiency resulted in the reduced expression levels
249 of some of these markers, most notably BLK (**Fig. 3C**), a finding that was consistent with the
250 decreased number of *Blk* transcripts observed in Fig. 2. Interestingly, as PLZF induction is often
251 associated with SLAM/SAP signaling, we noted that SAP did not affect overall PLZF expression
252 levels in E17 thymic γδ T cells (**Suppl. Fig. 5**).

253 In contrast to the decreased numbers of CD24^{pos}BLK^{pos}MAF^{pos}PLZF^{pos} RORγt^{pos} γδ T
254 cells, we observed a significant increase in the frequency and number of
255 CD24^{pos}BLK^{neg}MAF^{neg}PLZF^{neg}RORγt^{pos} γδ T cells (**Figs. 3A-B**), whose phenotype was consistent
256 with the αβ T cell-like c6 cluster in Fig. 2. Consistent with our finding that the c6 cluster was
257 enriched in CD4 and CD8, we found that the frequency and number of CD4 and CD8-expressing
258 CD24^{pos} TCRδ^{pos}TCRβ^{neg} BLK^{neg}MAF^{neg}RORγt^{pos} thymic γδ T cells was significantly increased
259 in B6.SAP$^{-/-}$ mice (**Fig. 3D**). Together, these analyses confirmed our single-cell CITEseq analysis,
260 and suggested that SAP regulated both the throughput of immature γδ T cells in the γδT17 cell

261 pathway as well as the αβ T cell-like pathway. More specifically, the data suggested that SAP
262 promoted progression to the CD24^{pos} BLK^{pos}MAF^{pos}PLZF^{pos}RORγt^{low} c2 cluster that is enriched
263 in a number of genes (e.g., *Sox13, Etv5, Blk, Maf)* known to regulate γδT17 development, but that
264 it inhibited entry into the CD24^{pos}44^{neg}BLK^{neg}MAF^{neg}RORγt^{pos} αβ–T cell-like pathway (c6
265 cluster).
266
267 *Identification of SAP-dependent developmental checkpoints during neonatal and adult thymus γδ*
268 *T cell developmental programming.*
269 The neonatal period is a time of rapid expansion of numerous γδ T cell subsets in the
270 thymus including Vγ4 γδT17 and γδNKT. Therefore, we conducted a comparison between B6 and
271 B6.SAP$^{-/-}$ neonatal and adult thymic γδ T cells, to identify novel SAP-dependent developmental
272 checkpoints and to track the outcome of the SAP-dependent alterations in γδ T cell development
273 observed in E17 thymus. Neonate datasets revealed a similar branched clustering pattern as in E17
274 with some notable differences. Similar to E17, we observed immature
275 CD24^{pos}73^{low}SLAMF1^{pos}SLAMF6^{pos} clusters (c0, c1, c2, c3, c9, c12, c14),
276 CD24^{pos}73$^{low/pos}$SLAMF1^{pos}SLAMF6^{pos} (c4, c5, c10, c15) *S1pr1*-enriched "naïve" clusters,
277 mature CD24^{neg}73^{low}SLAMF1^{pos}SLAMF6^{neg} (c6, c7) γδT17 clusters, and a mature
278 CD24^{neg}73^{pos}SLAMF1^{neg}SLAMF6$^{low/pos}$*Slamf7*^{high} (c8) γδT1 cluster (**Fig. 4A-B**, **Suppl. Fig. 6)**. In
279 general, we noted good correlation with cluster-specific gene expression between the E17 and D9
280 (Day 9) datasets. A notable exception was a striking decrease in *Zbtb16* expression among all
281 immature neonatal γδ T cells, which is consistent with previous reports[16, 40] (**Suppl. Fig. 6, Suppl.**
282 **Table 3**).

283 In contrast to the E17 dataset, the neonatal thymic γδ T cell dataset contained a
284 CD24^{neg}73^{pos}SLAMF1^{neg}SLAMF6^{high}*Slamf7*^{neg} (c13) γδT2 cluster enriched in *Il4, Il13, Zbtb16,*
285 *Cd40lig*, and *Nos1* (**Suppl. Fig. 6, Suppl. Table 1),** suggesting it represented IL-4-producing
286 γδNKT cells. Indeed, examination of the γδT2 (c13) and γδT1 (c8) cluster TCR repertoires
287 revealed a significant enrichment of canonical TRGV1 and TRAV15N-1 or TRAV15-1/DV6-1
288 sequences characteristic of γδNKT cells (**Fig. 4C, Fig. 5**)[27]. Analysis of the differentially
289 expressed genes in the γδT1 (c8) and γδT2 (c13) clusters revealed that *Zbtb16*, *Icos,* and *Slamf6*
290 were markers of γδT2 cells while *Tbx21*, *Klrb1c* (NK1.1), and *Slamf7* were markers of γδT1 cells
291 in neonatal thymus (**Suppl. Fig. 6**). Flow cytometric analysis confirmed that PLZF^{hi} γδT2
292 Vγ1Vδ6.3 cells co-express SLAMF6 and ICOS while Tbet^{hi} γδT1 Vγ1Vδ6.3 cells are NK1.1^{+} and
293 are either SLAMF6^{-}SLAMF7^{+} or SLAMF6^{+}SLAMF7^{+} **(Suppl. Fig. 7)**.

294 A comparison of B6 and B6.SAP$^{-/-}$ neonatal γδ T cells revealed multiple SAP-dependent
295 changes in clustering. Among the immature γδ T cells, we observed a decreased frequency of the
296 immature CD24^{high}73^{neg}SLAMF1^{pos}SLAMF6^{pos} c1 cluster (**Fig. 4D**) that was enriched in *Blk, Etv5,*
297 *Sox13, Rorc,* and *Maf* (**Suppl. Fig. 6**), suggesting it was analogous to the SAP-dependent c2
298 cluster in E17 γδ T cells. Similar to our observations in E17 γδ T cells, flow cytometric analysis
299 confirmed both a decrease in BLK^{pos}RORγt^{pos} and BLK^{pos}RORγt^{neg} γδ T cell populations, as well
300 as a decreased level of BLK expression (**Fig. 4E-F**). In addition, we observed an increased
301 frequency of immature CD24^{high}73^{neg}SLAMF1^{pos}SLAMF6^{pos} cluster with characteristics of αβ T
302 cells (c14) in B6.SAP$^{-/-}$ D9 thymic γδ T cells **(Fig. 4D, Suppl. Fig. 6**). While this increase did not
303 reach the level of significance, presumably due to the very low number of c14 cells in the dataset,
304 flow cytometric analysis revealed a significant increase in immature CD24^{pos}73^{neg}BLK^{neg}RORγt^{pos}
305 γδ T cells, a phenotype consistent with γδ T cells that have been diverted to the αβ developmental

306 pathway (**Fig. 4E**). Last, we observed an increased frequency of immature CD24^{pos}73$^{low/pos}$
307 SLAMF1^{pos}SLAMF6^{pos} *S1pr1*-enriched c4 and c5 clusters, but not the closely related *Cd200*-
308 enriched c10 cluster (**Fig. 4D).** While we did confirm an increased number of CD200^{neg}S1pr1^{pos}
309 γδ T cells in neonatal thymus by flow cytometry, this increase was relatively small and its
310 significance is unclear **(Suppl. Fig. 7).** Independent confirmation of these SAP-dependent changes
311 in neonatal γδ T cell gene expression was obtained by conducting bulk RNAseq analysis of
312 FACSs-sorted CD24^{high} neonatal thymic γδ T cells from B6 and B6.SAP$^{-/-}$ mice (**Suppl. Table 4**).
313 Among the mature neonatal γδ T cells, we observed a decreased frequency of the
314 CD24^{low}73^{neg}SLAMF1^{pos}F6^{low} γδT17 c6 cluster, which was consistent with our previous
315 observation of decreased IL-17 production in B6.SAP$^{-/-}$ neonatal γδ T cells[24]. Interestingly, we
316 observed a striking loss of the CD24^{low}73^{high}SLAMF1^{low}F6^{high}F7^{neg} γδT2 c13 cluster in B6.SAP$^{-/-}$
317 mice, as well as a decreased frequency of the mature CD24^{low}73^{high}SLAMF1^{low}F6^{low}F7^{high} γδT1
318 c8 cluster (**Fig. 4A - D**). These findings were consistent with a SAP-dependent loss of both the IL-
319 4- and IFN-γ-producing γδNKT as well as non-γδNKT γδT1 cells (discussed further below).
320 Unfortunately, while we were able to define mature SAP-dependent γδNKT subsets, we found no
321 evidence of immature γδNKT cells in our dataset, suggesting that they develop during a brief
322 developmental window between E17 and D9 after birth.
323 A comparison of B6 adult thymic γδ T cells between B6 and B6.SAP$^{-/-}$ mice recapitulated
324 many of our observations of the neonatal thymus, although to a somewhat lesser degree. For
325 example, we observed a small but significant decrease in the frequency of the CD24^{high}CD73^{low}
326 adult thymic c1 and c2 clusters in B6.SAP$^{-/-}$ mice that was coupled with an increased frequency of
327 the CD24^{pos}CD73$^{+/-}$ c0 cluster **(Suppl. Fig. 8)**. Like the SAP-dependent E17 c2 and D9 c1 clusters,
328 the adult thymus c1 and c2 clusters were enriched in γδT17-associated *Blk, Etv5, Sox13*, *Maf,* and

329 *Rorc* (mostly in c2) indicating that SAP regulates this γδ T cell thymic developmental checkpoint
330 at all ages. Likewise, both the adult thymus c0 and the neonatal c4 and c5 clusters that were
331 enriched in *Ms4a4b, Ms4a6b, Dgka, Klf2,* and *S1pr1* exhibited increased frequencies in B6.SAP^{-}
332 $^{/-}$ mice. Just as we observed in neonatal thymic γδ T cells, we noted a near complete loss of mature
333 γδNKT cells (*Zbtb16, Icos*, and *Il4*-enriched γδT2 c8 cells and *Tbx21, Slamf7*, and *Il2rb*-enriched
334 γδT1 c11 cells) as well as a decreased frequency of mature non-γδNKT γδT1 c10 cluster cells in
335 B6.SAP$^{-/-}$ adult thymus (**Suppl. Fig. 8**). Unlike the E17 and neonatal thymic datasets, however,
336 the frequency of γδ T cells with an αβ T cell-like signature in the adult thymic γδ T cell dataset
337 was minimal. Collectively, these data supported the presence of multiple SAP-dependent
338 developmental checkpoints during neonatal and adult γδ T cell development—a reduction in the
339 CD24^{pos}CD73^{neg} SLAMF1^{+}SLAMF6^{+} cluster enriched in γδT17 development-associated
340 transcripts, an increased frequency of immature *S1pr1*-enriched γδ T cells, and decreased
341 frequencies of both γδNKT cells (γδT1 and γδT2) as well as non-γδNKT γδT1 cells.
342
343 *SAP shapes the thymic γδ TCR repertoire*
344 Given our observation of altered γδ TCR clonotype distribution among E17 γδ T cells and
345 the substantial changes in clustering we observed in SAP-deficient mice, we were next interested
346 in determining the effect of SAP deficiency on the neonatal and adult γδ TCR repertoires. A
347 comparison of frequencies of the top 100 TCR clonotypes between B6 and B6.SAP$^{-/-}$ mice revealed
348 significant changes in the overall frequency of several TRGV1 and TRGV4 clonotypes (**Fig. 5A**).
349 Consistent with a SAP-dependent loss of γδNKT, we observed a profound loss of TRGV1
350 clonotypes utilizing the canonical TRAV15N-1 and TRAV15-1/TRDV6-1 γδNKT cell TCRs (**Fig.**

351 **5B**). Loss of these clonotypes was directly tied to the significant decrease of the γδT1 c8 and γδT2
352 c13 clusters, in which nearly all these clonotypes resided.

353 Within the B6 γδT2 c13 cluster the vast majority (~86%) of TCR sequences were highly
354 restricted canonical γδNKT cell clonotypes **(Suppl. Table 2**) and nearly all of these clonotypes
355 were also present in the γδT1 c8 cluster consistent with the ability of γδNKT cells to produce both
356 IFN-γ and IL-4. In contrast, while the B6 γδT1 c8 cluster contained a large proportion of canonical
357 γδNKT cell clonotypes (~46% of c8 TCRs), it also contained TCRs with a diverse pool of
358 clonotypes that utilized TRGV1 (~70% of c8 TCRs), TRGV4, TRGV5, TRGV6, and TRGV7 that
359 were present only in the c8 γδT1 cluster. Therefore, in neonates, the thymic γδT1 population is a
360 mixture of γδNKT and "non-γδNKT" γδT1 clonotypes, and each of these clonotype pools is SAP-
361 dependent. As noted above, these findings were largely reproduced in the adult thymus where the
362 γδNKT clonotypes associated with the c8 and c11 clusters were virtually absent in B6.SAP$^{-/-}$ mice,
363 and where the diverse pool of γδT1 c10 clonotypes was significantly diminished (**Suppl. Table**
364 **2)**.

365 Interestingly, a closer examination of the neonatal thymic TRGV4 clonotypes revealed a
366 significant decrease in the frequencies of γδT17-associated clonotypes with a germline-encoded
367 TRDV5[52] (**Fig. 5B**), some of which were identical to those that were redistributed to the αβ T cell-
368 like c6 cluster in E17 γδ T cells **(Fig. 2E)**. When these clonotypes were mapped to their D9 clusters,
369 we noted a significant decrease in the frequency of TRGV4/TRDV5 clonotypes in the mature
370 γδT17 c6 cluster (**Fig 5C**). We note that while we observed a trend toward an increased frequency
371 of TRGV4/TRDV5 and TRGV4/TRDV2 clonotypes in the *S1pr1*$^{+}$ c4/c5 clusters, analysis of these
372 sequences revealed that they largely exhibited diverse CDR3 rather than the restricted CDR3

373 observed in the γδT17 c6 cluster (**Suppl. Table 2**). Taken together, these data indicated that the
374 immature embryonic day 17 γδ TCR clonotypes that were redirected to the αβ T cell pathway in
375 B6.SAP$^{-/-}$ mice were underrepresented among the mature B6.SAP$^{-/-}$ neonatal γδ T cells.
376
377 *Restricted TCR repertoire in innate-like γδT1 as well as γδT17 in the periphery.*
378 We previously demonstrated that SAP-deficiency results in a significant impairment in γδ
379 T cell function in the periphery[24]. Specifically, we observed that γδ T cell IL-17 production is
380 impaired in the lungs of young mice, but that this had largely corrected itself as the mouse reached
381 maturity. In contrast, we observed that both Vγ1 and Vγ4 IFN-γ production were significantly
382 impaired in B6.SAP$^{-/-}$ adult lung and spleen. To better understand how SAP-dependent alterations
383 in thymic development ultimately affected the peripheral γδ T cell compartment, we compared B6
384 and B6.SAP$^{-/-}$ lungs using single-cell RNAseq with V(D)J profiling.
385 Our initial annotation of the B6 lung γδ T cell transcriptome revealed the presence of 11
386 clusters of the lung γδ T cells that we annotated based on cluster-specific gene expression and
387 TRGV and TRDV usage (**Figure 6A**). Based on their expression of signature cytokines and
388 transcription factors, we identified 2 γδT17 clusters (c1 and c4), 4 γδT1 clusters (c2, c3, c7, and
389 c9), 1 γδTNKT-like cluster (c10) with very few cells, as well as a *Cd24*-enriched cluster (c5) (**Fig.
390 6B and 6C, Suppl. Table 5**). Consistent with previous observations, we noted that the c1 and c4
391 γδT17 clusters were enriched in *Slamf1* and that the c2/c3/c7/c9 γδT1 clusters were enriched in
392 *Slamf7* and *Slamf6* (**Fig. 6B**). Indeed, flow cytometric analysis revealed that SLAMF7 expression
393 was restricted to the innate-like lung CD44^{+}CD45RB^{+} γδT1 cell population, and that γδT1 cells
394 are SLAMF1^{-}F6^{+}F7^{+}, while the CD44^{+}CD45RB^{-} γδT17 subsets are SLAMF1^{+}F6^{-}F7^{-} (**Fig. 6D**).
395 Further annotation using V(D)J profiling revealed that the c1 cluster corresponded to Vγ4 γδT17

396 (primarily TRGV4/TRDV5 and TRGV4/TRDV2-2) while the c4 cluster corresponded to lung Vγ6
397 (TRGV6/TRDV4) (**Fig. 6E, Suppl. Table 6**). The c10 cluster was enriched in *Zbtb16*, *Il4*, and
398 *Icos* (**Fig. 6B-C**) as well as TRGV1/TRAV15N-1 and TRGV1/TRDV6 sequences (**Fig. 6E**, **Suppl.**
399 **Table 6**) consistent with γδNKT cells. We did note, however, that the TRAV15N-1 and TRDV6
400 sequences in the c10 cluster were, for the most part, non-canonical γδNKT cell clonotypes,
401 suggesting a degree of flexibility in the TRAV15N-1 and TRDV6 CDR3 sequences that can be
402 utilized by γδNKT cells.

403 Interestingly, while the γδT1 c2/c3/c7/c9 clusters contained primarily Vγ1 and Vγ4 T cells
404 as expected, we noted that Vγ4 γδT1 cells exhibited a striking preference in the usage of TRAV13-
405 4(DV7), and that TRGV4/TRDV7 pairings accounted for 80% of all Vγ4 clonotypes in the γδT1
406 clusters **(Fig. 6E, Suppl. Table 6**). Analysis of the γδT1 TRAV13-4/DV7 CDR3 sequences
407 revealed a high level of diversity that showed no evidence of clonal expansions (**Fig. 6F**). This
408 was in contrast to the highly restricted Vγ6 repertoire in the c4 γδT17 cluster, as well as the
409 restricted Vγ4 repertoire in the c2 γδT17 cluster that was dominated by semi-invariant TRDV5
410 and TRDV2-2 sequences (**Fig. 6F**). As no Vδ7-specific antibody was available, we independently
411 confirmed this observation using single-cell PCR to assess the lung Vγ4 CDR3δ sequences from
412 13 individual mice. These data demonstrated that, other than TRDV2-2 and TRDV5, TRDV7 is
413 the only other TCR delta chain used at an appreciable frequency by Vγ4 T cells in the B6 mouse
414 lung and that it exhibits significant diversity in its CDR3 (**Suppl. Fig. 9**). Vγ1 γδT1 cells, in
415 contrast, exhibited a more mild pairing preference where 44% of the γδT1 clonotypes utilized
416 TRAV15N-1, TRAV15-1/DV6-1, or TRAV15D-2/DV6D-2 and 13% utilized TRAV13-4/DV7
417 (**Suppl. Table 6**). Together these data formed a comprehensive map of B6 lung γδ T cell
418 transcriptomes and revealed that lung innate-like γδT1, like γδT17 and γδNKT, are all

419 characterized by preferential TCR γ- and δ-chain pairings. This was especially notable for Vγ4 and
420 our data suggested that Vγ4 γδT1 exhibited a distinct preference for the utilization of TRAV13-
421 4(DV7) chains with diverse CDR3.
422
423 *SAP regulates peripheral Vγ4/Vδ7 γδT1 cells and shapes the lung γδT17 repertoire.*
424 Next, we assessed the effect of SAP deficiency on the lung γδ TCR repertoire by comparing
425 B6 and B6.SAP$^{-/-}$ lung γδ T cells (**Fig. 7A**). Consistent with our previous observation that lung γδ
426 T cell IFN-γ production is deficient in SAP-deficient mice[24], we observed a decrease in the
427 frequency of the γδT1 c2, c3, and c7 clusters (**Fig. 7B**). Moreover, we observed a striking decrease
428 in the frequency of TRGV4/TRDV7-expressing cells in the lungs of B6.SAP$^{-/-}$ mice (**Figs. 7C-D,**
429 **Suppl. Table 6),** and we noted that we found no evidence of a compensatory increase in the
430 frequency of other TRDV-expressing lung Vγ4 γδT1 cells in the B6.SAP$^{-/-}$ lung. We independently
431 confirmed this SAP-dependent decrease in TRAV13-4/TRDV7 in both lung and spleen using
432 qPCR (**Suppl. Fig. 10**), and we demonstrated a significant decrease in the number of
433 CD44^{+}SLAMF7^{+} Vγ4 T cells in both the lungs and spleen of B6.SAP$^{-/-}$ mice (**Fig. 7E, Suppl. Fig.**
434 **10**). The decreased lung γδT1 did not appear to be due to a SAP-dependent decrease in homeostatic
435 proliferation, nor to increased apoptosis, since we observed no significant change in lung γδ T cell
436 BrdU incorporation or Annexin V staining in B6.SAP$^{-/-}$ mice (**Suppl. Fig. 10**).
437 In addition to the decrease in lung γδT1, we also noted a loss of the c10 γδT2 cluster
438 consistent with the enrichment in SAP-dependent γδNKT TCRs in this cluster, and we observed
439 an increased frequency of the Vγ4 γδT17 c1 cluster (**Fig. 7B**). Given our previous observation of
440 a SAP-dependent decrease in lung γδ T cell IL-17 production in young, but not adult mice[24], and
441 our findings here of SAP-dependent alterations in γδT17 clonotypes, we were interested in

442 determining whether the adult lung γδT17 repertoire was altered in SAP-deficient mice. Indeed, a
443 comparison of the lung Vγ4 c1 γδT17 CDR3 sequences between B6 and B6.SAP$^{-/-}$ mice revealed
444 significant alterations in the γδT17 c1 cluster TCR repertoire. Specifically, we noted a decreased
445 frequency of TRGV4 chains that exhibited a germline-encoded CDR3γ (CSYGYSS) and an
446 increased frequency of TRGV4 chains with a CDR3γ exhibiting evidence of N/P additions
447 (CSYG(X)YSS). These changes were associated with a significant shift in the usage of TRDV2-2
448 CDR3δ sequence usage (**Fig. 7F**) and an altered c1 TCR clonotype frequency in B6.SAP$^{-/-}$ mice
449 (**Fig. 7G**). Although the number of germline-encoded invariant TRGV4/TRDV5 clone (clonotype
450 1 in Fig. 6B) was diminished in B6.SAP$^{-/-}$ lung γδ T cells (**Fig. 7G, Suppl. Table 6**), the low
451 numbers of cells available for analysis precluded us from making strong conclusions regarding the
452 loss of any one particular clonotype. Taken together, these data suggest that Vγ4 γδT1
453 preferentially utilize the TRAV13-4(DV7) chain in the lung and that the SAP-dependent decrease
454 in peripheral γδ T cell IFN-γ production is not due to dysregulated cytokine production, but rather
455 due to a specific loss of innate-like γδT1 subsets. This finding, together with our finding that the
456 adult lung γδT17 TCR repertoire is altered in SAP-deficient mice suggests that SLAM/SAP
457 signaling plays a role in shaping the γδ TCR repertoire.

458 **Discussion**

459 A common denominator in most innate-like T cell developmental programming is a
460 dependence on the SLAM/SAP signaling pathway[17, 24, 25, 61]. Within the γδ T cell lineage, SAP
461 plays a critical role in the development of IFN-γ and IL-4-producing γδNKT cells[27], as well as in
462 γδT1 and γδT17[24], but exactly when during γδ T cell development SAP functions, and how it exerts
463 these effects is unknown. Here, we provide evidence that SAP mediates its effects on immature,
464 uncommitted thymic γδ T cells and that it works to simultaneously promote progression through
465 the γδT17 developmental pathway while inhibiting the diversion of γδ T cells into the αβ T cell
466 pathway. The redirection of γδ T cell clonotypes into the αβ T cell pathway at E17 is associated
467 with a decreased frequency of these mature clonotypes in neonatal thymus, and an altered γδT17
468 TCR repertoire in the periphery. Finally, we identify Vγ4/Vδ7 T cells as a novel, SAP-dependent
469 IFN-γ-producing Vγ4 γδT1 subset.

470 The developmental pathway(s) that gives rise to γδ T cell functional subsets remains unclear.
471 γδ T cells develop at the DN2/DN3 stage after receiving a sufficiently strong γδTCR-mediated
472 signal[62]. Numerous reports support a model where, within the continuum of signals that can drive
473 γδ T cell development, it is the relatively weaker TCR signals that promote γδT17 programming
474 while the stronger TCR signals foster γδNKT and γδT1 programming[4, 14, 17, 20, 63, 64]. Despite
475 considerable effort, the precise thymic developmental stages at which γδ T cell lineage
476 diversification occurs remains unclear. Recent studies examining this issue have demonstrated that
477 effector programming can occur at a $CD44^{neg}CD45RB^{neg}$ stage[4, 20], and that c-Maf-directed γδT17
478 programming occurs at a $CD45RB^{low}$ stage[42]. In addition, by altering TCR signal strength in a
479 transgenic model, Chen et al., defined a *Ccr9*-enriched cluster as a point of effector lineage
480 diversification[16]. Our findings here suggest that SAP influences γδT17 developmental

481 programming during the immature uncommitted CD24^{hi}CD73^{neg} stage, either during or soon after
482 *Il2ra (*CD25) downregulation. The SAP-dependent c2 cluster we define here was highly enriched
483 in numerous genes (e.g., *Sox13*[46], *Blk*[41], *Maf*[42], *Etv5*[45], *Sh2d1a*[24]) previously associated with γδT17
484 development as well as *Ccr9*, and the cell surface phenotype of c2 γδ T cells is
485 SLAMF1^{pos}SLAMF6^{pos}CD44$^{low/high}$CD45RB^{low}. Altogether, these data suggest that the SAP-
486 dependent c2 cluster is identical to these previously defined developmental checkpoints. Given
487 that these previous studies have demonstrated that this developmental checkpoint is influenced by
488 TCR signaling, it is interesting to note that SLAM/SAP signaling has previously been
489 demonstrated to foster semi-invariant NKT cell differentiation through its ability to regulate TCR
490 signal strength[65].

491 To that end, we noted that the SAP-dependent c2 cluster in E.17 γδ T cells was enriched in
492 *Blk, Lck,* and *Fyn*, Src tyrosine kinase family members that have all been implicated in γδ T cell
493 development[41, 60]. Decreased expression of *Blk*, which is known to promote γδT17 development[41],
494 in B6.SAP$^{-/-}$ γδ T cells suggests one possible mechanism through which SAP may regulate γδT17
495 development via TCR signaling. The mechanism, however, through which SAP regulates *Blk* gene
496 expression remains unclear. Since SAP is known to regulate conventional αβ T cell signaling
497 through its ability to recruit FYN[66, 67] and LCK[68, 69] to SLAM family members, it seems reasonable
498 to hypothesize that SAP could regulate TCR signaling by recruiting one or more of these Src kinase
499 family members to the γδ TCR signalosome.

500 Our finding that SAP inhibited the number of γδ T cells that enter the αβ T cell
501 developmental pathway is reminiscent of previous work using transgenic TCR models
502 demonstrating that a reduction of TCR signal strength results in a redirection of γδ T cells to the
503 αβ T cell lineage[59, 70]. Fahl et al. recently demonstrated that both entry into the γδ T cell lineage

504 as well as γδ T cell effector programming involved repression of TCF1 expression by TCR-driven
505 increases in *Id3*[48]. Consistent with these results, we found that *Tcf7* (encoding TCF1) transcript
506 levels were highest in the αβ T cell-like c6 cluster, and we note that *Tcf7* transcripts levels were
507 noticeably higher in the *Il2ra*-enriched post-selection c5 cluster in B6.SAP$^{-/-}$ γδ T cells. *Id3*
508 expression, however, did not appear to be appreciably altered in SAP-deficient mice. Whether
509 SAP-mediated signals could alter γδ T cell *Tcf7* expression through a TCR-independent
510 mechanism remains an open question.

511 In addition to the considerable evidence supporting a role for TCR signal strength in γδ T
512 cell developmental programming, there is increasing support for a model in which γδT17
513 programming occurs earlier in development, prior to expression of the γδ TCR. Indeed, evidence
514 that some DN1 thymocytes possess a SOX13^{hi} IL-17-like phenotype and that Vγ4 γδT17 arise
515 from DN1 precursors[18, 71] indicates the existence of such a TCR-independent developmental
516 programming stage. In consideration of such a model, it may be possible that SLAM/SAP-
517 mediated signals could differentially regulate the survival and/or fitness of the functionally pre-
518 programmed γδ T cell subsets. Such a function would be consistent with the role of SLAMF6 and
519 SAP in promoting reactivation-induced cell death in conventional αβ T cells[69, 72].

520 While our data indicate that SAP regulates the diversion of at least some TCR clonotypes
521 into the αβ TCR pathway, the fate of those cells is unclear. Certainly, the fact that the clonotypes
522 that were diverted to the αβ T cell pathway in E17 thymus are under-represented in the mature D9
523 thymus γδT17 clusters suggests that this diversion has significant consequences on the γδ T cell
524 receptor repertoire, but whether these diverted γδ T cells contribute to the αβ T cell compartment
525 is unclear. Recently, a population of hybrid αβ-γδ T cells was described in both mouse and

526 human[73] that responds to peptide/MHC stimulation like conventional αβ T cells, as well as to IL-
527 1 and IL-23 which induce both IFN-γ and IL-17 production[73]. In the mouse, at least some of these
528 cells are Vγ4/Vδ5, Vγ4/Vδ4, or Vγ4Vδ7 and are present in the embryonic thymus, raising the
529 possibility that γδ T cells diverted to the αβ T cell pathway in B6.SAP$^{-/-}$ mice contribute to this
530 αβ-γδ T cell population. While we have not observed a significant increase in the overall numbers
531 of αβ-γδ T cells in B6.SAP$^{-/-}$ thymus (not shown), a direct comparison of B6 and B6.SAP$^{-/-}$ αβ-
532 γδ TCRs may be necessary to see such an effect.

533 Our previous observations that SAP deletion did not completely abolish the development of
534 IL-17- and IFN-γ producing γδ T cells[24] suggested the possibility that SAP may be critical for the
535 development of additional γδ T cell clonotypes other than the Vγ1Vδ6.3 subset. Therefore, we
536 compared the SAP-dependent and SAP-independent γδTCR repertoires using paired TCR
537 clonotype analysis, which allowed us to track clonotype fate during development. Our findings not
538 only confirmed previous results demonstrating highly restricted γδT17[51, 52], and γδNKT[27] TCR
539 repertoires, they also revealed that the vast majority of Vγ4 γδT1 subsets in the periphery
540 preferentially utilize TRGV4/TRAV13-4(DV7) clonotypes, thereby further highlighting the strong
541 links between γδ T cell function and the utilization of specific TCRs[29]. The reason for this
542 preferential TRDV usage in Vγ4/Vδ7 γδT1 is unclear. While the TRAV13-4(DV7) CDR3
543 sequences were diverse and did not suggest evidence of clonal expansion, it may be possible that
544 TRDV-encoded sequence motifs could be required to interact with a ligand, similar to the way that
545 TRGV-encoded sequences mediate recognition of butyrophilins[74, 75].

546 Exactly when during development SAP exerts its effects on Vγ4/Vδ7 T cells is still
547 somewhat unclear. We found comparatively low numbers of TRGV4/TRDV7 γδ T cells in
548 embryonic, neonatal, or adult thymus, and those that were identified were generally found in the

549 immature clusters. The increased frequency in B6.SAP$^{-/-}$ E17 thymus of TRGV4/TRDV7 γδ T
550 cells in the *Il2ra*$^{+}$ c5 cluster coupled with their decreased frequency in the emigrating *S1pr1*$^{+}$ c4
551 cluster suggests a model where SAP promotes progression through the early stages of development
552 through thymic egress. SAP deficiency, therefore, could result in lower Vγ4/Vδ7 output. However,
553 this model is at odds with our finding that the frequency of *S1pr1*$^{+}$ clusters in neonatal thymus is
554 increased in B6.SAP$^{-/-}$, and that these clusters contained increased numbers of TRGV4/TRDV7 γδ
555 T cells. A possible explanation could be found in a previous report demonstrating that a Vγ4/Vδ7
556 subset increases in frequency in the periphery of B6 mice over time and undergoes extrathymic
557 expansion[76]. Our finding here that that the Vγ4/Vδ7 T cells represent a SAP-dependent innate-like
558 γδT1 subset raise the possibility that SAP regulates the homeostatic expansion of this subset after
559 it leaves the thymus. The mechanism, however, through which SAP is regulating the number of
560 Vγ4/Vδ7 T cells remains unclear, as we have so far observed no evidence of changes in
561 homeostatic proliferation or apoptosis of these cells in the lungs.

562 We previously demonstrated that the SAP-dependent impairment in γδT17 function in the
563 neonatal periphery largely corrects itself as mice mature[24]. This suggested the possibility that SAP-
564 dependent γδT17 clonotypes originating in the embryonic thymus were being replaced over time
565 by SAP-independent γδT17 clonotypes. Although our data certainly point to a SAP-dependent
566 decrease in a germline-encoded Vγ4/Vδ5 clonotype in neonatal thymus, the low numbers of this
567 clonotype in the lung makes it difficult to draw definitive conclusions in the periphery. Still, we
568 did observe a role for SAP in shaping the peripheral γδT17 repertoire, as we noted a decreased
569 frequency of germline-encoded TRGV4 sequences (so-called "GYSS"[77]) coupled with an
570 increased frequency of TRGV4 sequences with more diverse CDR3 ("GXYSS") in the periphery.
571 Although the potential significance of this change on γδ T cell function is unclear, it does support

572 a model in which SAP regulates γδT17 developmental programming during embryonic thymic
573 development, where the low expression of terminal deoxynucleotide transferase results in a high
574 frequency of germline-encoded V-J junctions.

575 In summary, our findings reveal the presence of multiple SAP-dependent developmental
576 checkpoint during the very early stages of γδ T cell development in the thymus, indicating a more
577 complex role for this signaling pathway in γδ T cell developmental programming than previously
578 appreciated. Indeed, our data indicate that SAP functions to regulate entry into the γδ and αβ T
579 cell developmental pathways, and we make the striking observation that nearly all Vγ4 γδT1 cells
580 in the periphery preferentially use Vδ7 chains and that it is a decrease in the Vγ4/Vδ7 subset that,
581 in part, underlies the SAP-dependent decrease in γδ T cell IFN-γ production. Altogether, these
582 findings suggest that SAP regulates the balance of innate-like γδT1/γδT2/γδT17 subsets during
583 thymic development and in the periphery.

584 **Methods**

585 *Mice*

586 C57BL/6J (B6) and B6.*Sh2d1a*$^{-/-}$ (SAP$^{-/-}$) mice were purchased from the Jackson
587 Laboratory (Bar Harbor, ME) and were housed and bred in a specific pathogen-free facility at the
588 animal facility of the University of Vermont. For experiments using E17 mice, timed-pregnant
589 matings were used. The presence of a vaginal plug indicated day 0 of pregnancy. The flow
590 cytometry experiments included 8-13 weeks old B6 and B6.SAP$^{-/-}$ mice (age and sex-matched).
591 All experimental procedures on animals were carried out with the approval of the University of
592 Vermont Institutional Animal Care and Use Committee.

593

594 *Tissue Processing*

595 Single-cell suspensions from the spleen and thymus were obtained by gently passing tissue
596 through nylon mesh. Red blood cells (RBCs) were lysed with Gey's solution. Single-cell
597 suspensions from the lungs were prepared as described (Benoit et al., 2015). Briefly, dissected
598 lungs were finely minced in a digestion buffer containing DMEM, 1 mg/ml collagenase type IV
599 (Gibco), and 0.2 mg/ml DNase (Sigma-Aldrich). After shaking at 200 rpm at 37˚C for 20 min, the
600 lung digests were triturated with a 16-gauge needle, followed by an additional 20 min shaking at
601 200 rpm at 37˚C. Following the final trituration, red blood cells (RBC) were lysed with Gey's
602 solution. Finally, the digested lung tissues were filtered through a 70-µm filter and washed in
603 PBS/2%FBS. Cells were counted either on a MACSQuant VYB or using a hemacytometer
604 following trypan blue staining.

605 *Flow Cytometry*

606 Cells were incubated with LIVE/DEAD™ Fixable Blue Dead Cell stain (Thermo Fisher
607 Scientific, Grand Island, NY) for 30 min at 4^0C in PBS, after which they were resuspended in Fc-
608 Block (BioLegend) containing PBS/2% FCS/0.1% sodium azide buffer. After a 5-10 min
609 incubation on ice, antibodies specific for cell surface markers were added, incubated for 30 min
610 on ice, and washed in PBS/2% FCS/0.1% sodium azide buffer. Brilliant Violet Staining buffer
611 (BD Biosciences) was used in experiments contain more than one Brilliant Violet, Brilliant UV,
612 or SuperBright-conjugated Ab. Cells were fixed in PBS/1% PFA buffer and stored at 4^0 C prior to
613 data collection.

614 For nuclear staining, cells were permeabilized with Foxp3 transcription factor
615 fixation/permeabilization buffer (ThermoFisher) following surface staining. Cells were incubated
616 overnight at 4˚C, washed, and incubated with 25 micrograms/ml total rat IgG before adding Abs
617 against transcription factors. After staining, cells were washed and resuspended in PBS/2%
618 FCS/0.1% sodium azide buffer. For intracellular cytokine staining, cells were permeabilized with
619 PBS/1% FCS/0.1% sodium azide/0.1% saponin following surface staining and fixation. To reduce
620 unspecific binding, 25 μg/ml total rat IgG was added prior to cytokine staining with fluorescent-
621 labeled antibodies.

622 Flow cytometry data were collected on a Cytek® Aurora (Cytek Biosciences) spectral
623 cytometer, and data analysis was performed using FlowJo Software (Tree Star). In some cases,
624 visualization of flow cytometry data was conducted by concatenation of individual .fcs files,
625 followed by dimensionality reduction and clustering using UMAP and FlowSOM[78] in FlowJo.
626 Antibodies used in these experiments are anti-CD4 (RM4-5), anti-CD11b (M1/70), anti-CD11c
627 (N418), anti-CD19 (1D3), anti-CD24 (M1/69), anti-CD25 (PC61), anti-CD27 (LG.3A10), anti-

628 CD44 (IM7), anti-CD45RB (C363-16A) , anti-CD73 (TY/11.8), anti-CD150 (TC15-12F12.2),
629 anti-CD196 (29-2L17), anti-CD319 (4G2), anti-cMAF (sym0F1), anti-IFNγ (XMG1.2), anti-
630 IL17a (TC11-18H10.1), anti-IL4 (11B11), anti-PLZF (9E12), anti-T-bet (4B10), anti-TCRβ (H57-
631 597), anti-Vγ5 (536), and anti-Vd6.3 (C504.17c) from BioLegend; and anti-RORγt (Q31-378),
632 anti-TCRδ (GL3), anti-Vγ1 (2.11) from BD biosciences; and anti-CD8a (53-6.7), anti-CD45 (30-
633 F11), anti-CD200 (OX90), anti-CD278 (7E17G9), anti-Ki-67 (SolA15), anti-Ly108(13G3-19D),
634 anti-Vγ4 (UC3-10A6) from eBiosciences; anti-S1P1 (713412) from R&D systems; anti-Blk
635 (polyclonal) from Cell Signaling Technology; and anti-17D1
636
637 *In vivo proliferation and apoptosis*
638 For *in vivo* proliferation analysis, each mouse was intraperitoneally injected with 1 mg of
639 5-bromo-deoxyuridine (BrdU) (Sigma-Aldrich) each day for 3 days. Lung cell suspensions were
640 prepared as above, stained with surface markers, after which they staining with anti-BrdU antibody
641 according to the manufacturer's instructions (BrdU Flow Kit; BD Biosciences). For apoptotic cell
642 detection, annexin V staining was performed. Briefly, surface staining was followed by dead cell
643 staining with Fixable Viability Dye eFluor™ 780 dye. The cells were washed and resuspended in
644 an annexin-binding buffer (10 mM HEPES, 140 mM NaCl, and 2.5 mM CaCl2, pH 7.4). Finally,
645 1 µl of Annexin V Conjugate (Thermo Fisher Scientific, Grand Island, NY) was added to each
646 tube, and cells were incubated for 15 minutes at room temperature (RT) prior to data collection.
647
648 *Bulk RNA Sequencing and data analysis*
649 For the bulk RNA sequencing, thymocytes from 10-day old B6 (n=4 male, n=2 female)
650 and B6.SAP$^{-/-}$ (n=5 male, n=1 female) mice were prepared by depleting CD4+ cells from

651 thymocytes using the EasySepTM Mouse CD4 Positive Selection Kit II (STEMCELL
652 Technologies). Cells were then incubated with Fixable Viability Dye eFluor™ 780 (Thermo Fisher
653 Scientific, Grand Island, NY) for 30 min at 4^0C in PBS, after which they were resuspended in Fc-
654 Block (BioLegend) containing PBS/2% FCS. After washing, cells were stained with antibodies
655 against CD11b (M1/70), CD19 (1D3), CD24 (M1/67), CD45 (30-F11), TCRβ (H57-597), and
656 TCRδ (GL3) for 30 min at 4^0C. Following surface staining, $CD24^{hi}$TCRδ+ cells were sorted from
657 a $CD11b^-CD19^-$TCRb- population of live $CD45^+$ lymphocytes. Immature ($CD24^{high}$) thymocytes
658 from both B6 and B6.$SAP^{-/-}$ mice were sorted directly into 350 microliters of RLT lysis buffer
659 (Qiagen). RNA was extracted using the RNeasy Micro kit (Qiagen) according to manufacturer
660 instructions. After RNA quantification and quality assessment, cDNA libraries were prepared
661 using SMARTer Stranded Total RNA-Seq Kit v3 - Pico Input Mammalian (Takara, Japan)
662 according to the manufacturer's protocol. Following library clean-up and quantification, the
663 libraries were sequenced (single-end 75 bp) on an Illumina HiSeq1500.

664 The Fastq files were checked for data quality using FastQC and MultiQC[79] bioinformatics
665 tools. Cutadapt[80] was used to filter out low-quality sequences and to remove adapter sequences
666 from all reads. The expression of transcripts was quantified using the mapping-based mode of
667 Salmon[81], which quasi-mapped RNA-seq reads to an index created from a mouse reference
668 transcriptome (GRCm39). The transcript abundance estimates were imported using tximport[82] and
669 differential gene expression (DE) analysis was performed using DEseq2[83] employing the Wald
670 test of the negative binomial model coefficients to determine statistical significance. The results
671 were analyzed based on Log_2 fold change ($Log_2FC \geq 0.5$ or ≤ -0.5) and adjusted P-value (padj
672 ≤ 0.0001) to determine whether a gene was differentially expressed.

673

674 *Cell sorting and library preparation for CITE-seq and V(D)J enrichment*

675 For thymus single-cell transcriptome analysis, we used embryonic day 17 (E17) B6 (n=4)
676 and B6.*Sh2d1a*$^{-/-}$ (SAP$^{-/-}$) (n=4) mice, nine day-old (D9) B6 (n=3) and B6.SAP$^{-/-}$ (n=3) mice, and
677 six-week-old B6 (n=3 male) and B6.SAP$^{-/-}$ (n=2 male, n=1 female) mice. For single-cell analysis
678 of adult lung γδ T cells, we used 13 week old B6 and B6.SAP$^{-/-}$ littermates (pooled cells from 2
679 males and one female mouse in each group).

680 Analysis of gene expression, surface protein expression, and TCR V(D)J repertoire was
681 performed using the 10X Genomics Chromium Next GEM Single Cell 5' V(D)J with feature
682 barcoding kit (version 1.1). To sort cells for scRNAseq, thymocytes were stained with anti-TCRδ-
683 PE (GL3) antibody and enriched using anti-PE MicroBeads kit (Miltenyi Biotec). The exception
684 was E17 thymus which did not undergo TCRδ enrichment. Following live/dead staining with
685 Fixable Viability Dye eFluor™ 780 (Thermo Fisher Scientific, Grand Island, NY) for 30 min at
686 4° C in PBS, cells were resuspended in Fc-Block (BioLegend) containing PBS/2% FCS. Cells were
687 then simultaneously stained with oligonucleotide-conjugated antibodies targeting CD24, CD44,
688 CD45RB, CD73, SLAMF1, SLAMF6, Vγ1, and Vγ4 (TotalSeqC-BioLegend), oligonucleotide-
689 conjugated hashtag antibodies (TotalSeqC-BioLegend), and fluorophore-conjugated antibodies for
690 cell sorting which included the anti-CD11b (M1/70), anti-CD11c (N418), anti-CD19 (1D3), anti-
691 CD45.2 (104) and anti-TCRβ (H57-597) antibodies. Following surface staining of the enriched
692 population, TCRδ^{+} cells were sorted from a CD11b^{-}CD11c^{-}CD19^{-}TCRβ^{-} population of CD45.2^{+}
693 live lymphocytes.

694 Libraries were prepared according to the manufacturer's instructions with modifications to
695 the V(D)J enrichment procedure. Equal numbers of live GL3^{+} γδ T cells from B6 and B6.SAP$^{-/-}$
696 mice were pooled and captured (between 5000 – 7000 cells) using a 10x Chromium controller.

697 Following cDNA preparation, the gene expression and CSP libraries were created according to the
698 manufacturer's instructions. To obtain TCR gamma and delta chain sequences, we replaced kit-
699 provided enrichment primers with custom mouse γ and δ chain-specific primers and modified the
700 number of PCR cycles used from manufacturer recommended cycling conditions. In the first
701 enrichment step, an equal amount of cDNA was used as a template for PCR amplification of γ and
702 δ chains separately using a total of 12 and 10 PCR cycles, respectively. The primers used for the
703 first γ-chain enrichment are: Forward Primer 5'-AATGAT ACGGCGA CCACCG AG
704 ATCTACACTCTT TCCCTACAC GACGCTC-3' (2 μM) and Reverse Outer Primers 5'-GGAA
705 AGAACTT TTCAAGGAS ACAAAG-3' (1 μM), 5'-CCCTTATG ACTTCAGG AAAGAA
706 CTTT-3' (0.5 μM) . The primers used for the first δ-chain enrichment are: Forward Primer 5'-
707 AATGAT ACGGCGACCACCG AGATCTACACTC TTTCCCTAC ACGACGCTC-3' (2 μM)
708 and Reverse Outer Primer 5'-CCACAATC TTCTTGGATG ATCTGAG-3' (0.5 μM). Following
709 PCR product purification, the γ-chain and δ-chain amplicons went through the second round of
710 enrichment separately using a total of 12 and 10 PCR cycles, respectively. The primers used for
711 the second γ-chain enrichment are: Forward Primer 5'-AATGA TACGGCGACCA
712 CCGAGATCT-3' (0.5 μM) and Reverse Inner Primers 5'-ACAAA GGTATGTCCCA
713 GTCTTATGGA-3' (0.5 μM), 5'-GGAGACA AAGGTAGGT CCCAGC-3' (0.5 μM). The
714 primers used for the second δ-chain enrichment are: Forward Primer 5'-AATGATA
715 CGGCGACCACC GAGATCT-3' (0.5 μM) and Reverse Inner Primer 5'-GTCACCTC
716 TTTAGGGTAG AAATCTT-3'. Following PCR product cleanup, the second round PCR products
717 (γ-chain and δ-chain amplicons) were quantified and combined in equal quantity making the final
718 TCR V(D)J library. Finally, all three libraries (gene expression, cell surface protein expression,

719 and TCR V(D)J) were sequenced (paired-end 26 x 91 bp) on an Illumina HiSeq 1500 sequencer
720 or a NextSeq 2000.
721
722 *CITE-seq quality control, filtering and demultiplexing*
723 Raw sequence reads from the gene expression and CSP libraries were processed using the
724 Cell Ranger software (v4.0.0)[84]. Reads were mapped to the GRCm38 (mm10) mouse reference
725 genome. To exclude the possibility of TCR transcripts playing a role in UMAP clustering, all TCR
726 genes were omitted from the analysis using the "cellranger reanalyze" argument of Cell Ranger
727 software.
728 Quality control, filtering, UMAP projection, and clustering analysis were conducted using
729 Seurat (v4.3.0.1)[85] R package. Briefly, cells with a low number (≤2000 for E17 thymus dataset,
730 ≤1200 for D9 thymus dataset and ≤750 for lung dataset) of unique genes (nFeature_RNA), a
731 frequency of mitochondrial reads > 4% and a frequency of ribosomal protein < than ~12% were
732 eliminated from further analysis. To reduce cell cycle-related and stress-related heterogeneity in
733 the normalized data, selected cell cycle genes and stress-induced genes [86] were regressed out
734 during the data normalization step. Note that in some instances, contaminating clusters expressing
735 macrophage specific marker genes were manually removed using Seurat "CellSelector ()"
736 argument. We used the Seurat function "HTODemux()" to demultiplex single cells back to their
737 sample of origin [87].
738
739 *CITE-Seq and V(D)J enrichment data analysis*
740 The demultiplexed datasets were further analyzed for gene expression, cell surface protein
741 expression following the multimodal analysis pipeline of Seurat[85]. For each dataset, we performed

742 normalization and variance stabilization of the gene expression data using the scTransform[88].
743 Following identification of top significant principal components (PCs) using the principal
744 component analysis (PCA), we performed a graph-based (UMAP) semi-supervised clustering of
745 cells with similar gene expression patterns using specific number of top PCs (E17 = 25, D9 = 30,
746 W6 = 27, lung = 28) and resolution values (E17 = 1.2, D9 = 1.6, W6 = 0.65, lung =1.2) for each
747 dataset. The cell surface protein expression data (Centered Log Ratio (CLR) normalized) from
748 CSP libraries as well as the gene expression data were then visualized on the clustered cells using
749 the R package scCustomize[89]. The differentially expressed features of each cluster (cluster
750 biomarkers) were identified using FindAllMarkers() function using the Wilcoxon Rank Sum test.
751 For identifying differentially expressed genes (DEGs) between B6 and B6.SAP$^{-/-}$ samples, we
752 performed a pseudobulk DE (differential expression) analysis of aggregated read counts using the
753 DEseq2 package, which accounts for biological replicates making it a better approach than other
754 specialized single-cell DE analysis methods[90]. Briefly, for cells of a given sample type, we
755 aggregated RNAseq reads across biological replicates identified by individual hashtags. Then
756 transformed the genes-by-cell matrix to a genes-by-replicates matrix and performed DE analysis
757 using the DESeq2[83] package employing the Wald test of the negative binomial model coefficients
758 to determine statistical significance. Finally, the trajectory and pseudotime inference analysis was
759 performed using the partition-based graph abstraction (PAGA)[91] analysis, which is a part of the
760 Scanpy[92] python package.

761 For the analysis of V(D)J library sequences, Cell Ranger v6.1.2 ("cellranger vdj"
762 argument) was used to map the TCR V(D)J) reads to a custom-made reference containing
763 sequences from the IMGT database[93]. The Cell Ranger V(D)J output was then processed with
764 custom bashscripts. Briefly, the TRGV and TRAV/TRDV contigs identified by Cell Ranger V(D)J

765 were demultiplexed to individual barcodes after which the dominant TRGV and TRAV/DV
766 transcripts were selected per cell. Finally, the V(D)J information of each cell was integrated with
767 scCITE-seq data and visualized using a combination of Seurat and custom-made R scripts. We
768 note that since about half of Vγ1, Vγ4, and Vγ7 T cells contain functionally rearranged TRGV2
769 chains, but only a small percentage express Vγ2 on the cell surface[94], the methods used here cannot
770 adequately assess the true TRGV2 repertoire. Therefore, we report it here for accuracy but have
771 omitted TRGV2 from our analysis.
772
773 *Quantitative PCR*
774 Lung qPCR samples were prepared by positively selecting leukocytes using CD45 MicroBeads
775 (Miltenyi Biotec). Spleen qPCR samples were prepared by depletion of CD19+ TCRβ+ cells using
776 biotinylated antibodies and Streptavidin MicroBeads (Miltenyi Biotec) according to the
777 manufacturer's instructions. Total RNA was extracted from approximately 5-10 million cells from
778 each organ using the RNeasy Mini Kit (QIAGEN). SuperScript® IV Reverse Transcriptase
779 (Thermo Fisher Scientific, Grand Island, NY) was used to generate cDNA using 400 ng of RNA
780 and oligodT primer according to the manufacturer's instructions. qPCR was performed using 1µl
781 of cDNA template in iTaq Universal SYBR Green Supermix (Bio-Rad) containing TCR delta
782 chain specific primer pairs. The qPCR reaction was run on a Bio-Rad CFX96 qPCR machine using
783 the following cycling conditions: 95^0C for 30 sec; 40 cycles of [95^0C for 5 sec; 60^0C for 30 sec;
784 72^0C for 30 sec]. The β2M and TRDC genes were used as endogenous housekeeping controls.
785 Primers used were as follows: mb2mforward, 5'- CATGGCTCG CTCGGTGACC-3',
786 mb2mreverse, 5'-AATGTGAGGC GGGTGGAACTG-3', TRDCforward, 5'- CTCCGGCCA
787 AACCATCTGTT-3', mouseDV2, 5'-CCAAGAAG CATACAAGCAGT ATAATG-3',

788 mouseDV5, 5'- CCCATGA TGCAGATTT TGTTCAAGG-3', mouseDV7, 5'- GGAAG
789 MCTCGTCAGC CTGTTGT-3', mouseDCrev, 5'- CCACAATCTT CTTGGAT GATCTGAG-3'.
790 Some primer sequences were adopted from Wei. et. al. (2015)[51].
791
792 *Vγ4 single cell sorting and TCR Sequencing*
793 The plate-based based γδ TCR repertoire analysis of single-cell sorted Vγ4 cells involved
794 adult lungs from 8-10 weeks old B6 male (n=7) and female mice (n=6). Lung Vγ4 TCR sequences
795 were obtained using a protocol modified from Wei *et al.*, (2015)[51]. Briefly, lung cell suspensions
796 were prepared as described above. After washing, cells were resuspended in Fc-Block
797 (BioLegend) containing PBS/2% FCS buffer, and stained with anti-CD11b (M1/70), anti-CD11c
798 (N418), anti-CD19 (1D3), anti-CD45 (30-F11), anti-TCRδ (GL3) and anti-Vγ4 (UC3-10A6) from
799 for 30 min at 4^0C in PBS. Fixable Viability Dye eFluor™ 780 (Thermo Fisher Scientific, Grand
800 Island, NY) was used to identify dead cells. Single-cell sorting of lung $V\gamma4^+TCR\delta^+$ from a $CD11b^-$
801 $CD11c^-CD19^-TCR\beta^-$ population of $CD45^+$ live lymphocytes were performed using a FACS Aria
802 III cell sorter (BD Bioscience). Cells were sorted directly into 12.5 µl (per well) of OneStep RT-
803 PCR Buffer mix (QIAGEN) in a 96-well PCR plate (one cell/well).
804 TCR sequences were then amplified and barcoded according to (Wei *et al.*, 2015). Briefly,
805 the first two nested PCR reactions involved primer-specific amplification of gamma and delta TCR
806 sequences. In both the first and second PCR reactions, the final concentration of each V-region
807 primer is 0.36µM, and each C-region primer is 0.6µM. The first RT-PCR step was performed using
808 the following cycling conditions: 50^0C for 30 min; 95^0C for 5 min; 25 cycles of [94^0C for 30 sec;
809 62^0C for 1min; 72^0C for1 min]; 72^0C for 7 min; 4^0C. Next, 1 µl of the first round PCR product was
810 used as a template for the second nested PCR reaction using HotStartTaq Master Mix Kit

811 (QIAGEN). The cycling conditions for the second PCR reaction were 95^0C for 5 min; 25 cycles
812 of [94^0C for 30 sec; 64^0C for 1min; 72^0C for1 min]; 72^0C for 7 min; 4^0C. In the third PCR reaction,
813 1 µl of second round PCR product as the template in a new 14 µl reaction using HotStartTaq Master
814 Mix Kit (QIAGEN). Each well was barcoded. The final concentration of 5' and 3' barcoding
815 primers was 0.05µM each and paired-end primers were 0.5µM each. The cycling conditions for
816 the third PCR reaction were 95^0C for 5 min; 36 cycles of [94^0C for 30 sec; 62^0C for 1min; 72^0C
817 for1 min]; 72^0C for 7 min; 4^0C. The γ and δ chain products were run on 1.2% agarose gel separately
818 and purified using the Qiagen QIAquick Gel Extraction Kit according to kit instructions. The final
819 products were then analyzed using the 2100 Bioanalyzer (Agilent Technologies). Finally, the γ
820 and δ TCR products were mixed in equal concentration and sequenced on the Illumina MiSeq
821 platform using the Illumina MiSeq Reagent Kit v2 (500-cycles).

822 The paired-end TCR sequencing reads were analyzed using a custom software pipeline
823 capable of de-multiplexing barcoded sequences to individual cells. The resulting de-multiplexed
824 reads were then analyzed by MiGMAP software, which identifies CDR3 sequences using the
825 IgBlast 1.4.0 (NCBI) V(D)J mapping tool[95, 96]. The single-cell TCR V(D)J profiling data were then
826 visualized using custom R scripts.

827

828 *Statistical analysis*

829 Prism (GraphPad Software, San Diego, CA) was used for the statistical analysis of data.
830 Unpaired Student t-tests, one-way ANOVA, or two-way ANOVA were used where appropriate.
831 Tests were considered significant when p-values were less than 0.05. Error bars represent standard
832 deviation (SD) unless otherwise indicated.

833 **Acknowledgements**

834 We thank Marlana Winschel, Cameron Moquin, and Erin Mathieu for help in tissue preparation
835 and flow cytometry. We acknowledge Roxana del Rio Guerra for help in cell sorting. All flow
836 cytometry data were collected at the Harry Hood Bassett Flow Cytometry and Cell Sorting Facility
837 (Larner College of Medicine, University of Vermont) and was supported by NIH grant
838 (S10OD026843). We thank Jessica Hoffman, Kris Finstaad, and the Vermont Integrated Genome
839 Resource (Larner College of Medicine, University of Vermont) for help in scRNAseq, Julie
840 Dragon and Korin Eckstrom for help in bioinformatics analysis. We thank Fred Kolling at the
841 Genomics Shared Resource (Dartmouth Geisel School of Medicine) for help in sequencing. We
842 also thank Willi Born and Rebecca O'Brien for the 17D1 hybridoma and Pablo Pereira for helpful
843 discussion. This work benefitted from data assembled by the ImmGen consortium, and was
844 supported by NIH grants R21AIO66465 and R03AI153902, S10OD026843 (JEB) and an AAI
845 Careers in Immunology Fellowship (SKM, JEB).

846 **Author contributions**

847 S.K.M. and J.E.B. conceived and designed the project; S.K.M., J.E.B., E.A., K.J.H., B.M.H., R.S.,
848 and O.D. performed experiments and analyzed data; K.J.H., D.G., J.T.R., and N.S. aided with the
849 single-cell TCR sequencing; D.M. assisted with bulk RNA sequencing; S.K.M. and J.E.B.
850 performed the bioinformatics analysis of bulk RNA-seq and single-cell CITEseq (with immune
851 profiling) data; J.E.B. supervised the project; S.K.M. and J.E.B. prepared the manuscript.

852

853 **Data Availability**

854 All sequencing data in this manuscript have been deposited in NCBI GEO and have been assigned
855 the accession number GSE262064. All scripts used in these analyses have been made publicly
856 available on Github and can be accessed here: https://github.com/Boyson-
857 Lab/scRNAseq_with_immune_profiling_tutorial

858

859 **Competing interests**

860 All authors declare no competing interests.

861

862 **Materials and Correspondence**

863 Correspondence and requests for materials should be addressed to J.E.B. (email:
864 jonathan.boyson@med.uvm.edu)

865 **References**

866 1. Grigoriadou K, Boucontet L, Pereira P. Most IL-4-producing gamma delta thymocytes of
867 adult mice originate from fetal precursors. *J Immunol* **171**, 2413-2420 (2003).
868
869 2. Haas JD*, et al.* Development of interleukin-17-producing gammadelta T cells is restricted
870 to a functional embryonic wave. *Immunity* **37**, 48-59 (2012).
871
872 3. Ribot JC*, et al.* CD27 is a thymic determinant of the balance between interferon-gamma-
873 and interleukin 17-producing gammadelta T cell subsets. *Nat Immunol* **10**, 427-436
874 (2009).
875
876 4. Sumaria N, Grandjean CL, Silva-Santos B, Pennington DJ. Strong TCRgammadelta
877 Signaling Prohibits Thymic Development of IL-17A-Secreting gammadelta T Cells. *Cell*
878 *Rep* **19**, 2469-2476 (2017).
879
880 5. Chien YH, Zeng X, Prinz I. The natural and the inducible: interleukin (IL)-17-producing
881 gammadelta T cells. *Trends Immunol* **34**, 151-154 (2013).
882
883 6. He W*, et al.* Naturally activated V gamma 4 gamma delta T cells play a protective role in
884 tumor immunity through expression of eomesodermin. *J Immunol* **185**, 126-133 (2010).
885
886 7. Gao Y*, et al.* Gamma delta T cells provide an early source of interferon gamma in tumor
887 immunity. *J Exp Med* **198**, 433-442 (2003).
888
889 8. Girardi M*, et al.* Regulation of cutaneous malignancy by gammadelta T cells. *Science*
890 **294**, 605-609 (2001).
891
892 9. Coffelt SB*, et al.* IL-17-producing gammadelta T cells and neutrophils conspire to
893 promote breast cancer metastasis. *Nature* **522**, 345-348 (2015).
894
895 10. Wu P*, et al.* gammadeltaT17 cells promote the accumulation and expansion of myeloid-
896 derived suppressor cells in human colorectal cancer. *Immunity* **40**, 785-800 (2014).
897
898 11. Rei M*, et al.* Murine CD27(-) Vgamma6(+) gammadelta T cells producing IL-17A
899 promote ovarian cancer growth via mobilization of protumor small peritoneal
900 macrophages. *Proc Natl Acad Sci U S A* **111**, E3562-3570 (2014).
901
902 12. Wakita D*, et al.* Tumor-infiltrating IL-17-producing gammadelta T cells support the
903 progression of tumor by promoting angiogenesis. *Eur J Immunol* **40**, 1927-1937 (2010).
904
905 13. Turchinovich G, Hayday AC. Skint-1 identifies a common molecular mechanism for the
906 development of interferon-gamma-secreting versus interleukin-17-secreting gammadelta
907 T cells. *Immunity* **35**, 59-68 (2011).
908

14. Jensen KD*, et al.* Thymic selection determines gammadelta T cell effector fate: antigen-naive cells make interleukin-17 and antigen-experienced cells make interferon gamma. *Immunity* **29**, 90-100 (2008).

15. Munoz-Ruiz M*, et al.* TCR signal strength controls thymic differentiation of discrete proinflammatory gammadelta T cell subsets. *Nat Immunol*, (2016).

16. Chen ELY, Lee CR, Thompson PK, Wiest DL, Anderson MK, Zuniga-Pflucker JC. Ontogenic timing, T cell receptor signal strength, and Notch signaling direct gammadelta T cell functional differentiation in vivo. *Cell Rep* **35**, 109227 (2021).

17. Kreslavsky T*, et al.* TCR-inducible PLZF transcription factor required for innate phenotype of a subset of gammadelta T cells with restricted TCR diversity. *Proc Natl Acad Sci U S A* **106**, 12453-12458 (2009).

18. Spidale NA*, et al.* Interleukin-17 Producing gammadelta T Cells Originate from SOX13(+) Progenitors that Are Independent of gammadeltaTCR Signaling. *Immunity*, (2018).

19. Laird SM, Tuckerman EM, Cork BA, Linjawi S, Blakemore AI, Li TC. A review of immune cells and molecules in women with recurrent miscarriage. *Hum Reprod Update* **9**, 163-174 (2003).

20. Sumaria N, Martin S, Pennington Daniel J. Constrained TCRγδ-associated Syk activity engages PI3K to facilitate thymic development of IL-17A–secreting γδ T cells. *Science Signaling* **14**, eabc5884 (2021).

21. Muro R, Nitta T, Nakano K, Okamura T, Takayanagi H, Suzuki H. gammadeltaTCR recruits the Syk/PI3K axis to drive proinflammatory differentiation program. *J Clin Invest* **128**, 415-426 (2018).

22. Cannons JL, Tangye SG, Schwartzberg PL. SLAM family receptors and SAP adaptors in immunity. *Annu Rev Immunol* **29**, 665-705 (2011).

23. Nichols KE*, et al.* Regulation of NKT cell development by SAP, the protein defective in XLP. *Nat Med* **11**, 340-345 (2005).

24. Dienz O*, et al.* Critical Role for SLAM/SAP Signaling in the Thymic Developmental Programming of IL-17- and IFN-gamma-Producing gammadelta T Cells. *J Immunol*, (2020).

25. Legoux F, Gilet J, Procopio E, Echasserieau K, Bernardeau K, Lantz O. Molecular mechanisms of lineage decisions in metabolite-specific T cells. *Nat Immunol* **20**, 1244-1255 (2019).

954 26. Koay HF, *et al.* A divergent transcriptional landscape underpins the development and
955 functional branching of MAIT cells. *Sci Immunol* **4**, (2019).
956
957 27. Azuara V, Levraud JP, Lembezat MP, Pereira P. A novel subset of adult gamma delta
958 thymocytes that secretes a distinct pattern of cytokines and expresses a very restricted T
959 cell receptor repertoire. *Eur J Immunol* **27**, 544-553 (1997).
960
961 28. Havran WL, Allison JP. Developmentally ordered appearance of thymocytes expressing
962 different T-cell antigen receptors. *Nature* **335**, 443-445 (1988).
963
964 29. O'Brien RL, Born WK. gammadelta T cell subsets: a link between TCR and function?
965 *Semin Immunol* **22**, 193-198 (2010).
966
967 30. Stoeckius M, *et al.* Simultaneous epitope and transcriptome measurement in single cells.
968 *Nature methods* **14**, 865-868 (2017).
969
970 31. Coffey F, *et al.* The TCR ligand-inducible expression of CD73 marks gammadelta
971 lineage commitment and a metastable intermediate in effector specification. *J Exp Med*
972 **211**, 329-343 (2014).
973
974 32. In TSH, *et al.* HEB is required for the specification of fetal IL-17-producing gammadelta
975 T cells. *Nat Commun* **8**, 2004 (2017).
976
977 33. Satija R, Farrell JA, Gennert D, Schier AF, Regev A. Spatial reconstruction of single-cell
978 gene expression data. *Nat Biotechnol* **33**, 495-502 (2015).
979
980 34. Havran WL, Chien YH, Allison JP. Recognition of self antigens by skin-derived T cells
981 with invariant gamma delta antigen receptors. *Science* **252**, 1430-1432 (1991).
982
983 35. Itohara S, *et al.* Homing of a gamma delta thymocyte subset with homogeneous T-cell
984 receptors to mucosal epithelia. *Nature* **343**, 754-757 (1990).
985
986 36. Wencker M, *et al.* Innate-like T cells straddle innate and adaptive immunity by altering
987 antigen-receptor responsiveness. *Nat Immunol* **15**, 80-87 (2014).
988
989 37. Buus TB, Odum N, Geisler C, Lauritsen JPH. Three distinct developmental pathways for
990 adaptive and two IFN-gamma-producing gammadelta T subsets in adult thymus. *Nat*
991 *Commun* **8**, 1911 (2017).
992
993 38. Xu H, *et al.* MS4a4B, a CD20 homologue in T cells, inhibits T cell propagation by
994 modulation of cell cycle. *PloS one* **5**, e13780 (2010).
995
996 39. Howie D, *et al.* MS4A4B is a GITR-associated membrane adapter, expressed by
997 regulatory T cells, which modulates T cell activation. *J Immunol* **183**, 4197-4204 (2009).
998

40. Sagar, *et al.* Deciphering the regulatory landscape of fetal and adult gammadelta T-cell development at single-cell resolution. *EMBO J* **39**, e104159 (2020).

41. Laird RM, Laky K, Hayes SM. Unexpected role for the B cell-specific Src family kinase B lymphoid kinase in the development of IL-17-producing gammadelta T cells. *J Immunol* **185**, 6518-6527 (2010).

42. Zuberbuehler MK, *et al.* The transcription factor c-Maf is essential for the commitment of IL-17-producing gammadelta T cells. *Nat Immunol* **20**, 73-85 (2019).

43. Narayan K, *et al.* Intrathymic programming of effector fates in three molecularly distinct gammadelta T cell subtypes. *Nat Immunol* **13**, 511-518 (2012).

44. Lu Y, Cao X, Zhang X, Kovalovsky D. PLZF Controls the Development of Fetal-Derived IL-17+Vgamma6+ gammadelta T Cells. *J Immunol* **195**, 4273-4281 (2015).

45. Jojic V, *et al.* Identification of transcriptional regulators in the mouse immune system. *Nat Immunol* **14**, 633-643 (2013).

46. Malhotra N, *et al.* A network of high-mobility group box transcription factors programs innate interleukin-17 production. *Immunity* **38**, 681-693 (2013).

47. He Q, *et al.* TOX deficiency facilitates the differentiation of IL-17A-producing gammadelta T cells to drive autoimmune hepatitis. *Cellular & molecular immunology* **19**, 1102-1116 (2022).

48. Fahl SP, *et al.* The E protein-TCF1 axis controls gammadelta T cell development and effector fate. *Cell Rep* **34**, 108716 (2021).

49. DiToro D, *et al.* Insulin-Like Growth Factors Are Key Regulators of T Helper 17 Regulatory T Cell Balance in Autoimmunity. *Immunity* **52**, 650-667 e610 (2020).

50. Roberts NA, *et al.* Rank signaling links the development of invariant gammadelta T cell progenitors and Aire(+) medullary epithelium. *Immunity* **36**, 427-437 (2012).

51. Wei YL, *et al.* A Highly Focused Antigen Receptor Repertoire Characterizes gammadelta T Cells That are Poised to Make IL-17 Rapidly in Naive Animals. *Frontiers in immunology* **6**, 118 (2015).

52. Kashani E, *et al.* A clonotypic Vgamma4Jgamma1/Vdelta5Ddelta2Jdelta1 innate gammadelta T-cell population restricted to the CCR6(+)CD27(-) subset. *Nat Commun* **6**, 6477 (2015).

53. Sim GK, Augustin A. Dominantly inherited expression of BID, an invariant undiversified T cell receptor delta chain. *Cell* **61**, 397-405 (1990).

1045 54. Scaramuzzino S, *et al.* Single-cell transcriptomics uncovers an instructive T-cell receptor
1046 role in adult gammadelta T-cell lineage commitment. *EMBO J* **41**, e110023 (2022).
1047
1048 55. Prinz I, Sansoni A, Kissenpfennig A, Ardouin L, Malissen M, Malissen B. Visualization
1049 of the earliest steps of gammadelta T cell development in the adult thymus. *Nat Immunol*
1050 **7**, 995-1003 (2006).
1051
1052 56. Mingueneau M, *et al.* The transcriptional landscape of alphabeta T cell differentiation.
1053 *Nat Immunol* **14**, 619-632 (2013).
1054
1055 57. Passoni L, *et al.* Intrathymic delta selection events in gammadelta cell development.
1056 *Immunity* **7**, 83-95 (1997).
1057
1058 58. Kang J, Coles M, Cado D, Raulet DH. The developmental fate of T cells is critically
1059 influenced by TCRgammadelta expression. *Immunity* **8**, 427-438 (1998).
1060
1061 59. Haks MC, *et al.* Attenuation of gammadeltaTCR signaling efficiently diverts thymocytes
1062 to the alphabeta lineage. *Immunity* **22**, 595-606 (2005).
1063
1064 60. Laird RM, Hayes SM. Roles of the Src tyrosine kinases Lck and Fyn in regulating
1065 gammadeltaTCR signal strength. *PloS one* **5**, e8899 (2010).
1066
1067 61. Griewank K, *et al.* Homotypic interactions mediated by Slamf1 and Slamf6 receptors
1068 control NKT cell lineage development. *Immunity* **27**, 751-762 (2007).
1069
1070 62. Kreslavsky T, Garbe AI, Krueger A, von Boehmer H. T cell receptor-instructed alphabeta
1071 versus gammadelta lineage commitment revealed by single-cell analysis. *J Exp Med* **205**,
1072 1173-1186 (2008).
1073
1074 63. Fahl SP, *et al.* Role of a selecting ligand in shaping the murine gammadelta-TCR
1075 repertoire. *Proc Natl Acad Sci U S A* **115**, 1889-1894 (2018).
1076
1077 64. Verykokakis M, Boos MD, Bendelac A, Adams EJ, Pereira P, Kee BL. Inhibitor of DNA
1078 binding 3 limits development of murine slam-associated adaptor protein-dependent
1079 "innate" gammadelta T cells. *PloS one* **5**, e9303 (2010).
1080
1081 65. Lu Y, *et al.* SLAM receptors foster iNKT cell development by reducing TCR signal
1082 strength after positive selection. *Nat Immunol*, (2019).
1083
1084 66. Davidson D, *et al.* Genetic evidence linking SAP, the X-linked lymphoproliferative gene
1085 product, to Src-related kinase FynT in T(H)2 cytokine regulation. *Immunity* **21**, 707-717
1086 (2004).
1087
1088 67. Chan B, *et al.* SAP couples Fyn to SLAM immune receptors. *Nature cell biology* **5**, 155-
1089 160 (2003).
1090

1091 68. Simarro M*, et al.* SAP increases FynT kinase activity and is required for phosphorylation
1092 of SLAM and Ly9. *Int Immunol* **16**, 727-736 (2004).
1093
1094 69. Katz G, Krummey SM, Larsen SE, Stinson JR, Snow AL. SAP facilitates recruitment and
1095 activation of LCK at NTB-A receptors during restimulation-induced cell death. *J*
1096 *Immunol* **192**, 4202-4209 (2014).
1097
1098 70. Hayes SM, Li L, Love PE. TCR signal strength influences alphabeta/gammadelta lineage
1099 fate. *Immunity* **22**, 583-593 (2005).
1100
1101 71. Oh S*, et al.* Distinct subpopulations of DN1 thymocytes exhibit preferential gammadelta
1102 T lineage potential. *Frontiers in immunology* **14**, 1106652 (2023).
1103
1104 72. Snow AL*, et al.* Restimulation-induced apoptosis of T cells is impaired in patients with
1105 X-linked lymphoproliferative disease caused by SAP deficiency. *J Clin Invest* **119**, 2976-
1106 2989 (2009).
1107
1108 73. Edwards SC*, et al.* A population of proinflammatory T cells coexpresses alphabeta and
1109 gammadelta T cell receptors in mice and humans. *J Exp Med* **217**, (2020).
1110
1111 74. Rigau M*, et al.* Butyrophilin 2A1 is essential for phosphoantigen reactivity by
1112 gammadelta T cells. *Science* **367**, (2020).
1113
1114 75. Melandri D*, et al.* The gammadeltaTCR combines innate immunity with adaptive
1115 immunity by utilizing spatially distinct regions for agonist selection and antigen
1116 responsiveness. *Nat Immunol* **19**, 1352-1365 (2018).
1117
1118 76. Sperling AI, Decker DC, DiPaolo RJ, Stern DA, Shum A, Bluestone JA. Selective
1119 expansion of Vgamma2-Vdelta7 TCR gammadelta cells in C57BL/6 mice is postnatal
1120 and extrathymic. *J Immunol* **159**, 86-91 (1997).
1121
1122 77. Sim GK, Augustin A. Extrathymic positive selection of gamma delta T cells. V gamma
1123 4J gamma 1 rearrangements with "GxYS" junctions. *J Immunol* **146**, 2439-2445 (1991).
1124
1125 78. Van Gassen S*, et al.* FlowSOM: Using self-organizing maps for visualization and
1126 interpretation of cytometry data. *Cytometry Part A : the journal of the International*
1127 *Society for Analytical Cytology* **87**, 636-645 (2015).
1128
1129 79. Ewels P, Magnusson M, Lundin S, Käller M. MultiQC: summarize analysis results for
1130 multiple tools and samples in a single report. *Bioinformatics (Oxford, England)* **32**,
1131 (2016).
1132
1133 80. Martin M. Cutadapt removes adapter sequences from high-throughput sequencing reads.
1134 *2011* **17**, 3 (2011).
1135

1136 81. Patro R, Duggal G, Love MI, Irizarry RA, Kingsford C. Salmon provides fast and bias-
1137 aware quantification of transcript expression. *Nature methods* **14**, 417-419 (2017).
1138
1139 82. Soneson C, Love MI, Robinson MD. Differential analyses for RNA-seq: transcript-level
1140 estimates improve gene-level inferences. *F1000Research* **4**, (2015).
1141
1142 83. Love MI, Huber W, Anders S. Moderated estimation of fold change and dispersion for
1143 RNA-seq data with DESeq2. *Genome biology* **15**, 550 (2014).
1144
1145 84. Zheng GXY*, et al.* Massively parallel digital transcriptional profiling of single cells.
1146 *Nature Communications* **8**, 1-12 (2017).
1147
1148 85. Hao Y*, et al.* Integrated analysis of multimodal single-cell data. *Cell* **184**, 3573-3587
1149 e3529 (2021).
1150
1151 86. Denisenko E*, et al.* Systematic assessment of tissue dissociation and storage biases in
1152 single-cell and single-nucleus RNA-seq workflows. *Genome biology* **21**, 130 (2020).
1153
1154 87. Stoeckius M*, et al.* Cell Hashing with barcoded antibodies enables multiplexing and
1155 doublet detection for single cell genomics. *Genome biology* **19**, 224 (2018).
1156
1157 88. Hafemeister C, Satija R. Normalization and variance stabilization of single-cell RNA-seq
1158 data using regularized negative binomial regression. *Genome biology* **20**, 296 (2019).
1159
1160 89. Marsh SE. scCustomize: Custom Visualizations & Functions for Streamlined Analyses of
1161 Single Cell Sequencing.) (2021).
1162
1163 90. Squair JW*, et al.* Confronting false discoveries in single-cell differential expression. *Nat*
1164 *Commun* **12**, 5692 (2021).
1165
1166 91. Wolf FA*, et al.* PAGA: graph abstraction reconciles clustering with trajectory inference
1167 through a topology preserving map of single cells. *Genome biology* **20**, 59 (2019).
1168
1169 92. Wolf FA, Angerer P, Theis FJ. SCANPY: large-scale single-cell gene expression data
1170 analysis. *Genome biology* **19**, 15 (2018).
1171
1172 93. Lefranc MP. IMGT, the International ImMunoGeneTics Information System. *Cold*
1173 *Spring Harb Protoc* **2011**, 595-603 (2011).
1174
1175 94. Pereira P, Boucontet L. Rates of recombination and chain pair biases greatly influence
1176 the primary gammadelta TCR repertoire in the thymus of adult mice. *J Immunol* **173**,
1177 3261-3270 (2004).
1178
1179 95. M S*, et al.* VDJtools: Unifying Post-analysis of T Cell Receptor Repertoires. *PLoS*
1180 *computational biology* **11**, (2015).
1181

1182 96. J Y, N M, TL M, JM O. IgBLAST: an immunoglobulin variable domain sequence
1183 analysis tool. *Nucleic Acids Res* **41**, (2013).
1184
1185

1186 **Figure Legends**

1187 **Figure 1. SLAM family receptor expression marks transcriptionally distinct developmental**
1188 **stages among E17 γδ T cells. (A)** Schematic workflow depicting the methodology for single-cell
1189 RNA sequencing (scRNAseq) library preparation and subsequent data analysis pipeline employed
1190 in this study. **(B)** Uniform Manifold Approximation and Projection (UMAP) visualization
1191 displaying 11 distinct clusters of E17 B6 thymic γδ T cells, n = 4 individual mice. Clusters are
1192 annotated based on comprehensive protein and gene expression data. **(C)** Feature plots illustrating
1193 the cell surface protein expression profiles of CD24, CD73, CD44, CD45RB, SLAMF1, and
1194 SLAMF6 on B6 E17 thymic γδ T cells. Each data point represents a cell, color-coded to indicate
1195 varying protein expression levels (high: dark blue, low: yellow). **(D)** Feature plot illustrating the
1196 gene expression profiles of signature genes among individual B6 E17 thymic γδ T cells. Each data
1197 point represents a cell, color-coded based on gene expression levels (high: purple, low: yellow).
1198 **(E)** Dot plot demonstrating the scaled expression levels of selected genes in E17 B6 thymic γδ T
1199 cells. Normalized expression levels are depicted using a color scale ranging from low (yellow) to
1200 high (purple). Dot size corresponds to the fraction of cells within each cluster expressing the
1201 specific marker. **(F)** UMAP representation of E17 B6 thymic γδ T cells indicating the expression
1202 of selected TRGV (TCRγ; left) and TRDV (TCRδ; right) chain V-segment usage (in blue) across
1203 individual cells. **(G)** Violin plots illustrating the expression patterns of selected genes among E17
1204 B6 thymic γδ T cell clusters. **(H)** Visualization of single-cell trajectories using PAGA (partition-
1205 based graph abstraction) with single-cell embedding (left) showing connectivity between
1206 individual nodes (middle). Weighted edges represent statistical measures of interconnectivity. The
1207 diffusion pseudotime plot (right) delineates inferred pseudotime progression of cells along

1208 developmental trajectories using cluster 5 (C5) as the root, highlighting their developmental order
1209 (from purple to yellow).
1210
1211 **Figure. 2. Identification of SAP-dependent developmental checkpoints during E17 γδ T cell**
1212 **developmental programming. (A)** UMAP representation of B6 (left) and B6.SAP$^{-/-}$ (right) γδ T
1213 cells from E17 thymi (n = 4 mice per group) is shown at *left.* Clusters were annotated based on
1214 protein and gene expression data. The frequencies of B6 and B6.SAP$^{-/-}$ E17 γδ T cell clusters is
1215 shown at right. Bars represent the mean cluster frequency, error bars represent standard deviation,
1216 **$p \leq 0.01$, two-way ANOVA, Sidak multiple-comparisons test; n=4 mice/genotype. **(B)** Volcano
1217 plot of differentially expressed genes among immature CD24^{high}CD73^{neg} (clusters: C1, C2, C5, C6,
1218 C7, and C10) B6 and B6.SAP$^{-/-}$ γδ T cells using pseudobulk scRNAseq analysis. Genes exhibiting
1219 a $\log_2FC \geq 0.5$ or ≤ -0.5, and a $p_{adj} \leq 0.005$ in are shown in red. Only some selected genes are
1220 labelled for the sake of clarity. **(C)** Feature plots illustrating gene expression profiles of selected
1221 C2 and C6 cluster-specific genes among individual B6 and B6.SAP$^{-/-}$ E17 thymic γδ T cells. Each
1222 point represents a cell, color-coded by gene expression level (high: purple, low: yellow). **(D)** TCR
1223 clonotype bubble plot displaying the top 100 B6 and B6.SAP$^{-/-}$ TRGV4 clonotypes in E17 thymus.
1224 Bubbles represent unique TRGV4/TRDV clonotypes; size indicates frequency of clonotype among
1225 all Vγ4 T cells (n = 388 B6, 288 B6.SAP$^{-/-}$ cells), and colors denote specific TRDV chains utilized.
1226 Selected clonotypes are numbered and their respective CDR3γ and CDR3δ sequences displayed
1227 below. Data are **(E)** Altered TRGV/TRDV clonotype distribution between B6 and B6.SAP$^{-/-}$ E17
1228 thymic γδ T cells. Frequencies of selected clonotypes among different clusters of B6 and B6.SAP^{-}
1229 $^{/-}$ E17 γδ T cells is shown. Bars represent the mean clonotype frequency among the indicated

1230 TRGV/TRDV pairings shown, error bars represent standard deviation, *p ≤ 0.05, ***p ≤ 0.001,
1231 two-way ANOVA, Sidak multiple-comparisons test; n = 4 mice/genotype-age groups.
1232
1233 **Figure 3. Increased frequency and numbers of immature $CD4^+CD8^+$c-$MAF^-$$ROR\gamma t^+$ thymic**
1234 **γδ T cells in B6.$SAP^{-/-}$ E17 γδ T cells. (A)** Representative contour plots depicting $CD24^{pos}$ E17
1235 γδ T cells in B6 (top) and B6.$SAP^{-/-}$ (bottom) mice. Concatenated data from 2 B6 and 3 B6.$SAP^{-/-}$
1236 embryos are shown, and are representative of 2 independent experiments. Numbers in the plots
1237 represent the frequency as a percentage of $CD24^{pos}$ γδ T cells. **(B)** Cumulative frequency and
1238 number of immature $CD24^{pos}$ BLK- (left), c-MAF- (right), RORγt-expressing E17 thymic γδ T
1239 cells. The mean and standard deviation are indicated. Data are the cumulative data from 2
1240 independent experiments, n = 10 B6, 11 B6.$SAP^{-/-}$ pooled embryonic thymi, *p ≤ 0.05, **p ≤ 0.01,
1241 ***p ≤ 0.001, ****p ≤ 0.0001, two-way ANOVA, Sidak's multiple comparisons test. **(C)** Relative
1242 geometric mean of BLK, c-MAF, and RORγt expression in B6 and B6.$SAP^{-/-}$ E17 $CD24^+CD73^-$
1243 Vγ4 γδ T cells, *p ≤ 0.001, ****p ≤ 0.0001, two-way ANOVA, Sidak's multiple comparisons test.
1244 Data are representative of 2 independent experiments, 7-9 mice per group. **(D)** Cumulative
1245 frequency (left) and number (right) of immature CD4- and CD8- $MAF^{neg}ROR\gamma t^{pos}$ E17 thymic γδ
1246 T cells in B6 and B6.$SAP^{-/-}$ thymus. The mean and standard deviation are indicated. Data are the
1247 cumulative data from 2 independent experiments, n = 10 B6, 11 B6.$SAP^{-/-}$ pooled embryonic
1248 thymi, **p ≤ 0.01, ***p ≤ 0.001, ****p ≤ 0.0001, two-way ANOVA, Sidak's multiple
1249 comparisons test.
1250
1251 **Figure 4. Identification of SAP-dependent developmental checkpoints during neonatal γδ T**
1252 **cell developmental programming. (A)** UMAP representation of B6 (left) and B6.$SAP^{-/-}$ (right)

1253 γδ T cells from D9 neonatal thymi (n = 3 mice per strain). Cluster annotation is based on
1254 comprehensive protein and gene expression data. **(B)** Feature plots displaying cell surface protein
1255 expression patterns of CD24, CD73, SLAMF1, and SLAMF6 on D9 B6 thymus γδ T cells. Data
1256 are color-coded based on protein expression level (high: dark blue, low: yellow). **(C)** UMAP
1257 representation of D9 B6 thymic γδ T cells exhibiting selected TRGV4 (left) and TRDV (right)
1258 chain V-segment usage (in blue) in individual cells. **(D)** Frequencies of B6 and B6.SAP$^{-/-}$ D9
1259 thymic γδ T cell clusters. Bars represent the mean cluster frequency, error bars represent standard
1260 deviation, *p ≤ 0.05, **p ≤ 0.01, two-way ANOVA, Sidak multiple-comparisons test, 3
1261 mice/strain. **(E)** Representative contour plots depicting BLK and RORγt expression in B6 and
1262 B6.SAP$^{-/-}$ CD24^{pos}CD73^{neg} D9 Vγ4 T cells are shown *above*. Cumulative frequencies of BLK and
1263 RORγt expression are shown *below*. The mean and standard deviation are indicated. Data are the
1264 cumulative data from 3 independent experiments, n = 13 B6, 16 B6.SAP$^{-/-}$ mice, ****p ≤ 0.0001,
1265 two-way ANOVA, Sidak's multiple comparisons test. **(F)** Decreased BLK expression in immature
1266 B6.SAP$^{-/-}$ γδ T cells. Data represent the mean expression of the indicated proteins in D6 neonate
1267 BLK^{pos}, RORγt^{pos}, or c-Maf^{pos} thymic γδ T cells, **p ≤ 0.01.

1268

1269 **Figure 5. SAP shapes the neonatal γδ TCR repertoire. (A)** TCR clonotype bubble plots
1270 depicting the top 100 B6 and B6.SAP$^{-/-}$ TCR clonotypes among D9 thymic γδ T cells. Each bubble
1271 represents a unique clonotype, is sized according to its frequency as a percentage of all γδ T cells
1272 n = 1429 B6, 1354 B6.SAP$^{-/-}$ cells), and is colored based on specific TRGV chains utilized. **(B)**
1273 TCR clonotype bubble plots depicting the top 100 B6 and B6.SAP$^{-/-}$ TRGV1 (*above*) and TRGV4
1274 (*below*) clonotypes among D9 γδ T cells. Bubble size indicates clonotype frequency as a
1275 percentage of TRGV1^{+} (n = 198 B6, 98 B6.SAP$^{-/-}$) or TRGV4^{+} (n = 646 B6, 669 B6.SAP$^{-/-}$) cells,

1276 and colors correspond to specific TRDV chains. Selected clonotypes are numbered and their
1277 corresponding CDR3γ and CDR3δ sequences are displayed below. **(C)** Distribution of selected
1278 TRGV/TRDV clonotypes among B6 and B6.SAP$^{-/-}$ D9 thymic γδ T cell clusters. Data
1279 representative of 3 mice/strain, *$p \leq 0.05$, ***$p \leq 0.001$, two-way ANOVA, Sidak multiple-
1280 comparisons test.
1281
1282 **Figure 6. Restricted TCR repertoire in innate-like γδT1 as well as γδT17 in the periphery.**
1283 **(A)** UMAP representation of B6 adult lung γδ T cells. Clusters are annotated based on gene
1284 expression and TCR profiling data. **(B)** Feature plot displaying gene expression profiles of selected
1285 genes among individual B6 lung γδ T cells, color-coded based on gene expression levels. **(C)** Dot
1286 plot indicating scaled expression levels of selected genes in B6 lung γδ T cells, with dot size
1287 representing the fraction of cells within each cluster expressing the marker. **(D)** SLAMF6 and
1288 SLAMF7 co-expression marks CD44^{+}CD45RB^{+} IFN-γ-producing cells in the periphery.
1289 Representative dot plots (left) of CD44 and CD45RB expression on lung Vγ1 (top) and Vγ4
1290 (bottom) γδ T cells. SLAMF7-expressing cells are highlighted in blue. Representative contour
1291 plots (right) of SLAMF1, SLAMF6, and SLAMF7 expression on IFN-γ^{+} and IL-17^{+} lung γδ T
1292 cells. **(E)** UMAP representation of B6 lung γδ T cells indicating selected TRG and TRD chain V-
1293 segment usage (blue). **(F)** Amino acid length distribution of lung CDR3δ clonotypes among
1294 immature C0/C5, γδT1 C2/C3/C7/C9, γδT17 C1, and γδT17 C4 clusters. The top 10 clonotypes in
1295 each group are color-coded, while all other clonotypes are shown in gray.
1296
1297 **Figure 7. Specific decrease in Vγ4/Vδ7 γδT1 cells in the lungs of SAP-deficient mice. (A)**
1298 UMAP representation of B6 (left) and B6.SAP$^{-/-}$ (right) lung γδ T cells, pooled from 3 mice per

1299 strain. **(B)** SAP-dependent variation in lung γδ T cell cluster frequencies. The frequency of each
1300 B6 and B6.SAP$^{-/-}$ cluster as a percentage of all lung γδ T cells is shown. (**C**) UMAP representation
1301 of selected TRG and TRD chain V-segment usage (blue) among B6 and B6.SAP$^{-/-}$ lung γδ T cells.
1302 **(D)** SAP-dependent decrease in lung γδT1 TRGV4/TRDV7. Normalized TRDV counts in B6 and
1303 B6.SAP$^{-/-}$ lung TRGV4^{+} γδT1 clusters (C2/C3/C7/C9). **(E)** SAP-dependent decrease in SLAMF7^{+}
1304 lung Vγ4 T cells. Representative contour plots of CD44 and SLAMF7 expression in B6 (left) and
1305 B6.SAP$^{-/-}$ (right) lung Vγ4 γδ T cells are shown at *left*. Relative frequencies and counts of
1306 CD44^{+}SLAMF7^{+} lung Vγ4 cells is shown at *right*. Data represent the cumulative data from five
1307 independent experiments, ****$p < 0.0001$ using unpaired t-test. **(F)** SAP-dependent skewing of
1308 the lung γδT17 TCR repertoire. Amino acid length distributions of B6 and B6.SAP$^{-/-}$ TRGV4^{+}
1309 CDR3γ (left) and TRDV2^{+} CDR3δ (right) sequences in the lung Vγ4 γδT17 C1 cluster. The top
1310 10 clonotypes are color-coded and all other clonotypes are shown in gray. Bars represent the
1311 frequency of γδ T cells in the c1 cluster. **(G)** TCR clonotype bubble plots depicting the top 50 lung
1312 TRGV4 clonotypes in the C1 γδT17 cluster. Bubble size indicates clonotype frequency as a
1313 percentage of C1 Vγ4 (n = 62 B6, 104 B6.SAP$^{-/-}$) T cells, and colors correspond to specific TRDV
1314 chains. Selected clonotypes are numbered and their corresponding CDR3γ and CDR3δ sequences
1315 are displayed below.

1316 **Supplementary Figure Legends**
1317
1318 **Supplemental Figure 1: Quality control for single cell CITE-seq. (A)** Representative gating
1319 scheme used for FACS sorting γδ cells from B6 (top) and B6.SAP$^{-/-}$ (bottom) thymus. **(B)** *Left,*
1320 Violin plots of B6 E17 thymic γδ T cells. nFeaure_RNA represents number of genes detected in
1321 each cell. nCount_RNA represents total number of molecules detected within a cell, percent.mt
1322 represents the frequency of mitochondrial genes expressed in each cell, and percent.ribo represents
1323 the frequency of ribosomal genes expressed in each cell. *Middle,* ridge plots demonstrating
1324 successful enrichment for selected hashtags in E17 thymus γδ T cells following demultiplexing.
1325 *Right,* UMAP representations showing distribution of demultiplexed γδ T cells among individual
1326 B6 E17 thymus samples. **(C)** Violin plots depicting distribution of cell surface protein oligo-
1327 conjugated antibody derived tags (ADTs) among different B6 E17 thymus γδ T cells clusters. **(D)**
1328 Violin plots depicting expression levels of selected genes among individual E17 B6 thymic γδ T
1329 cells clusters. **(E)** Representative dot plots of CD24 and SLAMF7 staining on neonatal thymus γδ
1330 T cells. The position of CD44^{+}CD45RB^{+} cells are shown in blue. Data are representative of two
1331 independent experiments, n = 10 mice.
1332
1333 **Supplemental Figure 2: TCR repertoire profiling of B6 E17 thymus γδ T cells. (A)** *Left,* TCR
1334 clonotype bubble plot depicting the top 100 TCR clonotypes among B6 E17 γδ T cells (n = 2502
1335 γδ T cells). Each bubble represents a unique TRGV/TRDV clonotype; the bubble size corresponds
1336 to the clonotype frequency, and colors correspond to specific TRGV chains utilized. The 4 most
1337 frequent clonotypes are numbered and their corresponding CDR3γ and CDR3δ sequences are
1338 displayed below. *Right*, UMAP representations depicting the location of the four most frequent
1339 clonotypes E17 thymic γδ T cell clusters. **(B)** Diversity of the E17 γδ TCR repertoire, represented

1340 by the Inverse Simpson index. **(C)** Amino acid length distributions of E17 thymic γδ T cell CDR3γ
1341 (top) and CDR3δ (bottom) in immature *Blk*$^{+}$, *Etv5*$^{+}$, *Maf*$^{+}$ C2 and C7 (left), immature RORγt^{high}
1342 C1 (middle), and mature RORγt^{high} c8 (right) clusters. The top 10 clonotypes are color-coded, all
1343 other clonotypes are shown in gray.
1344
1345 **Supplemental Figure 3: Identification of a BLK^{neg}MAF^{neg}RORγt^{pos} E17 γδ T cell population**
1346 **expressing CD4 and CD8. (A)** *Left,* Representative dot plot of CD24 and CD25 expression on
1347 E17 B6 thymic Vγ4 T cells. *Right,* Histograms depicting BLK, PLZF, and RORγt expression in
1348 the gated populations at left. The geometric mean fluorescence intensity of individual populations
1349 is shown. **(B)** Feature plots showing cell surface protein expression of Vγ1 (top) and Vγ4 (bottom)
1350 on B6 E17 thymus γδ T cells. Each point represents a cell, color-coded based on the protein
1351 expression level (high: dark blue, low: yellow). **(C)** *Top left*, UMAP representation of E17 B6 γδ
1352 T cell flow cytometry data with selected FlowSOM clusters indicated by color. All other cells are
1353 shown in gray. *Right,* Individual dot plots overlaid with the selected FlowSOM clusters from the
1354 UMAP plot. Data represent concatenated data from 5 B6 TCRβ^{neg}TCRδ^{pos} γδ T cells and are
1355 representative of 2 independent experiments. **(D)** Increasing BLK^{neg}RORγt^{pos} frequency as
1356 thymocytes progress to DN4 stage. Representative contour plots of E17 DN thymocytes with
1357 selected gates shown (*left*) and BLK and RORγt expression associated with each gated population
1358 (*right*). Numbers indicate the percentage of cells in the gated population. **(E)** Immature Vγ1Vδ1 T
1359 cells comprise the major IL17-producing Vγ1 T cell population in E17 thymus. *Left,* representative
1360 contour plot of Vγ1 and Vδ1 (17D1) expression among E17 thymic γδ T cells. *Middle,* Dot plot of
1361 CD24 and SSC expression on E17 thymic γδ T cells. The position of Vγ1^{+}Vδ1^{+} E17 T cells is

1362 shown in red. *Right,* Dot plots of IL-17 and IFN-γ expression in E17 thymic $V\gamma1^{+}17D1^{+}$ and
1363 $V\gamma1^{+}17D1^{-}$ cells after PMA/ionomycin stimulation.
1364
1365 **Supplemental Figure 4:** Violin plots showing expression levels of selected genes among
1366 individual B6 and B6.SAP$^{-/-}$ E17 thymic γδ T cell clusters. **(A)** Genes whose expression decreased
1367 in B6.SAP$^{-/-}$ immature γδ T cells. **(B)** Genes whose expression increased in B6.SAP$^{-/-}$ immature
1368 γδ T cells.
1369
1370 **Supplemental Figure 5: SAP-dependent regulation of immature BLK^{+}PLZF^{+}RORγt^{+} and**
1371 **BLK^{-}PLZF$^{+/-}$RORγt^{+} E17 thymic γδ T cells. (A)** Total number of E17 thymic γδ T cells in B6
1372 and B6.SAP$^{-/-}$ E17 thymus. **(B)** E17 thymic Vγ4 developmental checkpoints. *Left, U*MAP
1373 representation of E17 B6 and B6.SAP$^{-/-}$ Vγ4 T cell flow cytometry data with selected FlowSOM
1374 clusters indicated by color. All other cells are shown in gray. *Right,* Individual dot plots overlaid
1375 with the selected FlowSOM clusters from the UMAP plot. Data represent concatenated data from
1376 4 B6 and 4 B6.SAP$^{-/-}$ TCRβ^{neg}TCRδ^{pos} γδ T cells and are representative of 2 independent
1377 experiments. **(C)** Cumulative frequency and number of the indicated FlowSOM populations shown
1378 in (B), *$p \leq 0.05$, **$p \leq 0.01$, ***$p \leq 0.001$, unpaired t-test, corrected for multiple comparison
1379 using Holm-Sidak's test. **(D)** Decreased BLK, but not PLZF expression in B6.SAP$^{-/-}$ γδ T cells.
1380 *Above,* histograms of BLK and PLZF in immature E17 γδ T cells. B6 BLK (dark gray) and PLZF
1381 (red) histograms are overlaid on B6.SAP$^{-/-}$ (light gray) histograms for comparison. *Below,* control
1382 stains lacking BLK or PLZF. **(E)** Representative contour plots of immature CD25^{neg} E.17 Vγ4 T
1383 cells in B6 and B6.SAP$^{-/-}$ mice.
1384

1385 **Supplemental Figure 6: Transcriptional heterogeneity in neonatal thymic γδ T cells. (A)** Dot
1386 plot showing scaled expression level of selected genes in B6 D9 thymic γδ T cells. Level of
1387 normalized expression is shown using a color scale ranging from low (yellow) to high (purple).
1388 Dot size represents the fraction of cells within each cluster that express the marker. **(B)** Violin
1389 plots showing the specificity of the oligo-conjugated antibody derived tags (ADT) to cell surface
1390 proteins (CD24, CD73, SLAMF1, SLAMF6) among different B6 D9 thymus γδ T cell clusters.
1391 **(C)** Violin plots showing expression levels of selected genes among individual clusters in the B6
1392 D9 thymic γδ T cells. **(D)** Violin plots showing expression levels of *Zbtb16* gene (expressing
1393 PLZF) among individual clusters in the B6 E17 (top) and D9 (bottom) thymic γδ T cells.
1394

1395 **Supplemental Figure 7: Flow cytometric analysis of D9 thymic γδ T cells. (A)** SLAMF6 and
1396 SLAMF7 expression defines γδNKT cell subsets. *Left*, representative dot plot of PLZF and T-bet
1397 expression in B6 D9 thymic Vγ1Vδ6.3 γδNKT cells. Representative contour plots of ICOS and
1398 NK1.1 (*top right)* and SLAMF6 and SLAMF7 (*bottom right*) staining in PLZF^{hi}T-bet^{low} and
1399 PLZF^{low}T-bet^{high} subsets are shown at right. Data are representative of two independent
1400 experiments with a total of ten mice. **(B)** *Left,* representative dot plot of SLAMF6 and SLAMF7
1401 expression in B6 D9 thymic Vγ1Vδ6.3 γδNKT cells. *Right,* representative dot plots of intracellular
1402 IL4 and IFN-γ expression in SLAMF6^{hi}SLAMF7^{low}, SLAMF6^{high}SLAMF7^{hi}, and
1403 SLAMF6^{low}SLAMF7^{hi} γδNKT cell subsets. Numbers indicate percentage. Cumulative data of IL-
1404 4 and IFN-γ expression is shown below. Data are representative of two independent experiments
1405 with a total of ten mice. **(C)** Increased number of immature CD200^{-}S1P1^{+} γδ T cells in SAP-
1406 deficient neonatal thymus.
1407

1408 **Supplemental Figure 8: scRNA-seq with TCR repertoire profiling of B6 and B6.SAP$^{-/-}$ adult**
1409 **thymic γδ T cells. (A)** UMAP representation of B6 and B6.SAP$^{-/-}$ adult thymus (6 weeks old) γδ
1410 T cells, n = 3 mice per strain. **(B)** Feature plots illustrating the cell surface protein expression
1411 profiles of CD24, CD73, SLAMF1, and SLAMF6 on adult thymic γδ T cells. Each data point
1412 represents a cell, color-coded to indicate varying protein expression levels (high: dark blue, low:
1413 yellow). **(C)** Frequencies of B6 and B6.SAP$^{-/-}$ γδ T cell clusters. Bars represent the mean cluster
1414 frequency, error bars represent standard deviation, *$p \leq 0.05$, **$p \leq 0.01$, ****$p \leq 0.0001$, two-
1415 way ANOVA, Sidak multiple-comparisons test. **(D)** Dot plot showing scaled expression level of
1416 selected genes in B6 adult thymic γδ T cells. Level of normalized expression is shown using a
1417 color scale ranging from low (yellow) to high (purple). Dot size represents the fraction of cells
1418 within each cluster that express the marker. **(E)** Expression of selected TRG (left) and TRDs chain
1419 (right) V-segment usage (blue) by individual adult thymus γδ T cells in B6 and B6.SAP$^{-/-}$ mice.
1420

1421 **Supplemental Figure 9: Lung Vγ4 exhibit a high usage of TRDV7 chains with a diverse**
1422 **CDR3. (A)** TRDV usage among FACS-sorted lung Vγ4 γδ T cells from 7 male and 6 female mice.
1423 **(B)** *Left,* amino acid length distribution of top lung TRDV5^{+} CDR3δ clonotypes in the lung Vγ4
1424 γδ T cell population. *Right*, distribution of the most frequent clonotypes among individual B6 mice.
1425 **(C)** *Left,* amino acid length distribution of top lung TRDV2^{+} CDR3δ clonotypes in the lung Vγ4
1426 γδ T cell population. *Right*, distribution of the most frequent clonotypes among individual B6 mice.
1427 **(D)** *Left,* amino acid length distribution of top lung TRDV7^{+} CDR3δ clonotypes in the lung Vγ4
1428 γδ T cell population. *Right*, distribution of the most frequent clonotypes among individual B6 mice.
1429 **(E)** *Left,* amino acid length distribution of top lung TRGV4^{+} CDR3γ clonotypes in the lung Vγ4
1430 γδ T cell population. *Right*, distribution of the most frequent clonotypes among individual B6 mice.

1431 **Supplemental Figure 10: Significant and specific reduction in peripheral TRGV4/TRDV7^{+}**
1432 **γδT1 in B6.SAP$^{-/-}$ mice. (A)** The relative expression of the specified TRDV transcripts in adult
1433 lung and spleen CD45^{+} leukocytes (normalized to total TRDC transcript levels) in B6 and B6.SAP^{-}
1434 $^{/-}$ mice, **p < 0.01, ****p < 0.0001, two-way ANOVA followed by Sidak multiple-comparisons
1435 test. **(B)** SAP-dependent decrease in CD44^{+}SLAMF7^{+} spleen Vγ4 T cells. The relative percentage
1436 and count of CD44^{+}SLAMF7^{+} Vγ4 cells in B6 and B6.SAP$^{-/-}$ spleen subsets are shown. Data are
1437 representative of five independent experiments with 3-5 mice per strain per experiment, ****p,
1438 <0.0001, as determined by unpaired t tests. **(C)** No difference in lung Vγ4 homeostasis in B6.SAP^{-}
1439 $^{/-}$ mice. *Top left,* Representative contour plots showing the frequency of BrdU staining in B6 and
1440 B6.SAP$^{-/-}$ lung γδ T cells. Cumulative data from two independent experiments are shown at *top*
1441 *right*. *Bottom left,* representative contour plots depicting Annexin V and Live/Dead staining in B6
1442 and B6.SAP$^{-/-}$ lung γδ T cells. Cumulative results are shown at *bottom right,* and are representative
1443 of 3 independent experiments.

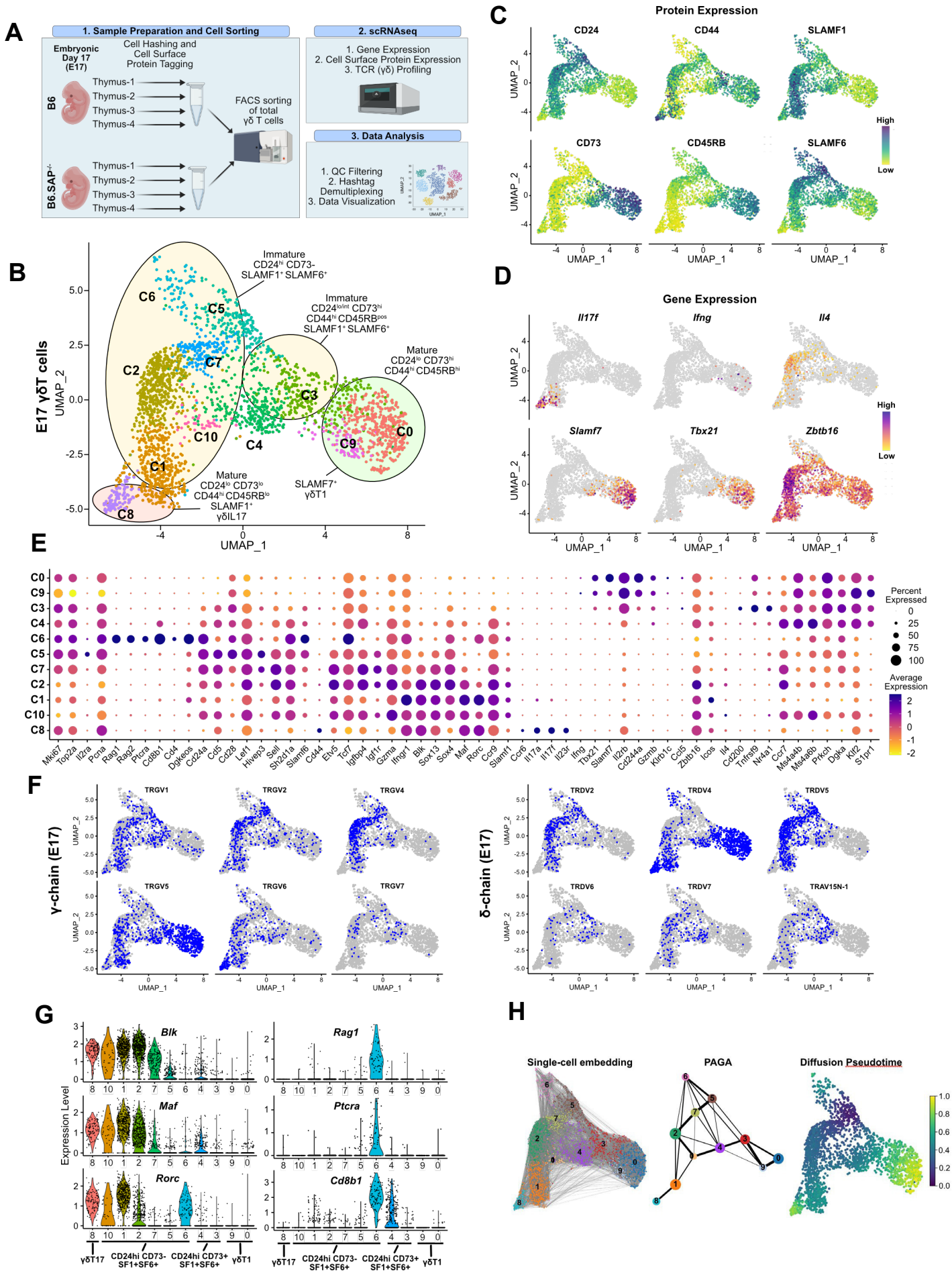
A
1. Sample Preparation and Cell Sorting
Embryonic Day 17 (E17)
Cell Hashing and Cell Surface Protein Tagging
B6
Thymus-1
Thymus-2
Thymus-3
Thymus-4
B6.SAP-/-
FACS sorting of total γδ T cells
2. scRNAseq
1. Gene Expression
2. Cell Surface Protein Expression
3. TCR (γδ) Profiling
3. Data Analysis
1. QC Filtering
2. Hashtag Demultiplexing
3. Data Visualization
B
E17 γδT cells
Immature CD24hi CD73- SLAMF1+ SLAMF6+
Immature CD24lo/int CD73hi CD44hi CD45RBpos SLAMF1+ SLAMF6+
Mature CD24lo CD73hi CD44hi CD45RBhi
Mature CD24lo CD73lo CD44hi CD45RBlo SLAMF1+ γδIL17
SLAMF7+ γδT1
C0
C1
C2
C3
C4
C5
C6
C7
C8
C9
C10
UMAP_1
UMAP_2
C
Protein Expression
CD24
CD44
SLAMF1
CD73
CD45RB
SLAMF6
High
Low
D
Gene Expression
Il17f
Ifng
Il4
Slamf7
Tbx21
Zbtb16
E
Percent Expressed
Average Expression
Mki67
Top2a
Il2ra
Pcna
Rag1
Rag2
Ptcra
Cd8b1
Cd4
Dgkeos
Cd24a
Cd5
Cd28
Lef1
Hlveps
Sell
Sh2d1a
Slamf6
Cd44
Etv5
Tcf7
Igfbp4
Igf1r
Gzma
Ifngr1
Blk
Sox13
Sox4
Maf
Rorc
Ccr9
Slamf1
Ccr6
Il17a
Il17f
Il23r
Ifng
Tbx21
Slamf7
Il2rb
Cd244a
Gzmb
Klrb1c
Cd5
Zbtb16
Icos
Il4
Cd200
Tnfrsf9
Nr4a1
Ccr7
Ms4a4b
Ms4a6b
Prkch
Dgka
Klf2
S1pr1
F
γ-chain (E17)
TRGV1
TRGV2
TRGV4
TRGV5
TRGV6
TRGV7
δ-chain (E17)
TRDV2
TRDV4
TRDV5
TRDV6
TRDV7
TRAV15N-1
G
Expression Level
Blk
Rag1
Maf
Ptcra
Rorc
Cd8b1
γδT17
CD24hi CD73- SF1+SF6+
CD24hi CD73+ SF1+SF6+
γδT1
H
Single-cell embedding
PAGA
Diffusion Pseudotime

Figure 1

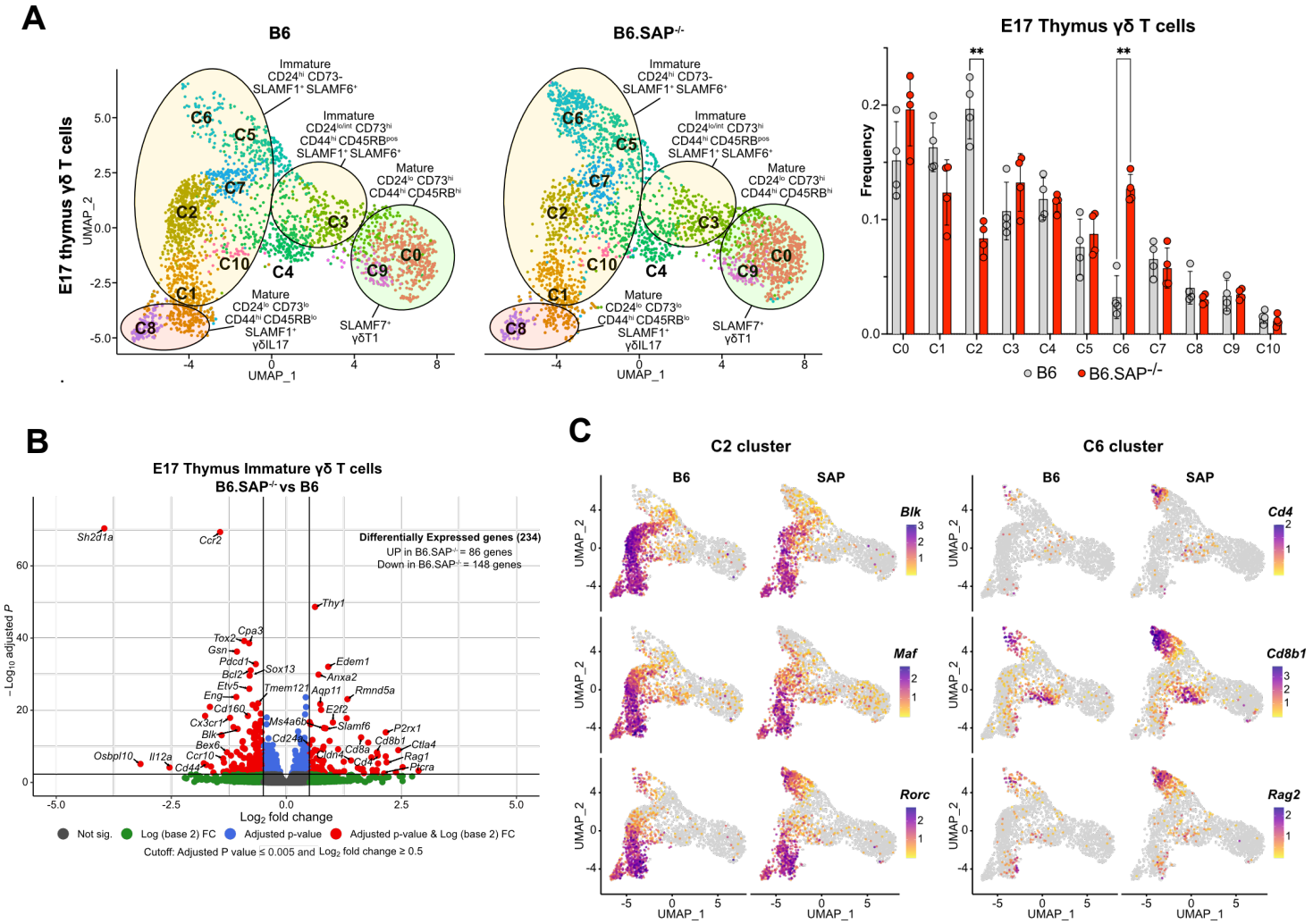
A
B6
B6.SAP-/-
E17 thymus γδ T cells
UMAP_1
UMAP_2
Immature CD24hi CD73- SLAMF1+ SLAMF6+
Immature CD24lo/int CD73hi CD44hi CD45RBpos SLAMF1+ SLAMF6+
Mature CD24lo CD73hi CD44hi CD45RBhi
Mature CD24lo CD73lo CD44hi CD45RBlo SLAMF1+ γδIL17
SLAMF7+ γδT1
C0 C1 C2 C3 C4 C5 C6 C7 C8 C9 C10
E17 Thymus γδ T cells
Frequency
B6
B6.SAP-/-
B
E17 Thymus Immature γδ T cells
B6.SAP-/- vs B6
Differentially Expressed genes (234)
UP in B6.SAP-/- = 86 genes
Down in B6.SAP-/- = 148 genes
Sh2d1a
Ccr2
Thy1
Cpa3
Tox2
Gsn
Pdcd1
Bcl2
Sox13
Etv5
Tmem121
Eng
Cd160
Cx3cr1
Blk
Bex6
Ccr10
Cd44
Osbpl10
Il12a
Ms4a6b
Cd24a
Edem1
Anxa2
Aqp11
Rmnd5a
E2f2
Slamf6
Cd8a
Cd4
Cdh1
P2rx1
Cd8b1
Ctla4
Rag1
Ptcra
Log2 fold change
Not sig.
Log (base 2) FC
Adjusted p-value
Adjusted p-value & Log (base 2) FC
Cutoff: Adjusted P value ≤ 0.005 and Log2 fold change ≥ 0.5
C
C2 cluster
C6 cluster
B6
SAP
Blk
Maf
Rorc
Cd4
Cd8b1
Rag2
UMAP_1
UMAP_2

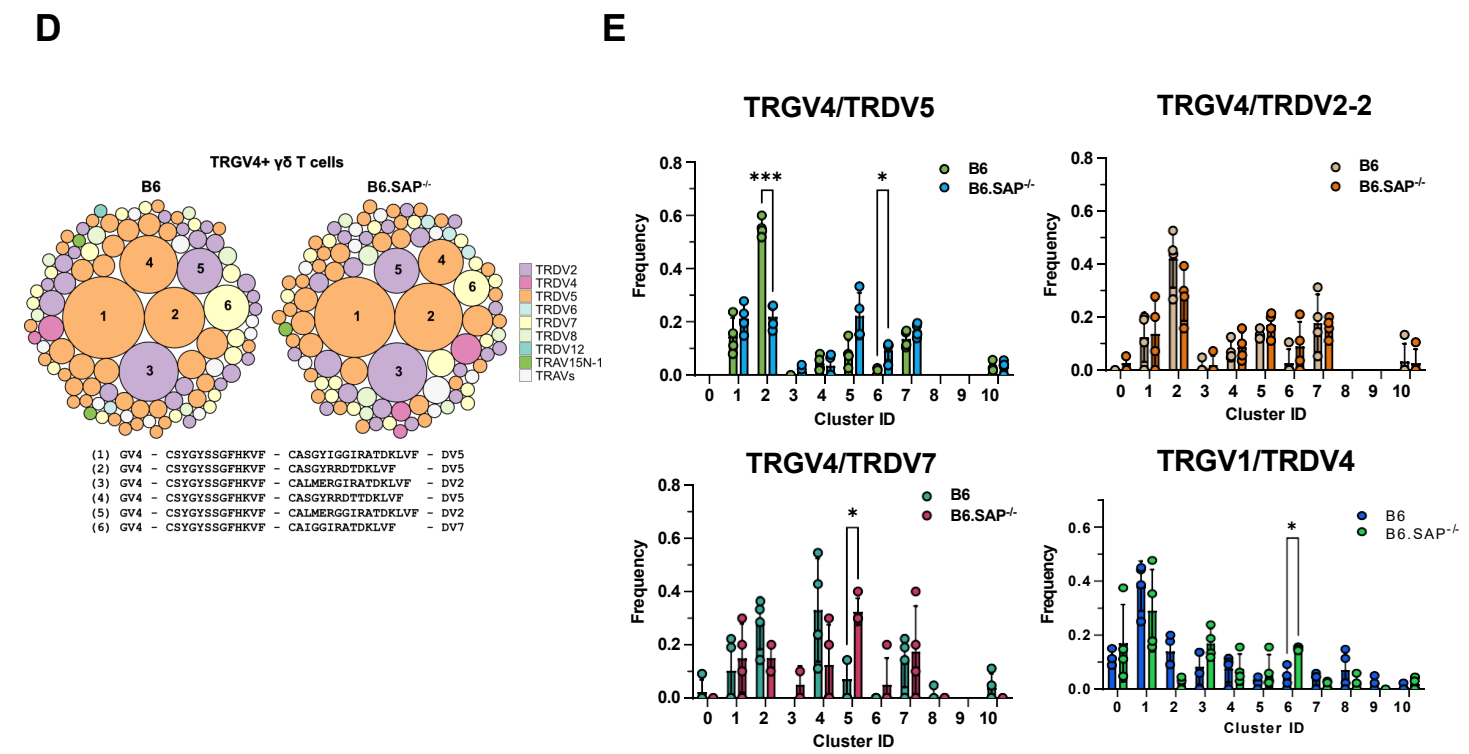
D
TRGV4+ γδ T cells
B6
B6.SAP-/-
TRDV2
TRDV4
TRDV5
TRDV6
TRDV7
TRDV8
TRDV12
TRAV15N-1
TRAVs
(1) GV4 - CSYGYSSGFHKVF - CASGYIGGIRATDKLVF - DV5
(2) GV4 - CSYGYSSGFHKVF - CASGYRRDTDKLVF - DV5
(3) GV4 - CSYGYSSGFHKVF - CALMERGIRATDKLVF - DV2
(4) GV4 - CSYGYSSGFHKVF - CASGYRRDTTDKLVF - DV5
(5) GV4 - CSYGYSSGFHKVF - CALMERGGIRATDKLVF - DV2
(6) GV4 - CSYGYSSGFHKVF - CAIGGIRATDKLVF - DV7
E
TRGV4/TRDV5
TRGV4/TRDV2-2
TRGV4/TRDV7
TRGV1/TRDV4
Frequency
Cluster ID
B6
B6.SAP-/-

Figure 2

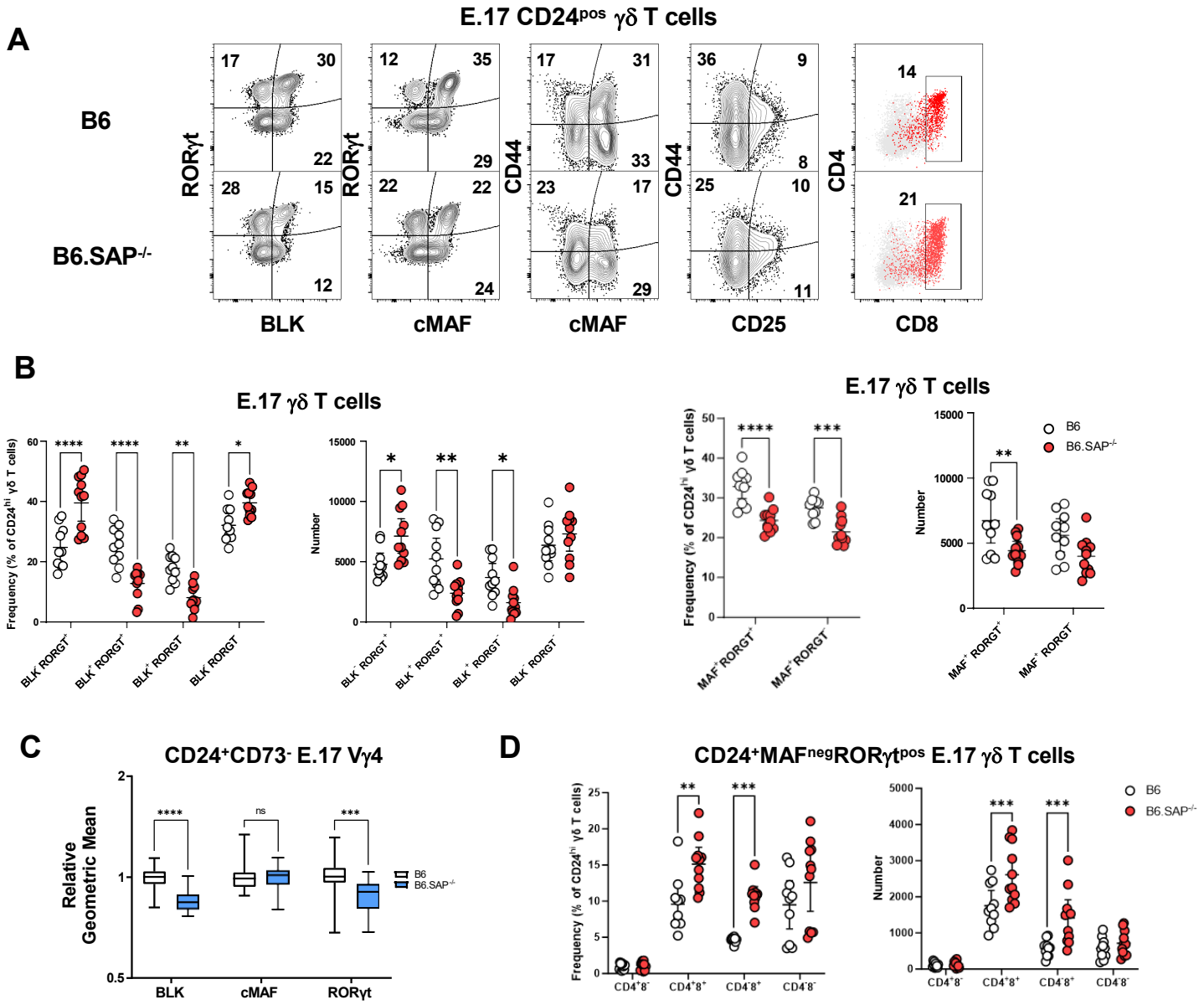
A
E.17 CD24pos γδ T cells
B6
B6.SAP-/-
RORγt
CD44
CD4
BLK
cMAF
CD25
CD8
B
E.17 γδ T cells
Frequency (% of CD24hi γδ T cells)
Number
BLK+RORGT+
BLK+RORGT-
BLK-RORGT+
BLK-RORGT-
MAF+RORGT+
MAF+RORGT-
MAF-RORGT+
MAF-RORGT-
B6
B6.SAP-/-
C
CD24+CD73- E.17 Vγ4
Relative Geometric Mean
ns
D
CD24+MAFnegRORγtpos E.17 γδ T cells
CD4+8-
CD4+8+
CD4-8+
CD4-8-

Figure 3

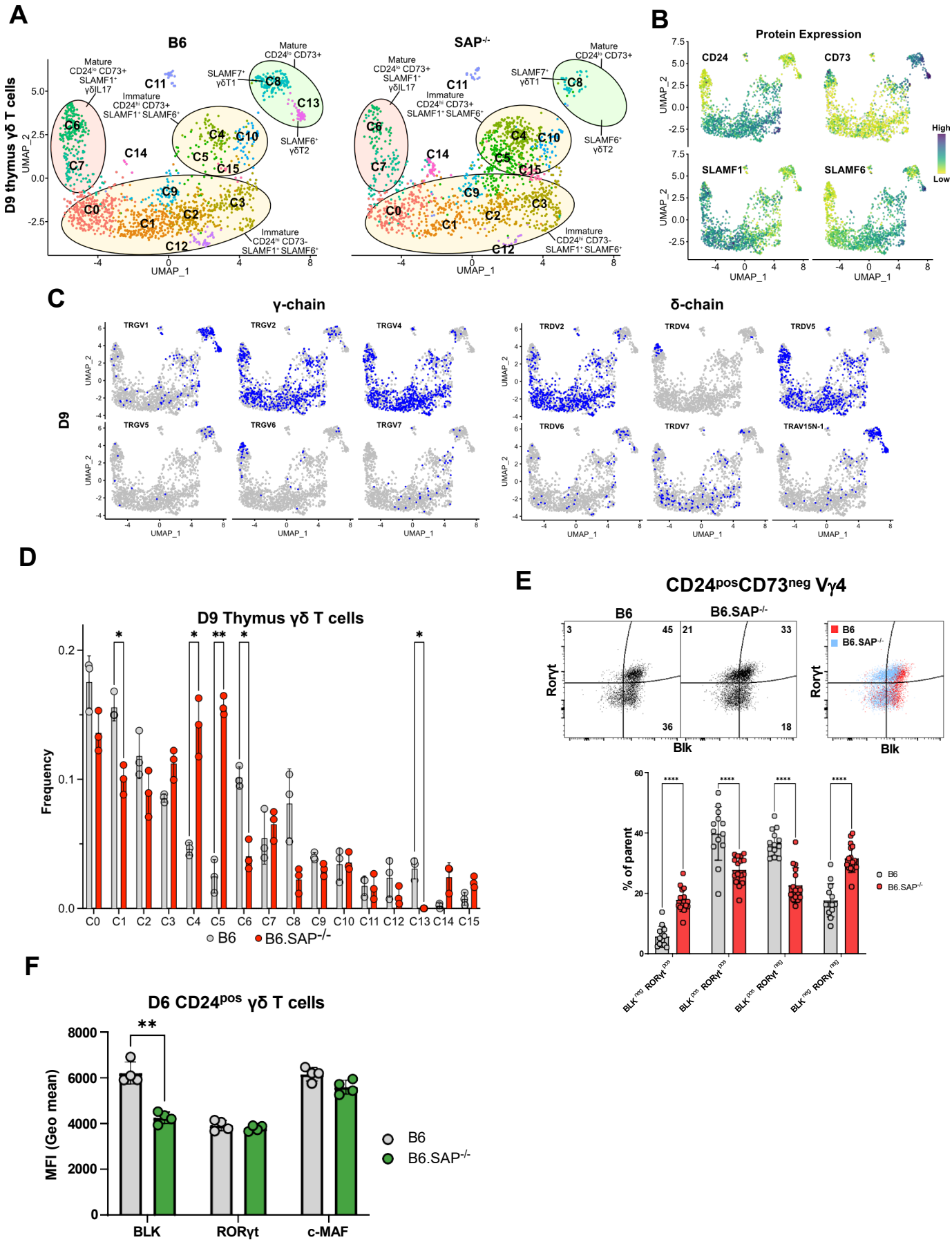
A
B6
SAP-/-
D9 thymus γδ T cells
Mature CD24lo CD73+ SLAMF1+ γδIL17
Immature CD24hi CD73+ SLAMF1+ SLAMF6+
SLAMF7+ γδT1
Mature CD24lo CD73+
SLAMF6+ γδT2
Immature CD24hi CD73- SLAMF1+ SLAMF6+
UMAP_1
UMAP_2
B
Protein Expression
CD24
CD73
SLAMF1
SLAMF6
High
Low
C
γ-chain
δ-chain
D9
TRGV1
TRGV2
TRGV4
TRGV5
TRGV6
TRGV7
TRDV2
TRDV4
TRDV5
TRDV6
TRDV7
TRAV15N-1
D
D9 Thymus γδ T cells
Frequency
B6
B6.SAP-/-
E
CD24posCD73neg Vγ4
B6
B6.SAP-/-
Roryt
Blk
% of parent
BLKneg RORγtpos
BLKpos RORγtpos
BLKpos RORγtneg
BLKneg RORγtneg
F
D6 CD24pos γδ T cells
MFI (Geo mean)
BLK
RORγt
c-MAF

Figure 4

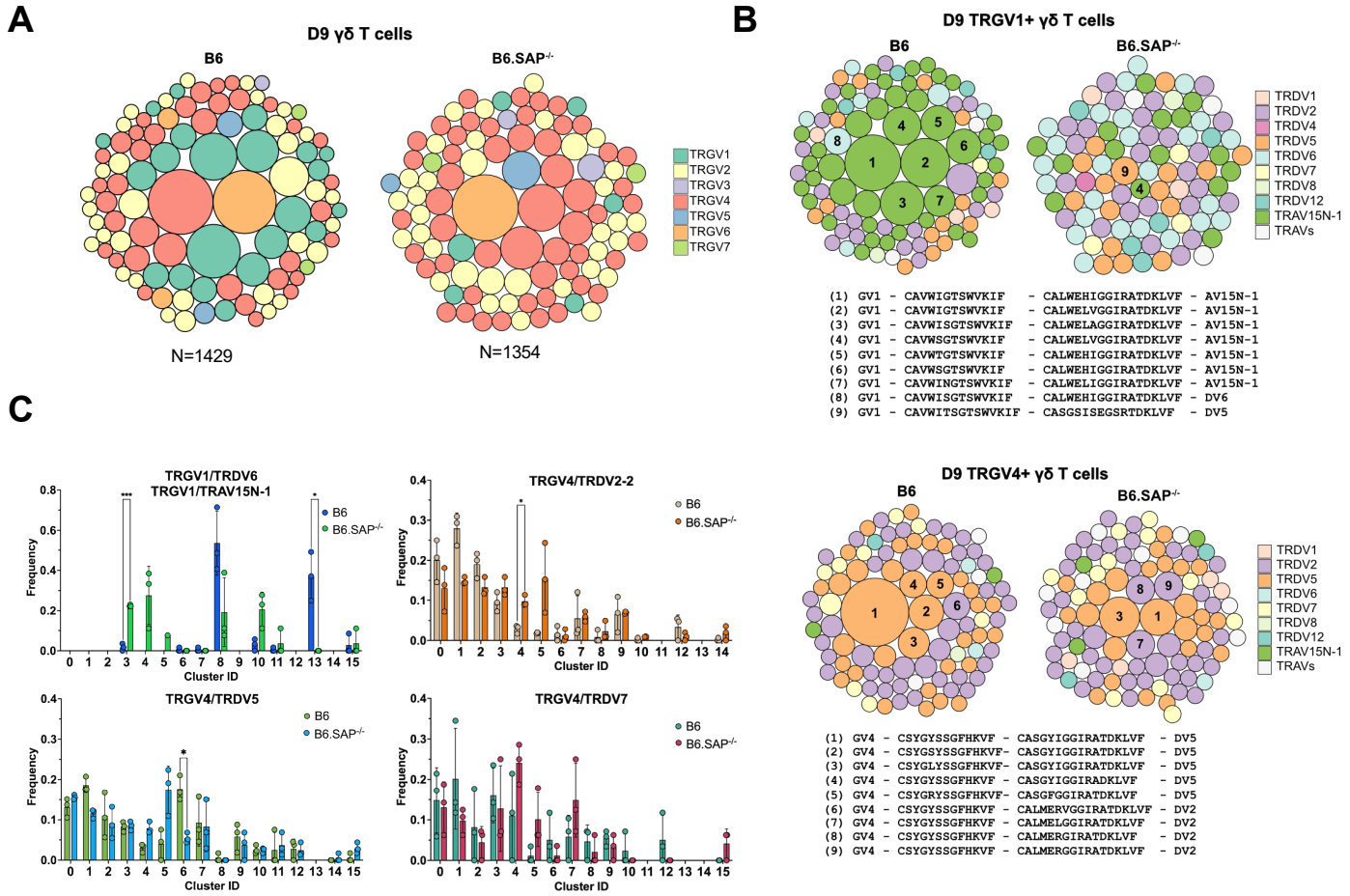
A
D9 γδ T cells
B6
B6.SAP-/-
N=1429
N=1354
TRGV1
TRGV2
TRGV3
TRGV4
TRGV5
TRGV6
TRGV7
B
D9 TRGV1+ γδ T cells
B6
B6.SAP-/-
TRDV1
TRDV2
TRDV4
TRDV5
TRDV6
TRDV7
TRDV8
TRDV12
TRAV15N-1
TRAVs
(1) GV1 - CAVWIGTSWVKIF - CALWEHIGGIRATDKLVF - AV15N-1
(2) GV1 - CAVWIGTSWVKIF - CALWELVGGIRATDKLVF - AV15N-1
(3) GV1 - CAVWISGTSWVKIF - CALWELAGGIRATDKLVF - AV15N-1
(4) GV1 - CAVWSGTSWVKIF - CALWELVGGIRATDKLVF - AV15N-1
(5) GV1 - CAVWTGTSWVKIF - CALWEHIGGIRATDKLVF - AV15N-1
(6) GV1 - CAVWSGTSWVKIF - CALWEHIGGIRATDKLVF - AV15N-1
(7) GV1 - CAVWINGTSWVKIF - CALWELIGGIRATDKLVF - AV15N-1
(8) GV1 - CAVWISGTSWVKIF - CALWEHIGGIRATDKLVF - DV6
(9) GV1 - CAVWITSGTSWVKIF - CASGSISEGSRTDKLVF - DV5
C
TRGV1/TRDV6
TRGV1/TRAV15N-1
TRGV4/TRDV2-2
TRGV4/TRDV5
TRGV4/TRDV7
B6
B6.SAP-/-
Frequency
Cluster ID
D9 TRGV4+ γδ T cells
B6
B6.SAP-/-
TRDV1
TRDV2
TRDV5
TRDV6
TRDV7
TRDV8
TRDV12
TRAV15N-1
TRAVs
(1) GV4 - CSYGYSSGFHKVF - CASGYIGGIRATDKLVF - DV5
(2) GV4 - CSYGSYSSGFHKVF- CASGYIGGIRATDKLVF - DV5
(3) GV4 - CSYGLYSSGFHKVF- CASGYIGGIRATDKLVF - DV5
(4) GV4 - CSYGYSSGFHKVF - CASGYIGGIRADKLVF - DV5
(5) GV4 - CSYGRYSSGFHKVF- CASGFGGIRATDKLVF - DV5
(6) GV4 - CSYGYSSGFHKVF - CALMERVGGIRATDKLVF - DV2
(7) GV4 - CSYGYSSGFHKVF - CALMELGGIRATDKLVF - DV2
(8) GV4 - CSYGYSSGFHKVF - CALMERGIRATDKLVF - DV2
(9) GV4 - CSYGYSSGFHKVF - CALMERGGIRATDKLVF - DV2

Figure 5

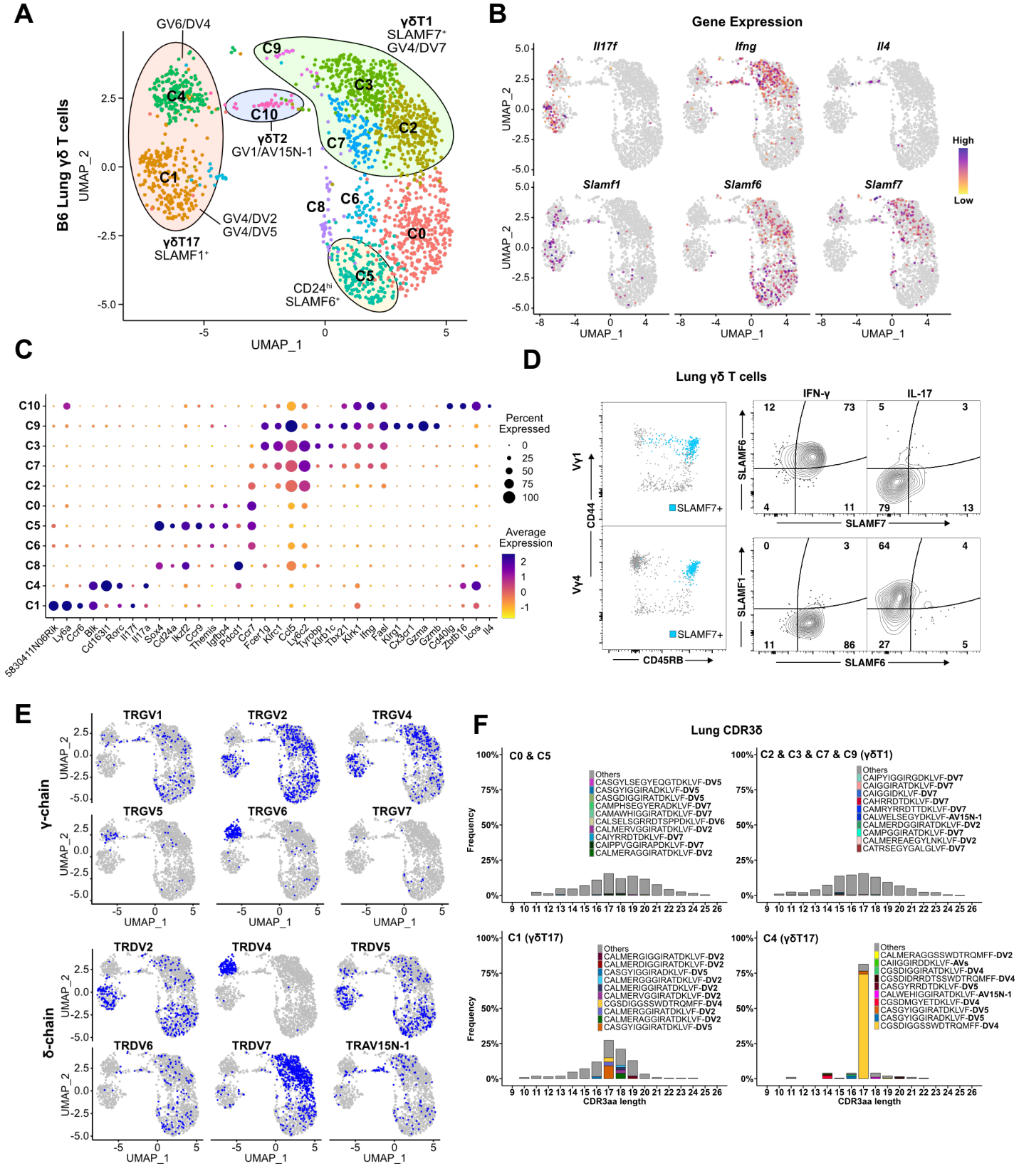
A
B6 Lung γδ T cells
UMAP_2
UMAP_1
GV6/DV4
γδT1
SLAMF7+
GV4/DV7
γδT2
GV1/AV15N-1
GV4/DV2
GV4/DV5
γδT17
SLAMF1+
CD24hi
SLAMF6+
C0
C1
C2
C3
C4
C5
C6
C7
C8
C9
C10
B
Gene Expression
Il17f
Ifng
Il4
Slamf1
Slamf6
Slamf7
High
Low
C
Percent Expressed
Average Expression
5830411N06Rik
Lyl6a
Ccr6
Blk
Cd163l1
Rorc
Il17f
Il17a
Sox4
Cd24a
Ikzf2
Ccr9
Themis
Igfbp4
Pdcd1
Ccr7
Fcer1g
Klrc1
Ccl5
Ly6c2
Tyrobp
Klrb1c
Tbx21
Klrk1
Ifng
Fasl
Klrg1
Cx3cr1
Gzma
Gzmb
Cd40lg
Zbtb16
Icos
Il4
D
Lung γδ T cells
IFN-γ
IL-17
Vγ1
Vγ4
CD44
CD45RB
SLAMF7+
SLAMF6
SLAMF7
SLAMF1
E
γ-chain
δ-chain
TRGV1
TRGV2
TRGV4
TRGV5
TRGV6
TRGV7
TRDV2
TRDV4
TRDV5
TRDV6
TRDV7
TRAV15N-1
F
Lung CDR3δ
C0 & C5
C2 & C3 & C7 & C9 (γδT1)
C1 (γδT17)
C4 (γδT17)
Frequency
CDR3aa length
Others
CASGYLSEGYEQGTDKLVF-DV5
CASGYIGGIRADKLVF-DV5
CASGDIGGIRATDKLVF-DV5
CAMPHSEGYERADKLVF-DV7
CAMAWHIGGIRATDKLVF-DV7
CALSELSGRRDTSPPDKLVF-DV6
CALMERVGGIRATDKLVF-DV2
CAIYRRDTDKLVF-DV7
CAIPPVGGIRAPDKLVF-DV7
CALMERAGGIRATDKLVF-DV2
CAIPYIGGIRGDKLVF-DV7
CAIGGIRATDKLVF-DV7
CAIGGIDKLVF-DV7
CAHRRDTDKLVF-DV7
CAMRYRRDTTDKLVF-DV7
CALWELSEGYDKLVF-AV15N-1
CALMERDGGIRATDKLVF-DV2
CAMPGGIRATDKLVF-DV7
CALMEREAEGYLNKLVF-DV2
CATRSEGYGALGLVF-DV7
CALMERGIGGIRATDKLVF-DV2
CALMERDIGGIRATDKLVF-DV2
CASGYIGGIRADKLVF-DV5
CALMERGGGIRATDKLVF-DV2
CALMERIGGIRATDKLVF-DV2
CALMERVGGIRATDKLVF-DV2
CGSDIGGSSWDTRQMFF-DV4
CALMERGGIRATDKLVF-DV2
CALMERAGGIRATDKLVF-DV2
CASGYIGGIRATDKLVF-DV5
CALMERAGGSSWDTRQMFF-DV2
CAIIGGIRDDKLVF-AVs
CGSDIGGIRATDKLVF-DV4
CGSDIDRRDTSSWDTRQMFF-DV4
CASGYRRDTDKLVF-DV5
CALWEHIGGIRATDKLVF-AV15N-1
CGSDMGYETDKLVF-DV4
CASGYIGGIRATDKLVF-DV5
CASGYIGGIRADKLVF-DV5
CGSDIGGSSWDTRQMFF-DV4

Figure 6

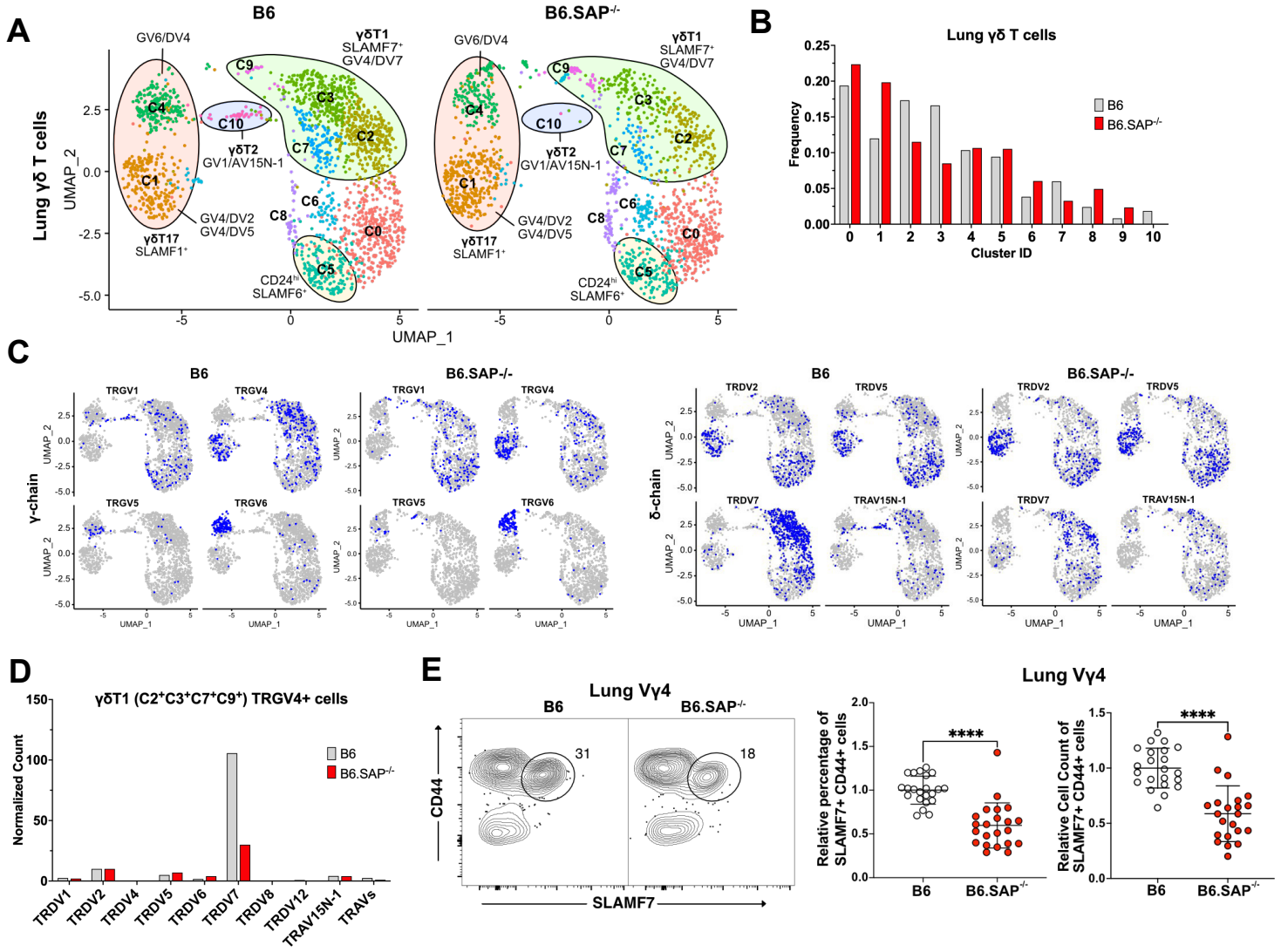
A
B6
B6.SAP-/-
Lung γδ T cells
UMAP_2
UMAP_1
GV6/DV4
γδT1
SLAMF7+
GV4/DV7
γδT2
GV1/AV15N-1
GV4/DV2
GV4/DV5
γδT17
SLAMF1+
CD24hi
SLAMF6+
C0
C1
C2
C3
C4
C5
C6
C7
C8
C9
C10
B
Lung γδ T cells
Frequency
Cluster ID
B6
B6.SAP-/-
C
γ-chain
δ-chain
TRGV1
TRGV4
TRGV5
TRGV6
TRDV2
TRDV5
TRDV7
TRAV15N-1
D
γδT1 (C2+C3+C7+C9+) TRGV4+ cells
Normalized Count
TRDV1
TRDV2
TRDV4
TRDV5
TRDV6
TRDV7
TRDV8
TRDV12
TRAV15N-1
TRAVs
E
Lung Vγ4
CD44
SLAMF7
31
18
Relative percentage of SLAMF7+ CD44+ cells
Relative Cell Count of SLAMF7+ CD44+ cells
****

F

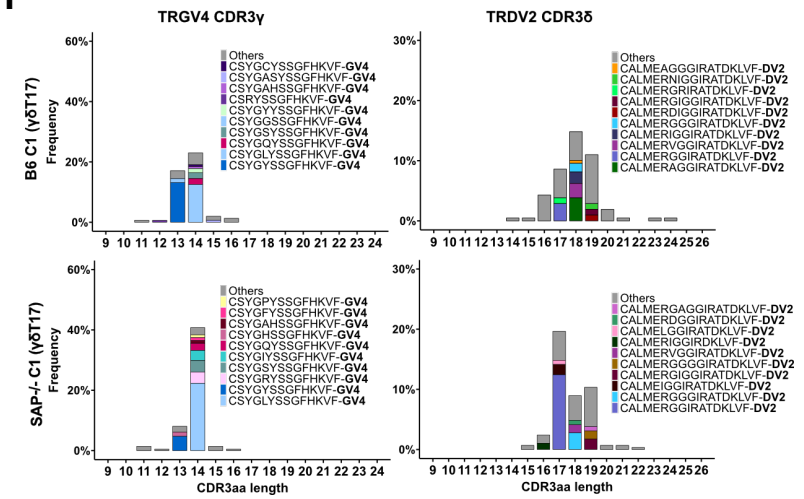
TRGV4 CDR3γ
TRDV2 CDR3δ
B6 C1 (γδT17)
SAP-/- C1 (γδT17)
Frequency
CDR3aa length
Others
CSYGCYSSGFHKVF-GV4
CSYGASYSSGFHKVF-GV4
CSYGAHSSGFHKVF-GV4
CSRYSSGFHKVF-GV4
CSYGYYSSGFHKVF-GV4
CSYGGSSGFHKVF-GV4
CSYGSYSSGFHKVF-GV4
CSYGQYSSGFHKVF-GV4
CSYGLYSSGFHKVF-GV4
CSYGYSSGFHKVF-GV4
CSYGPYSSGFHKVF-GV4
CSYGFYSSGFHKVF-GV4
CSYGAHSSGFHKVF-GV4
CSYGHSSGFHKVF-GV4
CSYGIYSSGFHKVF-GV4
CSYGRYSSGFHKVF-GV4
CALMEAGGGIRATDKLVF-DV2
CALMERNIGGIRATDKLVF-DV2
CALMERGRIRATDKLVF-DV2
CALMERGIGGIRATDKLVF-DV2
CALMERDIGGIRATDKLVF-DV2
CALMERGGGIRATDKLVF-DV2
CALMERIGGIRATDKLVF-DV2
CALMERVGGIRATDKLVF-DV2
CALMERGGIRATDKLVF-DV2
CALMERAGGIRATDKLVF-DV2
CALMERGAGGIRATDKLVF-DV2
CALMERDGGIRATDKLVF-DV2
CALMELGGIRATDKLVF-DV2
CALMERIGGIRDKLVF-DV2
CALMERVGGIRATDKLVF-DV2
CALMERGGGIRATDKLVF-DV2
CALMERIGGIRATDKLVF-DV2
CALMEIGGIRATDKLVF-DV2
CALMERGGGIRATDKLVF-DV2
CALMERGGIRATDKLVF-DV2

G

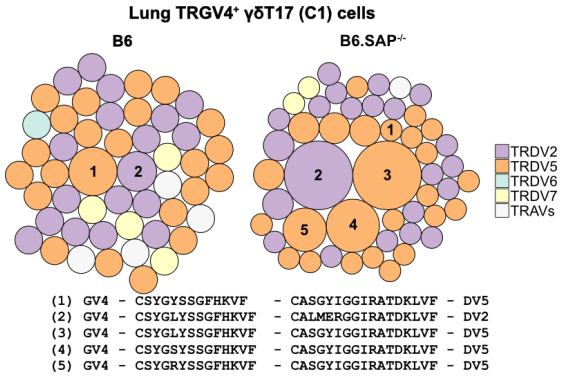
Lung TRGV4+ γδT17 (C1) cells
B6
B6.SAP-/-
TRDV2
TRDV5
TRDV6
TRDV7
TRAVs
(1) GV4 - CSYGYSSGFHKVF - CASGYIGGIRATDKLVF - DV5
(2) GV4 - CSYGLYSSGFHKVF - CALMERGGIRATDKLVF - DV2
(3) GV4 - CSYGLYSSGFHKVF - CASGYIGGIRATDKLVF - DV5
(4) GV4 - CSYGSYSSGFHKVF - CASGYIGGIRATDKLVF - DV5
(5) GV4 - CSYGRYSSGFHKVF - CASGYIGGIRATDKLVF - DV5

Figure 7

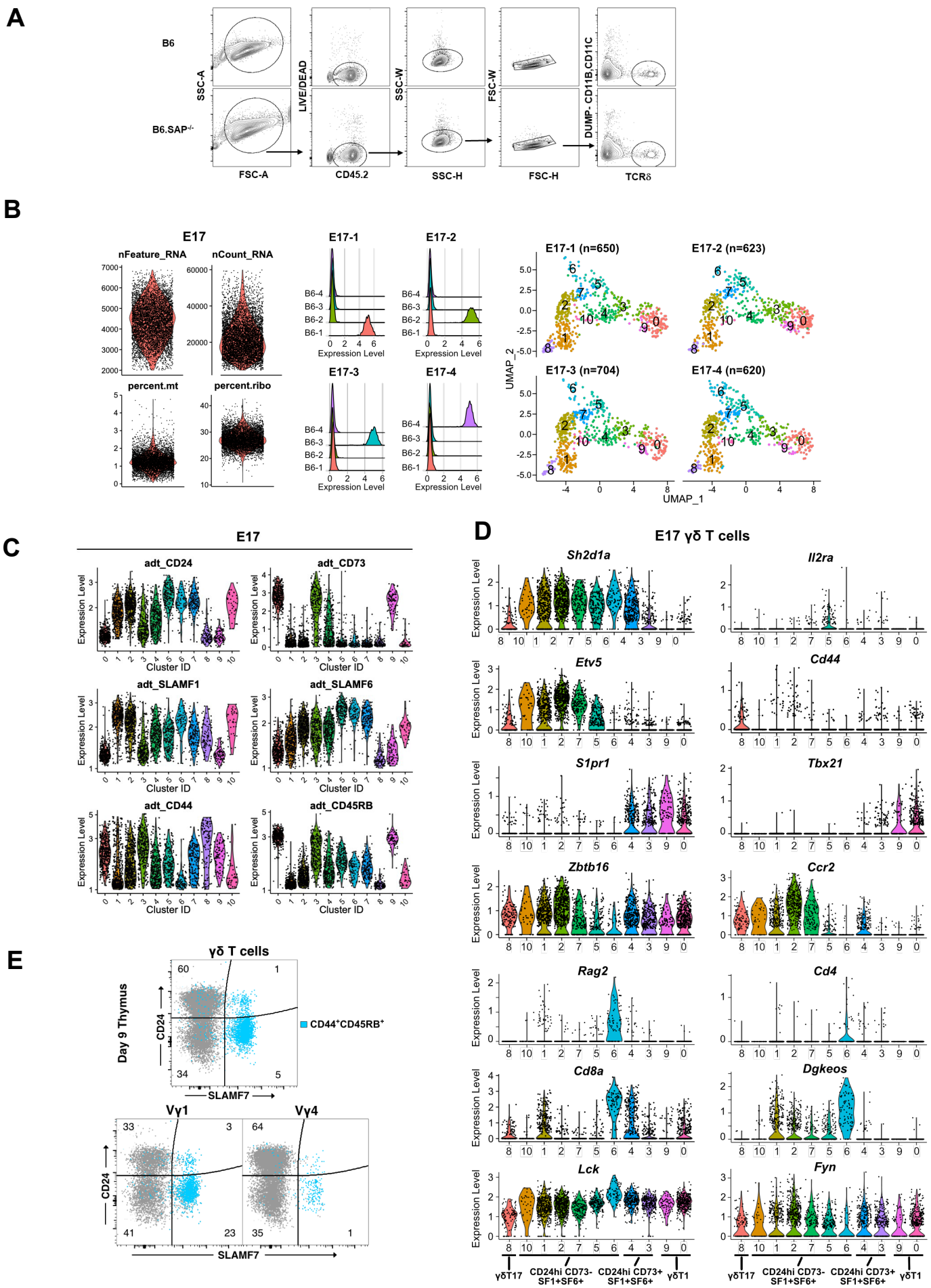

Supplemental Fig. 1

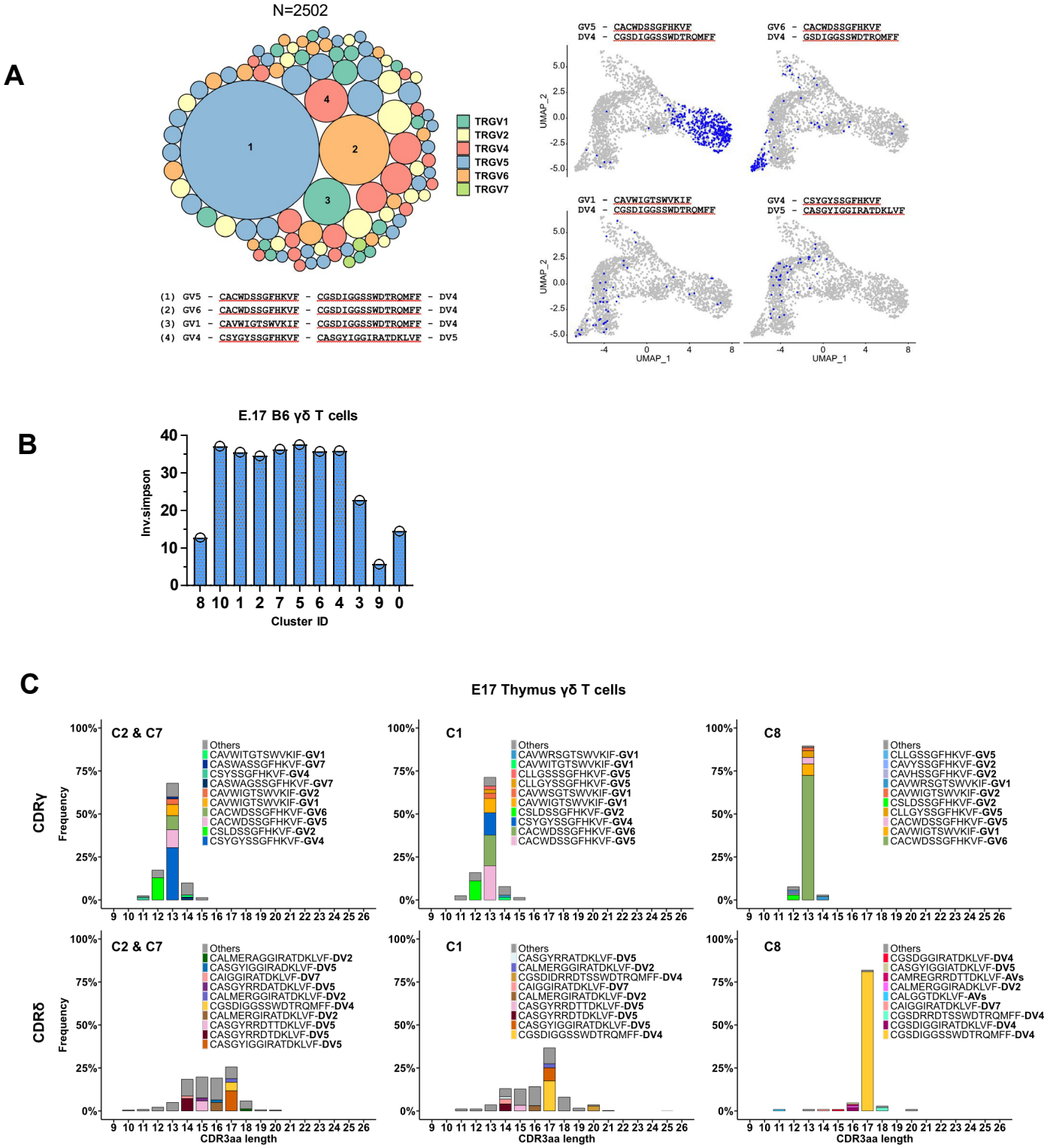

Supplemental Fig. 2

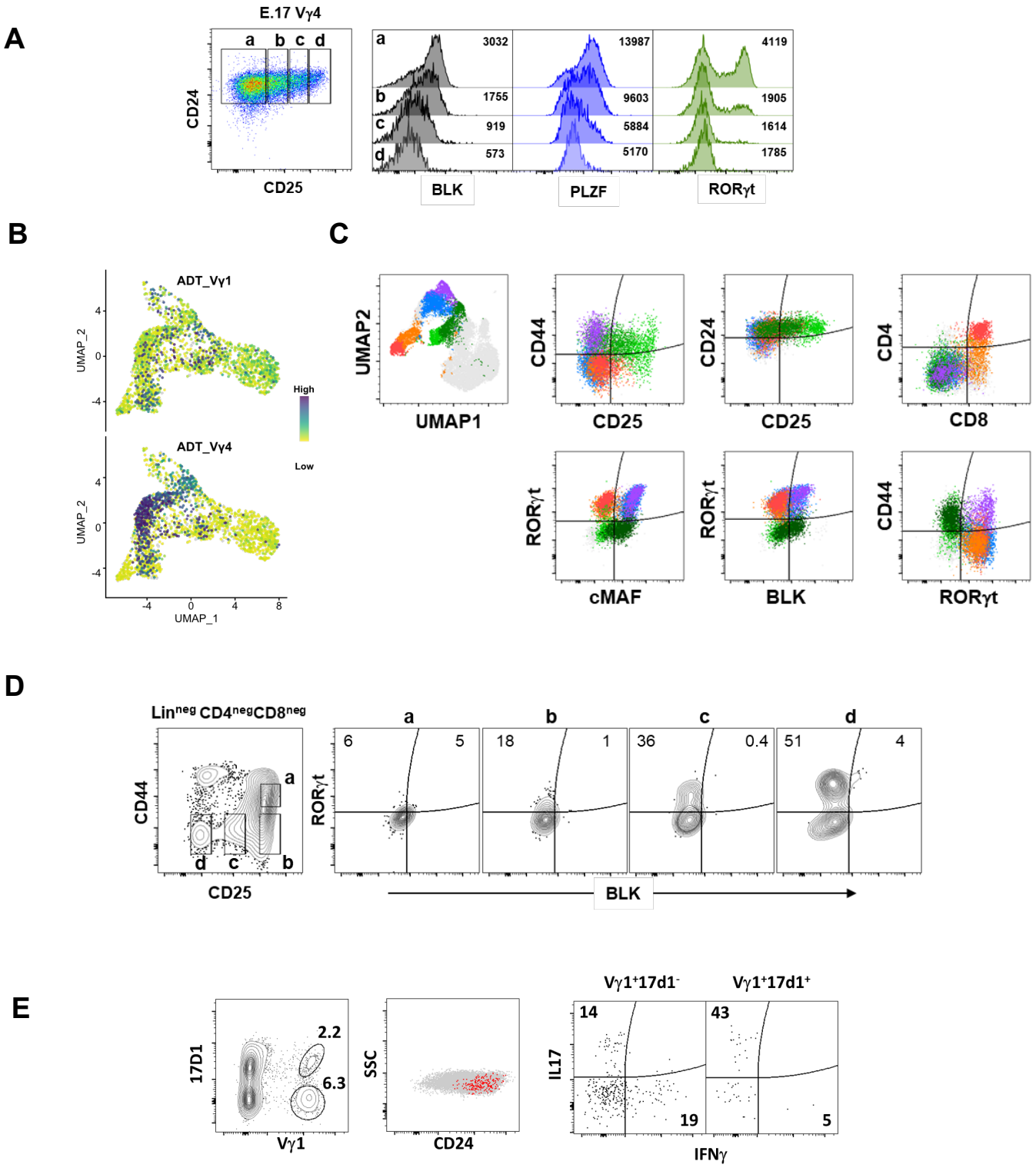

Supplemental Fig 3

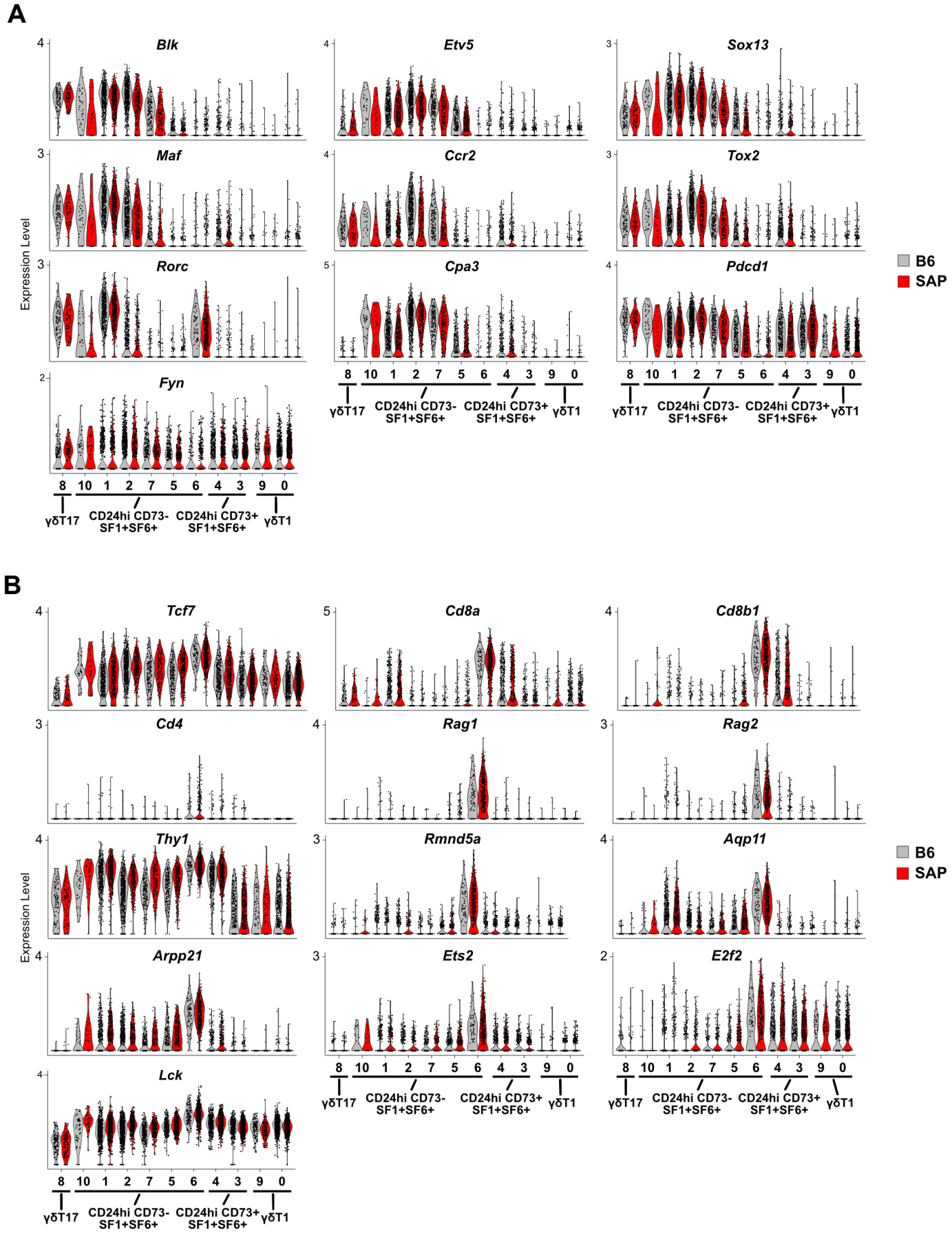

Supplemental Fig 4

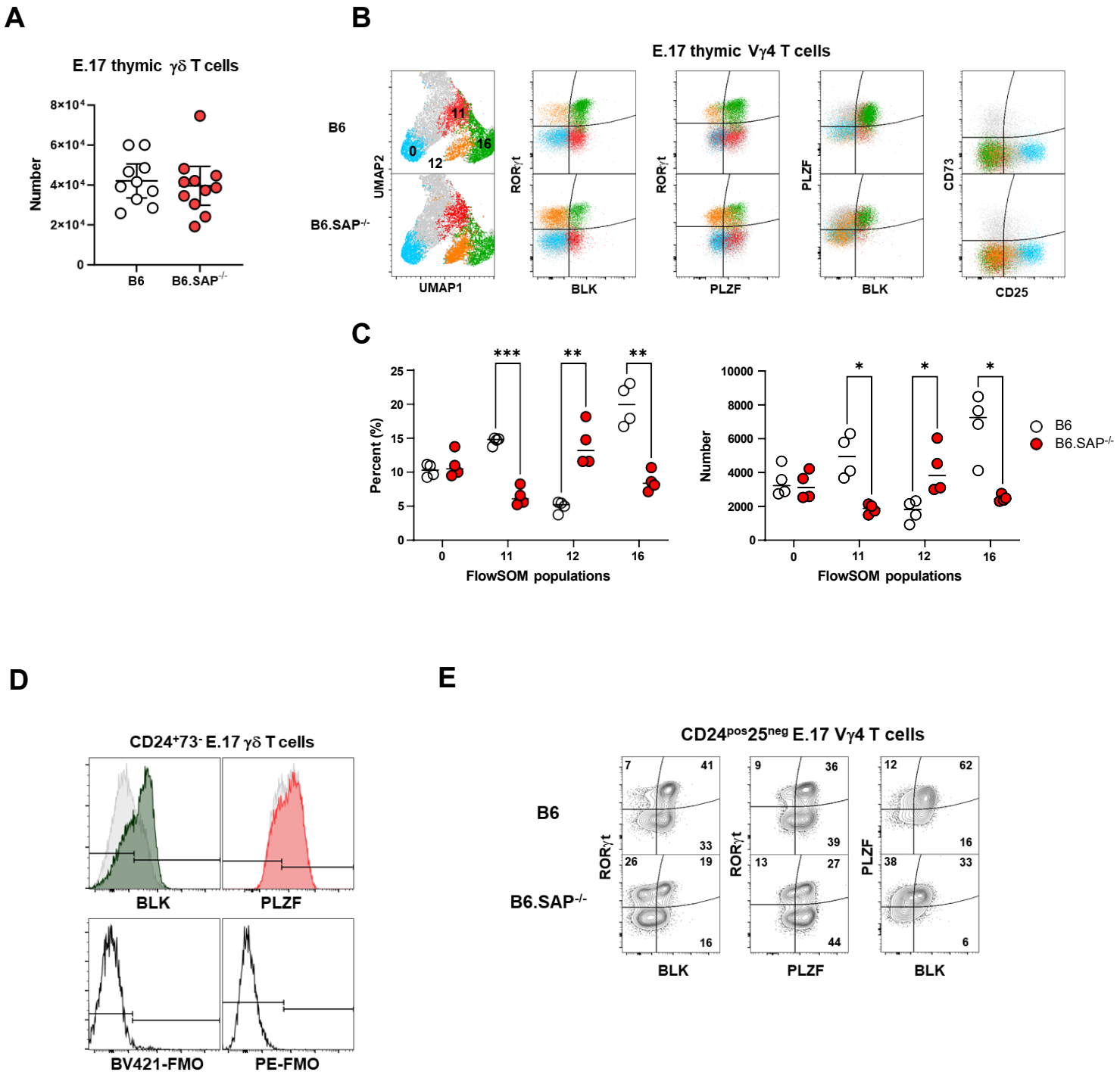
A
E.17 thymic γδ T cells
Number
8×10⁴
6×10⁴
4×10⁴
2×10⁴
0
B6
B6.SAP-/-
B
E.17 thymic Vγ4 T cells
B6
B6.SAP-/-
UMAP2
UMAP1
0
11
12
16
RORγt
BLK
PLZF
CD73
CD25
C
Percent (%)
Number
FlowSOM populations
***
**
*
B6
B6.SAP-/-
D
CD24+73- E.17 γδ T cells
BLK
PLZF
BV421-FMO
PE-FMO
E
CD24pos25neg E.17 Vγ4 T cells
B6
B6.SAP-/-
RORγt
PLZF
BLK
7
41
33
26
19
16
9
36
39
13
27
44
12
62
16
38
33
6

Suppl. Fig. 5

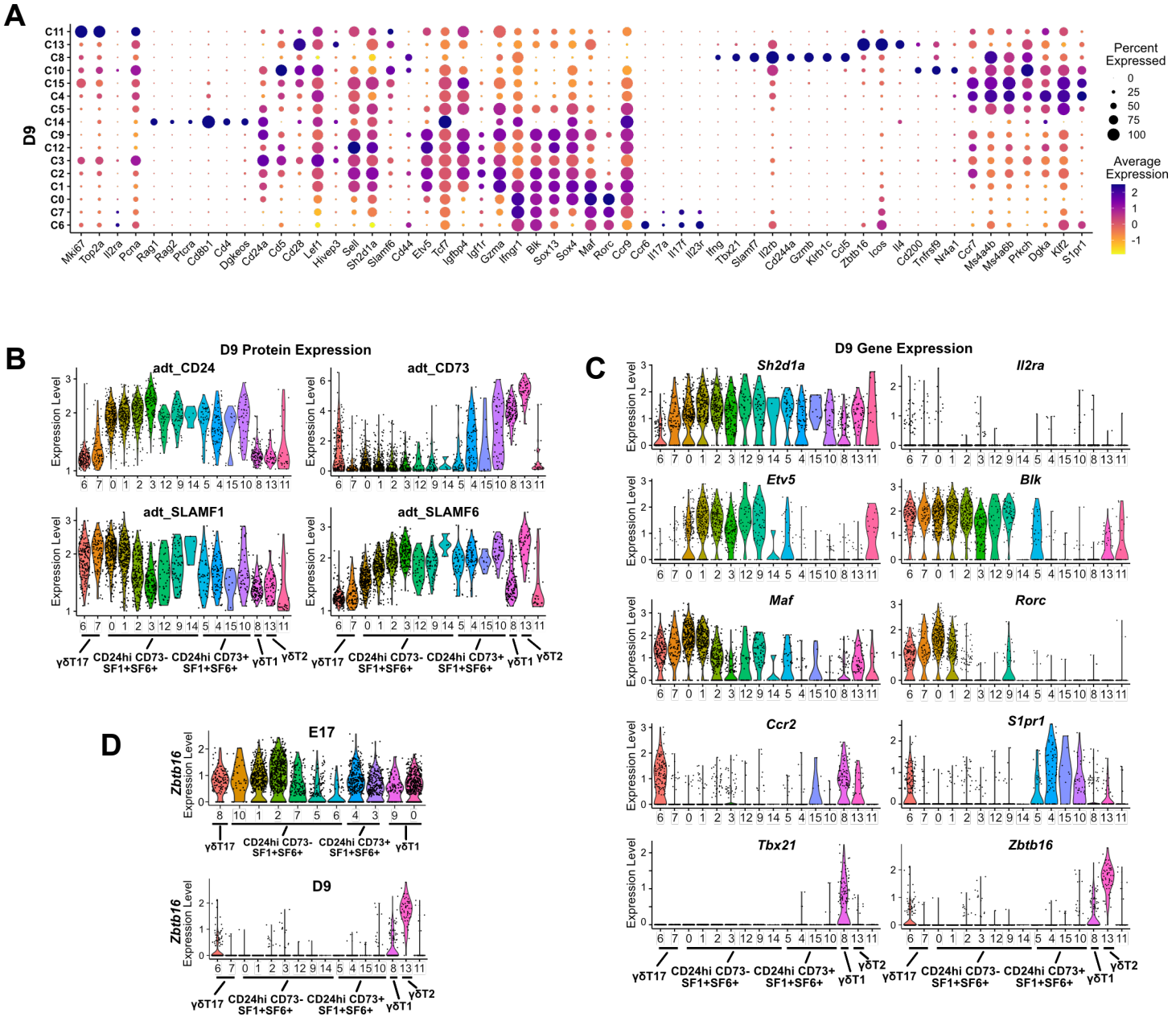
A
D9
C11
C13
C8
C10
C15
C4
C5
C14
C9
C12
C3
C2
C1
C0
C7
C6
Mki67 Top2a Il2ra Pcna Rag1 Rag2 Ptcra Cd8b1 Cd4 Dgkeos Cd24a Cd5 Cd28 Lef1 Hivep3 Sell Sh2d1a Slamf6 Cd44 Etv5 Tcf7 Igfbp4 Igf1r Gzma Ifngr1 Blk Sox13 Sox4 Maf Rorc Ccr9 Ccr6 Il17a Il17f Il23r Ifng Tbx21 Slamf7 Il2rb Cd244a Gzmb Klrb1c Cd6 Zbtb16 Icos Il4 Cd200 Tnfrsf9 Nr4a1 Ccr7 Ms4a4b Ms4a6b Prkch Dgka Klf2 S1pr1
Percent Expressed
0
25
50
75
100
Average Expression
2
1
0
-1
B
D9 Protein Expression
adt_CD24
adt_CD73
adt_SLAMF1
adt_SLAMF6
Expression Level
6 7 0 1 2 3 12 9 14 5 4 15 10 8 13 11
γδT17
CD24hi CD73- SF1+SF6+
CD24hi CD73+ SF1+SF6+
γδT1
γδT2
C
D9 Gene Expression
Sh2d1a
Il2ra
Etv5
Blk
Maf
Rorc
Ccr2
S1pr1
Tbx21
Zbtb16
D
E17
Zbtb16
Expression Level
8 10 1 2 7 5 6 4 3 9 0
D9

Suppl. Fig. 6

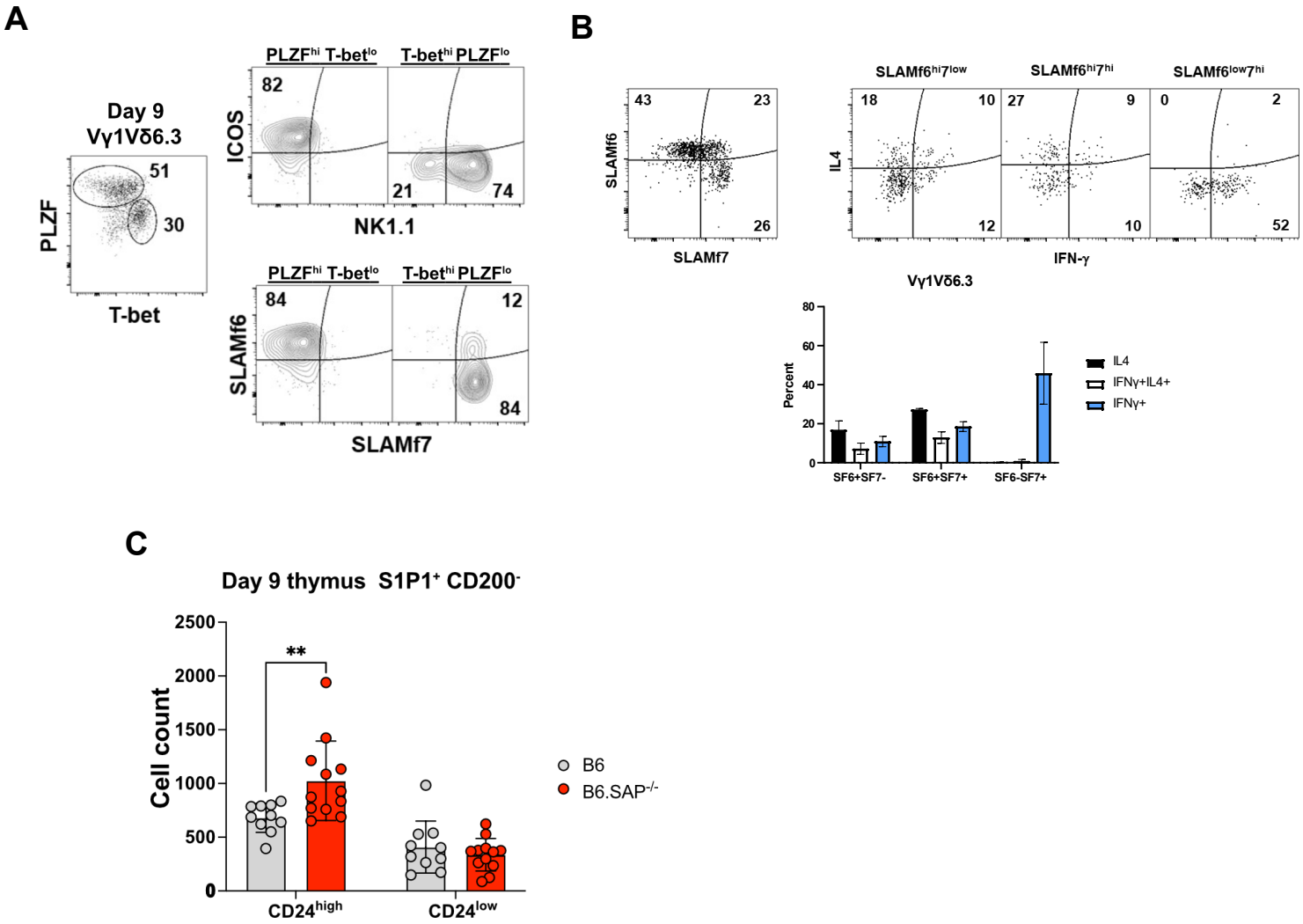
A
Day 9
Vγ1Vδ6.3
PLZF
T-bet
51
30
PLZFhi T-betlo
T-bethi PLZFlo
ICOS
NK1.1
82
21
74
SLAMf6
SLAMf7
84
12
84
B
SLAMf6hi7low
SLAMf6hi7hi
SLAMf6low7hi
SLAMf6
SLAMf7
43
23
26
IL4
IFN-γ
18
10
12
27
9
10
0
2
52
Vγ1Vδ6.3
Percent
IL4
IFNγ+IL4+
IFNγ+
SF6+SF7-
SF6+SF7+
SF6-SF7+
C
Day 9 thymus S1P1+ CD200-
Cell count
**
B6
B6.SAP-/-
CD24high
CD24low

Suppl. Fig. 7

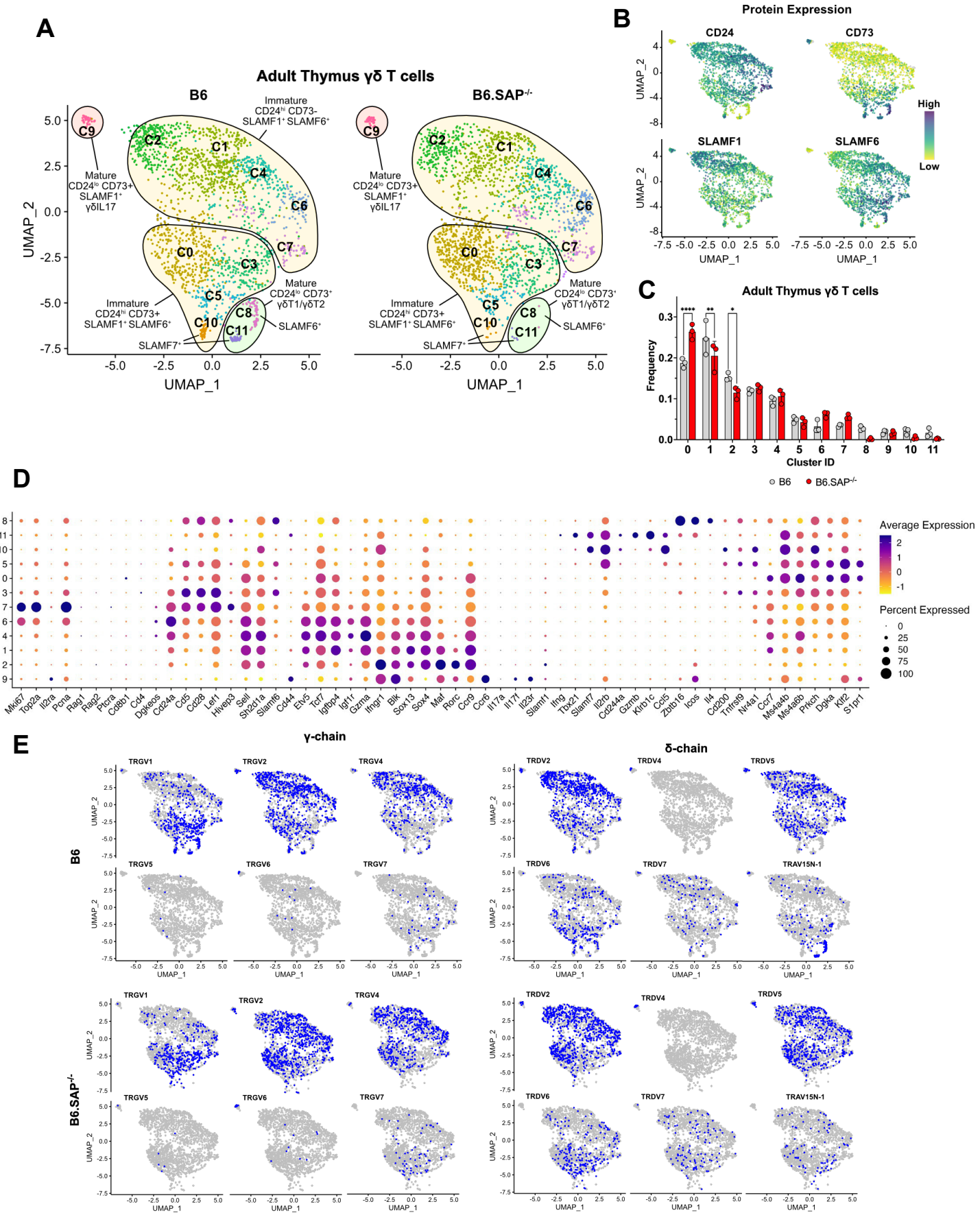

Supplemental Fig 8

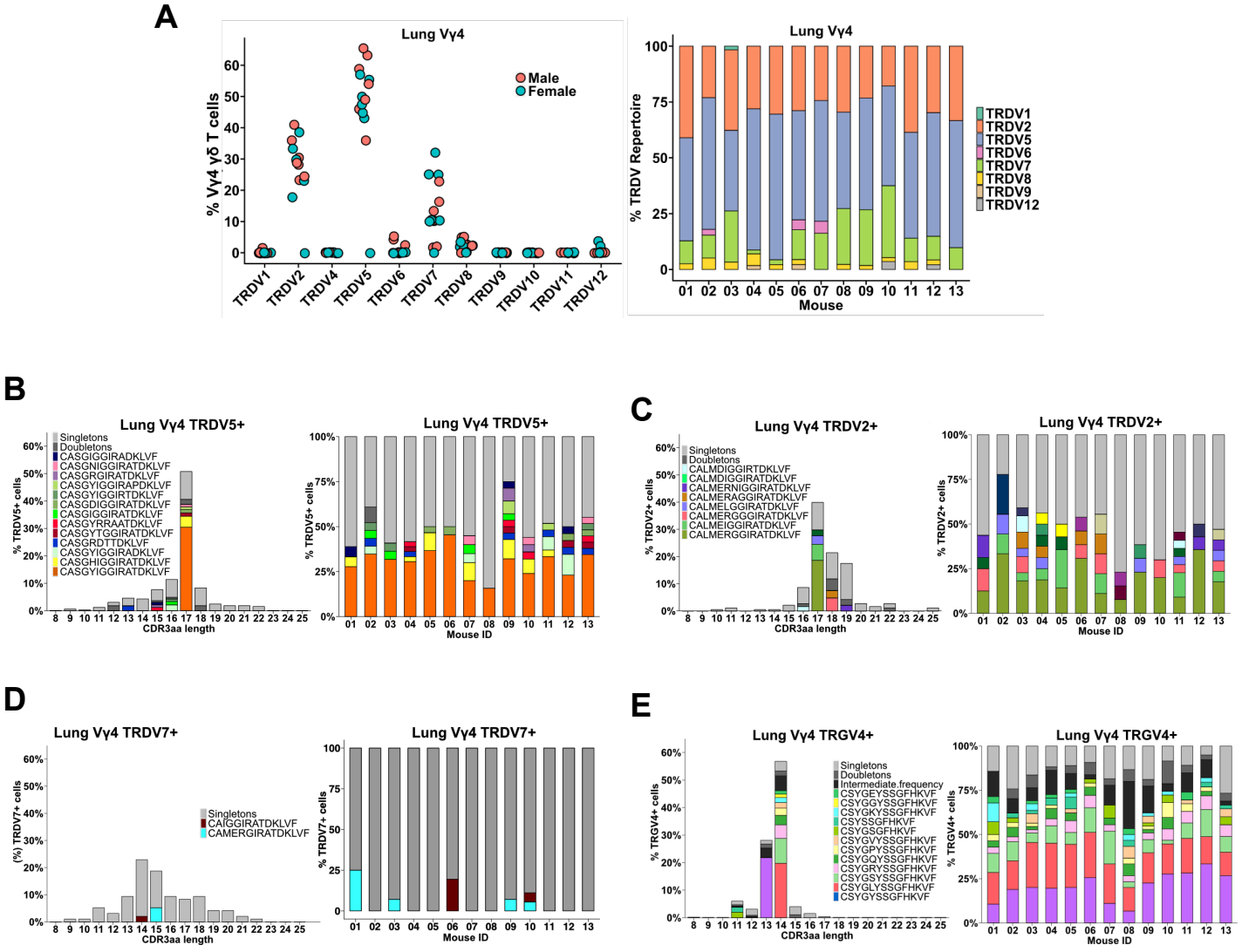

Supplemental Fig 9

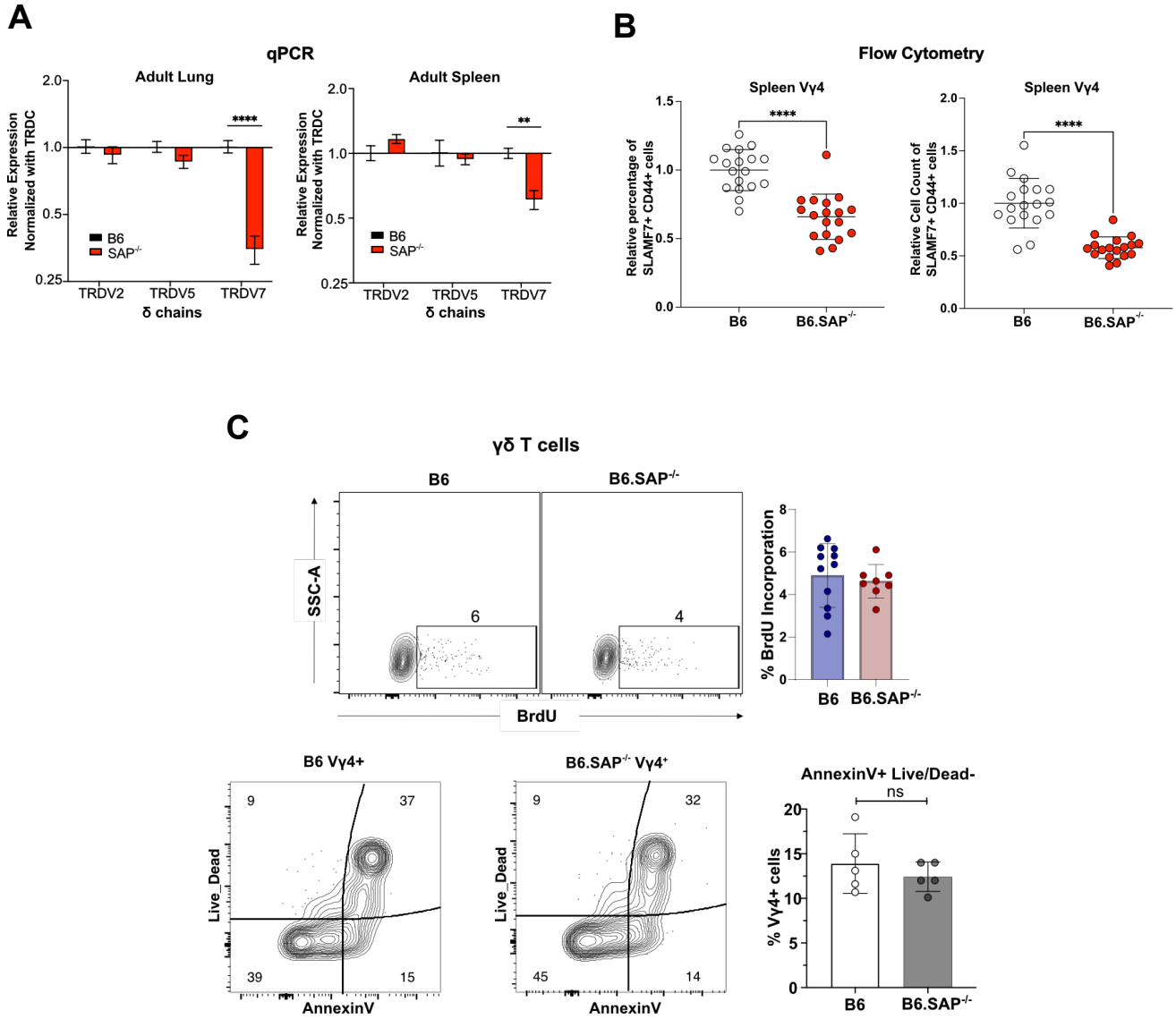

Supplemental Fig 10